Published June 24, 2019

Reviews and Analyses

Core Ideas

- Land surface models (LSMs) show a large variety in describing and upscaling infiltration.
- Soil structural effects on infiltration in LSMs are mostly neglected.
- New soil databases may help to parameterize infiltration processes in LSMs.

Received 22 Oct. 2018.
Accepted 16 Feb. 2019.

Citation: Vereecken, H., L. Weihermüller, S. Assouline, J. Šimůnek, A. Verhoef, M. Herbst, N. Archer, B. Mohanty, C. Montzka, J. Vanderborght, G. Balsamo, M. Bechtold, A. Boone, S. Chadburn, M. Cuntz, B. Decharme, A. Ducharne, M. Ek, S. Garrigues, K. Goergen, J. Ingwersen, S. Kollet, D.M. Lawrence, Q. Li, D. Or, S. Swenson, P. de Vrese, R. Walko, Y. Wu, and Y. Xue. 2019. Infiltration from the pedon to global grid scales: An overview and outlook for land surface modeling. Vadose Zone J. 18:180191. doi:10.2136/vzj2018.10.0191

Affiliations: H. Vereecken, L. Weihermüller, M. Herbst, C. Montzka, J. Vanderborght, K. Goergen, and S. Kollet, Agrosphere Institute IBG-3, Forschungszentrum Jülich GmbH, 52425 Jülich, Germany; H. Vereecken, International Soil Modeling Consortium (ISMC), Forschungszentrum Jülich GmbH, 52425 Jülich, Germany; S. Assouline, Dep. of Environmental Physics and Irrigation, Institute of Soils, Water and Environment Sciences, A.R.O. Volcani Center, Bet Dagan, Israel; J. Šimůnek, Dep. of Environmental Sciences, Univ. of California, Riverside, CA 92521; A. Verhoef, Dep. of Geography and Environmental Science, Univ. of Reading, Reading, RG6 6AB, UK; N. Archer, British Geological Survey, The Lyell Centre, Edinburgh, EH14 4AP, Scotland; B. Mohanty, Dep. of Biological and Agricultural Engineering, Texas A&M Univ., College Station, TX 77843; G. Balsamo, European Centre for Medium-Range Weather Forecasts, Reading, RG2 9AX, UK; M. Bechtold, Dep. of Earth and Environmental Sciences and Dep. of Computer Science, KU Leuven, 3001 Heverlee, Belgium; A. Boone and B. Decharme, CNRM, UMR3589 (Météo-France, CNRS), Toulouse, France; S. Chadburn, School of Earth and Environment, Univ. of Leeds, Leeds, LS2 9JT, UK; S. Chadburn, Univ. of Exeter, Exeter, EX4 4QE, UK; M. Cuntz, Univ. de Lorraine, INRA, AgroParisTech, UMR Silva, 54000 Nancy, France; A. Ducharne, Sorbonne Univ., CNRS, EPHE, UMR 7619 METIS, Paris, France; (continued on next page)

© 2019 The Author(s). This is an open access article distributed under the CC BY-NC-ND license (http://creativecommons.org/licenses/by-nc-nd/4.0/).

Infiltration from the Pedon to Global Grid Scales: An Overview and Outlook for Land Surface Modeling

Harry Vereecken, Lutz Weihermüller, Shmuel Assouline, Jirka Šimůnek, Anne Verhoef, Michael Herbst, Nicole Archer, Binayak Mohanty, Carsten Montzka, Jan Vanderborght, Gianpaolo Balsamo, Michel Bechtold, Aaron Boone, Sarah Chadburn, Matthias Cuntz, Bertrand Decharme, Agnès Ducharne, Michael Ek, Sebastien Garrigues, Klaus Goergen, Joachim Ingwersen, Stefan Kollet, David M. Lawrence, Qian Li, Dani Or, Sean Swenson, Philipp de Vrese, Robert Walko, Yihua Wu, and Yongkang Xue

Infiltration in soils is a key process that partitions precipitation at the land surface into surface runoff and water that enters the soil profile. We reviewed the basic principles of water infiltration in soils and we analyzed approaches commonly used in land surface models (LSMs) to quantify infiltration as well as its numerical implementation and sensitivity to model parameters. We reviewed methods to upscale infiltration from the point to the field, hillslope, and grid cell scales of LSMs. Despite the progress that has been made, upscaling of local-scale infiltration processes to the grid scale used in LSMs is still far from being treated rigorously. We still lack a consistent theoretical framework to predict effective fluxes and parameters that control infiltration in LSMs. Our analysis shows that there is a large variety of approaches used to estimate soil hydraulic properties. Novel, highly resolved soil information at higher resolutions than the grid scale of LSMs may help in better quantifying subgrid variability of key infiltration parameters. Currently, only a few LSMs consider the impact of soil structure on soil hydraulic properties. Finally, we identified several processes not yet considered in LSMs that are known to strongly influence infiltration. Especially, the impact of soil structure on infiltration requires further research. To tackle these challenges and integrate current knowledge on soil processes affecting infiltration processes into LSMs, we advocate a stronger exchange and scientific interaction between the soil and the land surface modeling communities.

Abbreviations: BC, boundary condition; CLM, common land model; FTC, freeze–thaw cycle; GCM, global climate model; LSM, land surface model; pdf, probability density function; PDM, probability-distributed model; PTF, pedotransfer function; SWR, soil water repellency.

Infiltration or water entry into the soil profile is a key process in the hydrological cycle. Its rate and dynamics affect the partitioning of precipitation at the land surface and determines the onset of ponding and, consequently, the formation of overland flow and runoff. Infiltration affects irrigation efficiency on managed lands and the resulting stored soil water available to vegetation (e.g., Verhoef and Egea-Cegarra, 2013), overland flow and soil erosion processes (e.g., Assouline and Ben-Hur, 2006; Garrote and Bras, 1995; Poesen et al., 2003), groundwater recharge (e.g., Dahan et al., 2008), the exchange of water and energy between the soil and atmosphere by controlling soil water content at the surface (Kim et al., 2017; MacDonald et al., 2017), and with this the flux partitioning into latent and sensible heat flux with multiple atmospheric feedbacks (e.g., Keune et al., 2016; Seneviratne et al., 2010), stream flow and flooding events (Garrote and Bras, 1995), and various soil physical processes such as the onset of landslides (Lehmann and Or, 2012) and soil mechanical

M. Ek, Environmental Modeling Center, National Centers for Environmental Prediction, College Park, MD 20740; S. Garrigues, French National Institute for Agricultural Research (INRA) CESBIO, Toulouse, France, and Centre for Ecology and Hydrology, CEH, Wallingford, UK; K. Goergen, Centre for High-Performance Scientific Computing in Terrestrial Systems, Geoverbund ABC/J, 52425 Jülich, Germany; J. Ingwersen, Institute of Soil Science and Land Evaluation, Biogeophysics, Univ. Hohenheim, 70599 Stuttgart, Germany; D.M. Lawrence, National Center for Atmospheric Research, Boulder, CO 80305; Q. Li, Center for Monsoon Research, Institute of Atmospheric Physics, Chinese Academy of Sciences, Beijing 100029, China; D. Or, ETH Zurich, Institut für Biogeochemie und Schadstoffdynamik, 8092 Zürich, Switzerland; S. Swenson, Climate and Global Dynamics Lab., Terrestrial Sciences, NCAR, Boulder, CO 80307; P. de Vrese, Max-Planck Institut for Meteorology, Land in the Earth System, 20146 Hamburg, Germany; R. Walko, Rosenstiel School of Marine and Atmospheric Science, Univ. of Miami, Miami, FL 33149; Y. Wu, Environmental Modeling Center, National Centers for Environmental Prediction and I.M. System Group at NCEP, College Park, MD 20740; Y. Xue, Dep. of Atmospheric and Oceanic Sciences and Dep. of Geography, Univ. of California, Los Angeles, CA 90095. *Corresponding author (h.vereecken@fz-juelich.de).

stress–strain behavior. The spatial distribution of infiltration rates is affected by soil type, local topography, and attributes of surface cover. Infiltration feedbacks have been shown to drive the formation of vegetation patterns. Infiltration rates are crucial inputs to the design of any irrigation system and many soil and water conservation practices. The significance of infiltration has made it a subject of studies in many domains ranging from hydrology to agricultural, environmental, and civil engineering.

Even at the single profile scale, infiltration exhibits strong dynamics that are dependent on soil properties, rainfall characteristics, wetting rates, vegetation cover and type, soil and crop management, and initial and boundary conditions within the soil flow domain. Based on the definition of Hillel (1980) and Brutsaert (2005), infiltration is defined as "the entry of water into the soil surface and its subsequent movement through the soil profile." The sources of liquid water for infiltration include direct precipitation (rainfall, dewfall, and snowmelt), leaf drip and stem flow, irrigation, or runoff that was routed over the land surface and reinfiltrates (a process termed *run-on*). A detailed understanding of the primary controls on infiltration rates and the onset of ponding with subsequent runoff, and their translation into model equations, is of great importance at all scales. The accurate process representation of infiltration is also essential for crop water use studies, the design of irrigation systems, and the optimal management of water resources. Different approaches have thus been developed over the past decades to provide quantitative tools able to describe and predict infiltration into porous media such as soils, ranging from empirical expressions to analytical and numerical solutions of the basic flow equations.

Infiltration dynamics are determined by soil properties (hydraulic conductivity, sorptivity), the hydraulic gradients that drive flow, and initial and boundary conditions (Philip, 1957). Depending on the initial soil water content in the soil profile, the water supply rate, and the corresponding soil wetting dynamics, all the available water can infiltrate in different amounts into the soil. Hence, these factors will influence the infiltration curve (the change with time of the infiltration rate during a wetting event) (Mein and Larson, 1973).

The infiltration capacity or potential infiltration rate of a soil, $q_{cap}(t)$, is the maximum rate at which the soil surface can take up water for given initial conditions (Horton, 1940). The actual infiltration capacity is also affected by the initial soil water content of the soil, but for practical considerations it may be considered a time-dependent soil property where water inputs in excess of this maximum infiltration rate will pond and likely generate runoff. For surface fluxes at rates lower than the soil's infiltration capacity, the realized infiltration rate will depend on the state of the soil (as shaped by the temporal history of the application rates and the consecutive sequences of wetting and drying). Two infiltration regimes in unsaturated soils can be distinguished and lead to different occurrence times of ponding and thus runoff generation: constant water supply (occurring during irrigation or simulated rainfall) and variable-rate supply (during natural rainfall), as is shown in Fig. 1 and 2 in terms of rates (top panel) or cumulative depths (bottom panel; in this case uppercase symbols are used).

The dashed curves in Fig. 1 and 2 represent the infiltration capacity, $q_{cap}(t)$ [L T^{-1}] or $Q_{cap}(t)$ [L], of a given soil profile, the dotted line depicts the water supply rate, $r(t)$ [L T^{-1}] or $R(t)$ [L], for the constant precipitation rate (Fig. 1) or for the variable precipitation rate, as is often the case during natural rainfall (Fig. 2), and the solid line shows the actual infiltration rate, $q(t)$ [L T^{-1}] or $Q(t)$ [L], during these events. In the case of constant $r(t)$, all the applied water can infiltrate in the first stage of wetting (Fig. 1), and $q(t) = r(t)$. Compared with $q_{cap}(t)$ corresponding to an unlimited water application rate, $q(t)$ can be higher than $q_{cap}(t)$ because the hydraulic gradients resulting from the unsaturated condition generated by the limited wetting rate, $r(t)$, are larger than the ones that result from the saturated condition inherent to the unlimited wetting rate. However, both curves tend toward a similar "quasi-steady" infiltration rate corresponding to a gradient of unity but approach it at different rates resulting from the difference in the rate of decrease of the hydraulic gradients corresponding to each wetting condition. As wetting progresses,

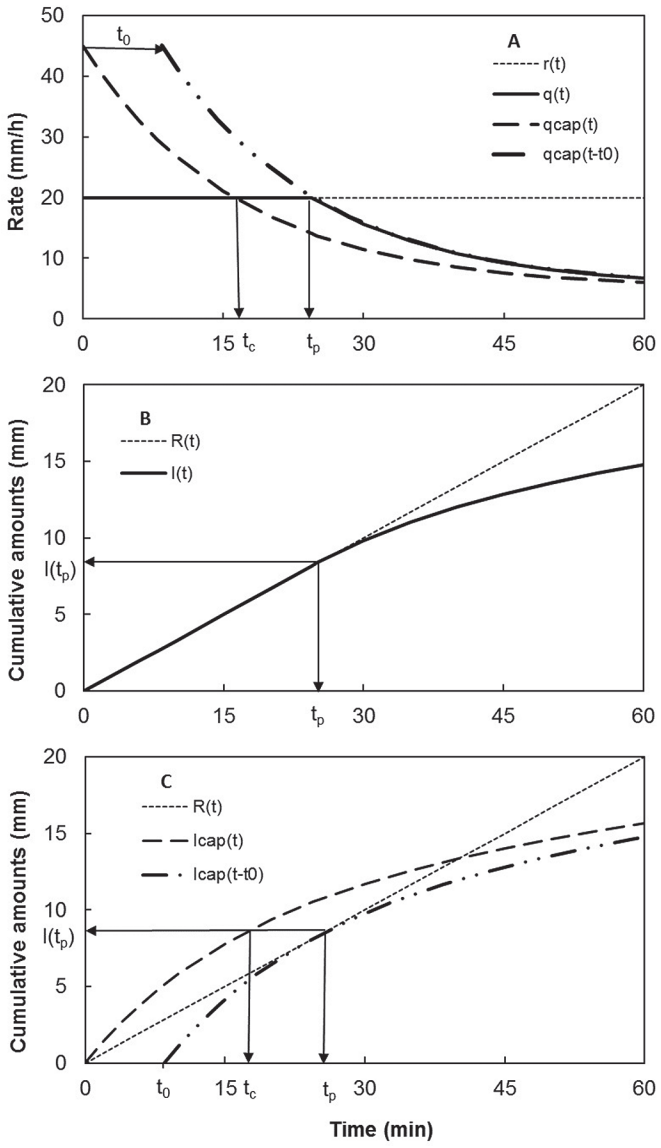

Fig. 1. (A) Illustrative representation of the infiltration capacity rate, $q_{cap}(t)$ (dashed curve) and the actual infiltration rate, $q(t)$ (solid line) of a soil profile exposed to a rainfall event with constant intensity $r(t)$ (dotted line), where the time t_c denotes the moment where $q_{cap}(t) = r(t)$, while the time t_p denotes the ponding time where $q(t) = r(t)$, and shifting the representation of $q_{cap}(t)$ by $t_0 = (t_p - t_c)$ (dashed-dotted line) allows estimation of t_p; (B) illustration of t_p in terms of the cumulative infiltration, with $I(t_p) = R(t_p)$; and (C) cumulative infiltration capacity $I_{cap}(t)$ (dashed line) and cumulative rainfall $R(t)$ (dotted line); the ponding time t_p can be estimated by means of $I_{cap}(t - t_0)$ (dashed-dotted line).

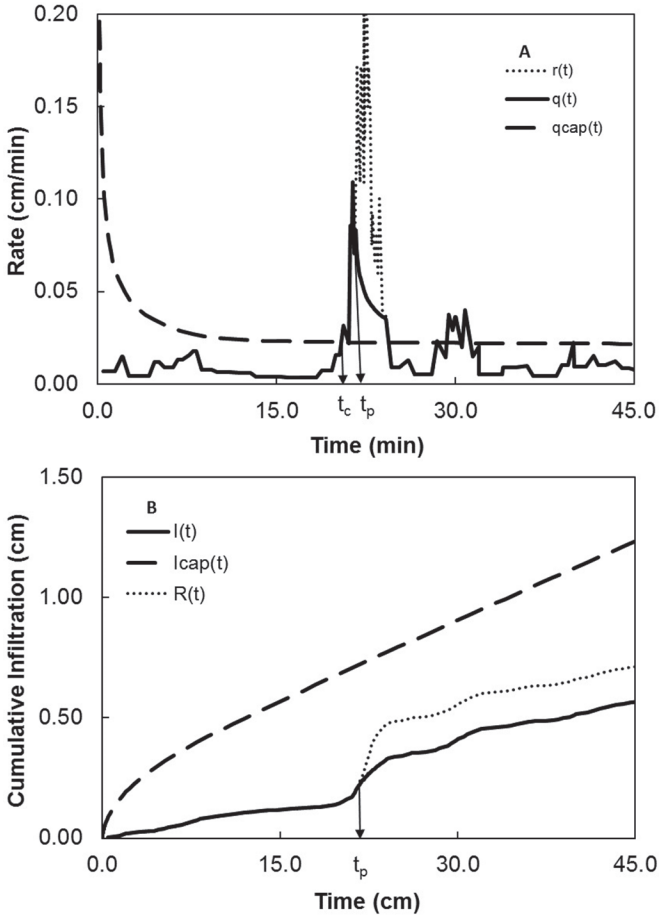

Fig. 2. (A) Illustrative representation of the infiltration capacity rate, $q_{cap}(t)$ (dashed curve) and the actual infiltration rate, $q(t)$ (solid line) of a soil profile exposed to a rainfall event with variable intensity $r(t)$ (dotted line)—for low $r(t)$ values below $q_{cap}(t)$, $q(t) = r(t)$, and the result is that t_c is close to t_p; and (B) cumulative infiltration capacity $I_{cap}(t)$ (dashed line), cumulative actual infiltration, $I(t)$ (solid line), and cumulative rainfall $R(t)$ (dotted line)—in this case, t_p cannot be estimated by means of $I_{cap}(t_p - t_0)$. Adapted from Assouline et al., 2007.

$q(t)$ begins to decrease, and at the time of ponding, t_p, where the infiltration rate, $q(t_p)$ is smaller than the wetting rate, $r(t_p)$, ponding occurs at the soil surface.

In terms of cumulative infiltrating volumes of water (or water depths, which are volumes per unit area) (Fig. 1B), $Q(t)$ is always smaller than $Q_{cap}(t)$ even when $q(t)$ is higher than $q_{cap}(t)$ (Fig. 1A), indicating that the concept of infiltration capacity corresponds to cumulative infiltration rather than to infiltration rates. Because the rainfall rate is constant, the picture in terms of infiltration rates (Fig. 1A) and cumulative depths (Fig. 1B and 1C) provide a similar condition for t_p, corresponding to the time when $Q(t)$ departs from $R(t)$. It is interesting to note that if it is assumed that ponding occurs when $r(t)$ exceeds $q_{cap}(t)$, t_p is underestimated (Fig. 1A and 1C). The infiltration regime under variable $r(t)$ and the prediction of t_p is much more complicated because $q(t)$ depends on the pattern of $r(t)$ (Fig. 2A). The picture is much simpler when expressed in terms of cumulative depths (Fig. 2B). Assouline et al. (2007) have proposed a simple method to estimate t_p under variable $r(t)$.

The cases described in Fig. 1 and 2 represent one mechanism of runoff formation termed *infiltration excess* or *Hortonian overland flow* (Horton, 1933). Another important mechanism corresponds to the formation of a saturated topsoil layer that enhances runoff formation. This mechanism is termed *saturation excess* or *Dunne overland flow* (Dunne, 1978; Freeze, 1980). Dunne overland flow occurs when the soil reaches saturation from above, via direct precipitation, or below and no additional water supplied

from the top can be stored in the soil profile. This can happen, for example, when the local water table is high or a hydraulically impeding layer close to the soil surface exists (causing a so-called "perched" water table). In general, the Dunne mechanism occurs in areas close to the channels of the drainage network of a catchment or in areas in the low-lying parts of a catchment where the depth to the water table is shallow. It is therefore more common in humid climates. These saturated runoff source areas vary in size, seasonally, and during individual storm events. Therefore, they are often referred to as variable source areas (Dunne and Black, 1970) and the runoff generated on them as variable source area runoff (as, e.g., in TOPMODEL [Beven and Kirkby, 1979], which is implemented [sometimes in modified form] in many LSMs). On the other hand, Hortonian overland flow is more common in semiarid climates (Entekhabi and Eagleson, 1989).

Infiltration theory, and related numerical and analytical solutions, was originally the domain of soil physicists. Several reviews on different aspects of infiltration into soils have been published (Assouline, 2013; Barry et al., 2007; Clothier, 2001; Gardner, 1960; Hopmans et al., 2007; Parlange, 1980; Parlange et al., 1999; Philip, 1969; Philip and Knight, 1974; Raats, 2001; Raats et al., 2002; Skaggs, 1982) and also constitute key chapters in textbooks (e.g., Bear, 1972; Brutsaert, 2005; Childs, 1969; Chow et al., 1988; Delleur, 2006; Hillel, 1998; Warrick, 2003). The fundamental concepts of infiltration have been applied in hydrology to deal with the prediction of infiltration at the field scale (Corradini et al., 2011; Govindaraju et al., 2012; Morbidelli et al., 2006), on hillslopes (e.g., Morbidelli et al., 2018), for heterogeneous soil systems (Govindaraju et al., 2001), and to handle the impact of complex precipitation events and patterns on infiltration (Corradini et al., 1994, 1997).

With the advent of efforts to model the global water and energy cycles at the large scale, infiltration theory was taken up by the climate and hydrological modeling community. Largely due to the (originally) limited computing power and the difficulty in defining spatially distributed and appropriately upscaled soil parameters, simplifications and approximations of the infiltration process were introduced into the LSMs embedded in weather and climate models. The main role of a LSM is to compute the energy partitioning at the interface between land surface and atmosphere. At the land surface, net radiation is converted into latent heat, sensible heat, and ground heat flux, where the latent heat flux is the equivalent of the evapotranspiration flux in the water balance but in this case expressed in energy units. The energy partitioning at the land surface directly affects the state of the atmosphere. For example, the relative magnitude of the latent and sensible heat fluxes will modify atmospheric state variables such as relative humidity and the height of the atmospheric boundary layer, which in turn will affect cloud-forming processes and ultimately rainfall. Infiltration acts on this energy partitioning indirectly via its control on soil moisture content. Near-surface soil moisture content is an important state variable in both the water and energy balance. For example, it affects net radiation due to its effects on land surface radiative properties, albedo, and emissivity. Also, both soil evaporation and transpiration depend strongly on soil moisture content. A reduction in soil moisture content will lower evaporation via a reduced soil–atmosphere vapor gradient and decreased replenishment of water to the evaporation front due to reduced hydraulic conductivity, whereas transpiration is affected via a decrease in root water uptake under drought conditions. Finally, because soil thermal conductivity and heat capacity are functions of soil moisture, infiltration also indirectly affects the soil heat regime. Anwar et al. (2018) showed that the choice of the infiltration scheme had a significant effect on the simulated regional climate. An infiltration scheme with a lower soil infiltration rate yielded lower topsoil soil moisture, which led to a lower latent heat flux and a higher sensible heat flux, resulting in a net warming effect within the simulation domain.

With regard to the simulation of infiltration, a range of approaches at different levels of complexity currently exists in these models. Paniconi and Putti (2015) reviewed the last five decades of physically based numerical models in hydrology and addressed the treatment of infiltration from local via hillslope to catchment scale. They focused on the flow path heterogeneity, where analysis has been focused on the nonlinearity and upscaling in hydrology with a specific focus on numerical methods used in hydrological models and related computational challenges. They briefly discussed the seminal work of Horton (1933), Betson and Marius (1969), and Dunne and Black (1970) in identifying the main mechanisms of runoff generation, which is closely related to the infiltration process.

Zhao and Li (2015) reviewed the different approaches to model land surface processes across complex terrain. The main focus was on the role of grid-scale spatial heterogeneity of land surface variables and parameters (e.g., soil moisture content, net primary productivity, leaf area index, fraction of vegetation cover) and the topographic impact on key atmospheric controls (e.g., precipitation, air temperature, wind speed, air pressure). The role of infiltration and its different parameterization was briefly addressed in relation to the spatial variability of soil hydraulic properties in complex terrains.

Clark et al. (2015) analyzed the state-of-the-art of infiltration processes in LSMs. They concluded that the main challenges are in the appropriate treatment of the small-scale heterogeneity to describe the large-scale fluxes of infiltration and surface runoff and the need for an improved description of wetting front dynamics, which may lead to improved simulations of infiltration and surface runoff during heavy rainfall. More recently, Mueller et al. (2016) examined the potential of the LSMs SWAP, JULES, and CH-TESSEL to produce surface runoff for intense rainfall events. Based on the results, they recommend that future work should consider a correction of the maximum infiltration rate in JULES and investigate its numerical scheme to make it suitable for high vertical resolution. Recently, Morbidelli et al. (2018) reviewed the role of slope on infiltration. They pointed out the need to further develop upscaling approaches up to catchment and subgrid scales

and to establish a theoretical framework to describe infiltration on hillslopes to better explain experimental observations that have become available in recent years.

In this review, we briefly recapitulate the main approaches and solutions derived from soil physical theory to describe infiltration processes at the point and field scales and the techniques used to numerically solve the infiltration processes and finally to quantify the impact of spatial variability on infiltration. Here, we focus on infiltration processes in non-frozen soils. We present the infiltration approaches used in various LSMs and address how maximum infiltration capacity is quantified, how soil moisture and spatial variability of soil properties are parameterized, and how the areal saturation fraction, F_{sat}, important for Hortonian runoff, is estimated. We also identify key soil parameters that affect the soil infiltration and runoff and present upscaling approaches for soil hydraulic parameters applicable to the grid scale of LSMs. Finally, we will present an outlook and future perspectives on modeling infiltration in LSMs. Table 1 shows the content and organization of the review, referring to the specific sections.

Table 1. Contents.

General Introduction 1
Quantitative Expression of the Infiltration Process at the Point Scale 5
Basic Physical Models of Soil Water Flow and Infiltration 5
Empirical Infiltration Equations 6
Analytical and Semi-analytical Infiltration Description 6
Numerical Solutions of Profile Scale Infiltration Processes 8
Numerical Methods 8
Governing Flow Equations 8
Boundary Conditions 8
Vertical and Temporal Discretization 9
Upscaling Approaches toward Larger Scales 10
Upscaling Spatially Heterogenous Parameters Relevant for Infiltration 10
Topography-based Aggregation 12
Homogenization 12
Similarity Scaling 12
Bayesian Upscaling 12
Machine Learning Based Upscaling 13
Multiscale Parameter Regionalization 13
Other Parameter Scaling Approaches 13
Upscaling Infiltration Processes 13
Similarity Scaling 14
Stochastic Upscaling 15
Infiltration Processes in Land Surface Models 16
Grid-Scale Infiltration Processes 16
The Maximum Infiltration Rate in Land Surface Models 19
Spatial Heterogeneity in Soil Water Content Using Probability Densities 22
Representing Spatial Heterogeneity of Surface Properties that Control Infiltration in a Single Parameter 23
Estimating the Areal Saturation Fraction 24
Characterizing the Surface Saturated Hydraulic Conductivity 24
Spatial Distribution of the Saturated Hydraulic Conductivity 24
Estimators for the Saturated Hydraulic Conductivity 25
Use of Soil Maps to Estimate the Saturated Hydraulic Conductivity 25
Saturated Hydraulic Conductivity and Infiltration in Organic Soils 25
Numerical Treatment of Infiltration in Land Surface Models 26
Sensitivity of Infiltration–Runoff Process to Model Parameters 27
Improving the Infiltration Process in Land Surface Models 28
Soil Structure 29
Hysteresis in the Soil Water Retention Curve and Thermal Effects on Hydraulic Properties 29
Soil Water Repellency 30
Compaction, Swelling, and Shrinkage 30
Freeze and Thaw 31
Impermeable Soil Layers 31
Instability of Different Flow Regimes 32
Solution of Numerical Issues 32
Summary and Conclusion 33
Appendix A1 37
Appendix A2 37
Appendix A3 39
Appendix A4 42

Quantitative Expression of the Infiltration Process at Point Scale

Basic Physical Models of Soil Water Flow and Infiltration

In the chronological development of the conceptual modeling of infiltration in porous media, there have been three main approaches.

Darcy (1856) formulated the first quantitative description of flow through a saturated porous medium, known as Darcy's law:

$$J = -K_s \frac{\partial H}{\partial z} \quad [1]$$

where J is the Darcian flux of water [L T^{-1}] at time t [T], K_s is a proportionality constant characterizing the medium and named the *saturated hydraulic conductivity* [L T^{-1}], and $\partial H/\partial z$ (dimensionless) is the hydraulic gradient calculated from the differences in total hydraulic head (H) and the (vertical) distance z [L] within the saturated porous medium (in saturated soils, the total head H is the sum of pressure [h] and elevation heads [z]).

Buckingham (1907) proposed to extend Darcy's law to unsaturated water flow, where the actual water content in the porous medium, θ, is lower than its maximum value at saturation, θ_s. The main assumption is that the constant saturated hydraulic conductivity value, K_s, could be replaced by a function of soil water content, θ, or matrix potential, h, as the characteristic of the unsaturated porous medium. That function was named the *unsaturated hydraulic conductivity function* and given the symbol $K(\theta)$ or $K(h)$. Following the notation of Eq. [1], the resulting unsaturated flow equation resulting from Buckingham's assumptions is

$$J = -K(h)\frac{\partial H}{\partial z} = -K(h)\left(\frac{\partial h}{\partial z} + 1\right) \quad [2]$$

where z [L] is the vertical coordinate being positive upward, and $z = 0$ represents a prescribed reference level. In this case, the total head H is the sum of the matrix potential in head units, h, and the gravitational head z.

Finally, Richards (1931) combined the flow equation of Buckingham (1907) (Eq. [2]) and the principle of continuity assuming an infinitely mobile air phase in the soil (zero resistance to air flow). The resulting well-known and widely used one-dimensional expression for vertical water flow is

$$\frac{\partial \theta}{\partial t} = \frac{\partial}{\partial z}\left[K(h)\left(\frac{\partial h}{\partial z} + 1\right)\right] \quad [3]$$

Equation [3] requires the definition of an additional characteristic of the porous medium, which is the soil water retention curve, where the actual water content is a function of the matrix potential, $\theta(h)$.

The $\theta(h)$ and $K(h)$ functions represent the hydraulic properties of the porous medium. An up-to-date presentation of the mathematical expressions (e.g., Brooks and Corey, 1964; van Genuchten, 1980) used to quantify these properties in soils can be found in the review of Assouline and Or (2013).

The Brooks and Corey (1964) retention function is given by

$$S_e(h)=\left(\frac{h}{h_c}\right)^{-\lambda_p};\ h<h_c \qquad [4]$$

$$S_e(h)=1;\qquad h\geq h_c$$

where h_c is the matric potential at air-entry value [L^{-1}], λ_p is a dimensionless pore size distribution index, h is the pressure head [L], and S_e is the effective saturation (dimensionless). given by

$$S_e=\frac{\theta-\theta_r}{\phi-\theta_r} \qquad [5]$$

where S_e is the effective saturation (dimensionless), θ is the actual water content [$L^3\ L^{-3}$], θ_r is the residual water content [$L^3\ L^{-3}$], and ϕ is the porosity [$L^3\ L^{-3}$], which can be related to θ_s as the saturated water content.

The corresponding unsaturated hydraulic conductivity function is

$$K=K_s S_e^{3+2/\lambda_p} \qquad [6]$$

where K_s is the saturated hydraulic conductivity [$L\ T^{-1}$].

The water retention function proposed by van Genuchten (1980) is

$$\theta(h)=\theta_r+\frac{\theta_s-\theta_r}{\left(1+\left|h/h_c\right|^{n_{vG}}\right)^m} \qquad [7]$$

where m is a shape factor (dimensionless) often assumed to be related to n_{vG} by $m = 1 - 1/n_{vG}$. This function is continuous in h and presents an inflection point, making it more appropriate for application in numerical solutions.

Applying the model of Mualem (1976) to Eq. [7] leads to the following unsaturated hydraulic conductivity function:

$$K(h)=K_s S_e^l\left[1-\left(1-S_e^{1/m}\right)^m\right]^2 \qquad [8]$$

where l is a fitting parameter dependent on the soil type (dimensionless).

The Richards equation (Eq. [3]) represents the actual physical model that can be used to simulate and illustrate the infiltration process in porous media. It addresses only the macroscale behavior and is valid for a representative volume for which the prescribed hydraulic properties can be applied. The solution of the Richards equation requires the definition of initial and boundary conditions. When water is ponding at the soil surface, infiltration is governed by the hydraulic head at the soil surface, a concentration type boundary condition (BC) known also as a Dirichlet BC. When the water application rate is below the soil infiltration capacity, a flux or Neumann BC can be applied at the soil surface. Because Eq. [3] is highly nonlinear due to the nonlinear character of the hydraulic conductivity function [$K(h)$ or $K(\theta)$], analytical solutions can be derived only for specific initial and boundary conditions and with knowledge of the soil hydraulic properties. Consequently, solutions to practical soil water flow problems generally require the use of numerical schemes designed to solve partial differential equations.

Empirical Infiltration Equations

The necessity to describe quantitatively such a crucial hydrological process as infiltration combined with the complexity of the solution of the flow equation (Eq. [3]) led to the development of empirical expressions relating the infiltration rate, q, to time, t. From Fig. 1 it can be seen that, for a constant water supply, $r(t)$, the infiltration rate $q(t)$ gradually decreases and tends toward a steady final infiltration rate, q_f. Consequently, the different forms of the suggested empirical equations describing infiltration are all monotonically decreasing functions based on exponential or power law decays, for which the parameters do not generally have a physical meaning and are evaluated by fitting to experimental data.

In general, there are two main families of equations used to describe the infiltration process—one is based on the original formulation of Horton (1941) and the other on those presented by Kostiakov (1932). Over time, both equations have been modified and extended by various researchers such as the Kostiakov model by Lewis (1937), Mezencev (1948), Smith (1972), Parhi et al. (2007), and Furman et al. (2006) to account for different initial and boundary conditions. The original formulation proposed by Horton (1941) predicts an exponential decay of the infiltration flux q over time t as

$$q(t)=q_f+(q_i-q_f)\exp(-\alpha_K t) \qquad [9]$$

where q is the infiltration rate [$L\ T^{-1}$], q_f is the final (constant) infiltration rate [$L\ T^{-1}$], q_i is the initial infiltration rate [$L\ T^{-1}$], and α_K is the decay constant [T^{-1}]. For $t \rightarrow \infty$, q_f can be related to the hydraulic conductivity of the wetted soil layer.

On the other hand, Kostiakov (1932) introduced a power law equation with two fitting parameters, n_K and β_K, in the form

$$q(t)=q_f+n_K\beta_K t^{(\beta_K-1)} \qquad [10]$$

where n_K and β_K depend on the initial and boundary conditions of the soil system.

Analytical and Semi-analytical Infiltration Description

Compared with the empirical models, analytical and semi-analytical equations based on the Richards equation were also developed; Philip (1957) and Philip (1969) presented the first analytical solution to the Richards equation. It considers infiltration as a sorption process with a perturbation generated by the presence of gravity. Therefore, this method corresponds by definition to the first stages of infiltration into a relatively dry soil profile where gravity plays only a minor role. It can therefore be expected to be applicable for small and intermediate values of time (Brutsaert, 2005; Hillel, 1998). Because the original solution, in the form of a power series, diverges for large values of time, Philip (1957) proposed to use a truncated version of the original solution, considering the first two terms of the series:

$$q(t)=\frac{1}{2}S_{op}t^{-1/2}+A \qquad [11]$$

where S_{op} is defined as the soil sorptivity [L T^{-2}], t is time [T], and A is a fitting parameter (dimensionless). Note that Eq. [11] is equivalent to Eq. [10] for $\beta_K = 1/2$, $n_K = S_{op}$, and $q_f = A$. For long infiltration times (during ponded infiltration), the term A approaches the value of K_s. Philip (1969) and Talsma and Parlange (1972) have shown that even for long infiltration times (of practical interest), the inequality $\frac{1}{3}K_s \leq A \leq \frac{2}{3}K_s$ holds. The spatial vertical water content distribution in the soil profile following infiltration and wetting is quite complex and can be illustrated by Fig. 3. Experimental results from Davidson et al. (1963) and Rubin and Steinhardt (1964) have shown the sigmoid-like nature of the distribution of $\theta(z)$ (here, the data of Davidson et al. [1963] are depicted in Fig. 4).

Green and Ampt (1911) presented an approach that is based on fundamental physics but makes strong assumptions about the soil hydraulic properties and the shape of $\theta(z)$. Their key assumption is the presence of a sharp infiltration front moving downward with time instead of the sigmoid distribution of water content with depth representing a more realistic wetting front, as shown in Fig. 3 and 4. The presented infiltration function integrated macroscale physical entities such as pressure head differences with depth, soil porosity, and saturated hydraulic conductivity over the wetter soil layer. The Green–Ampt model, for the case of ponding infiltration with a negligible ponded water depth at the surface, is represented by an implicit expression for the infiltration rate, $q(t)$, which needs to be solved iteratively for the cumulative infiltration $Q(t)$:

$$q(t) = K_s\left[\frac{h_f(\theta_s - \theta_i)}{Q(t)} + 1\right] \qquad [12]$$

where $Q(t)$ is the cumulative infiltration [L] at time t [T], h_f is the capillary head at the wetting front [L], K_s is the soil saturated hydraulic conductivity [L T^{-1}], and θ_i is the initial water content of the soil profile. The matrix head h_f is related to soil hydraulic properties (Bouwer, 1964; Neuman, 1976).

Generalized and exact solutions for $Q(t)$ were developed by Parlange et al. (1982, 1985), Haverkamp et al. (1990), Swartzendruber (1987), Ross et al. (1996), and Barry et al. (1995, 2005). Selker and Assouline (2017) presented a simple explicit solution for the position of the wetting front in time based on approximating the term describing early infiltration behavior by means of the sum of gravitational flow and the exact solution for capillary imbibition:

$$q(t) = K_s\frac{A_f K_s + \sqrt{n_f K_s h_f / 2t}}{1 + A_f\left(K_s t / n_f h_f\right) + \sqrt{\left(2/n_f h_f\right)K_s t}} \qquad [13]$$

where A_f is a fitting parameter that can be approximated by ($^2/_3$). For infiltration into a completely dry soil profile, $n_f = \theta_s - \theta_r$, whereas for a profile with known initial water content θ_i, $n_f = \theta_s - \theta_i$.

The result of Eq. [13] is within 1% of the exact implicit solution of vertical Green and Ampt infiltration (Eq. [12]). Hence, the proposed approximation adds essentially no error to the Green and Ampt approach but greatly simplifies the computation of infiltration by allowing an explicit expression that is, in theory, easy to implement in LSMs.

For near-constant rainfall rates, $q(Q)$ is independent of the applied rate r (Skaggs, 1982; Smith et al., 2002), and infiltration capacity at any given time depends only on the cumulative infiltration volume, regardless of the previous rainfall history. The

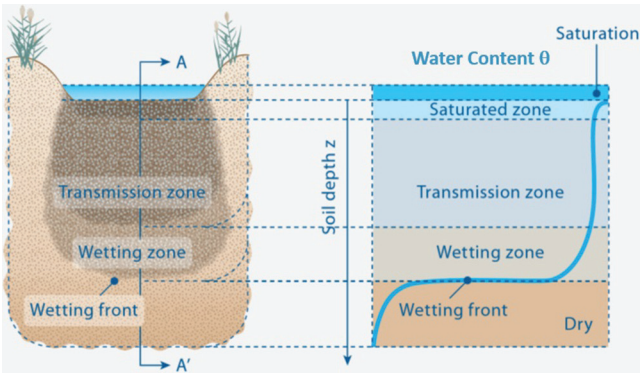

Fig. 3. Illustration of the two-dimensional spatial distribution of soil moisture content within a wetted soil profile during infiltration (left) and its corresponding soil moisture profile (right). A–A′ is the vertical transect depicted on the right-hand side of the left panel. (From Or et al. class notes with permission.)

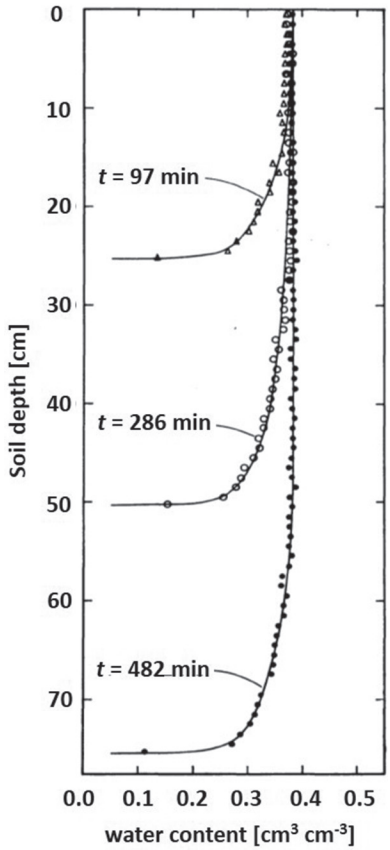

Fig. 4. Infiltration into Hesperia sandy loam soil (initially air dry) showing the soil water content with depth and the propagation of the wetting front with time during infiltration. (Reprinted with permission from Davidson et al., 1963.)

time invariance of $q(Q)$ holds true also when a layered profile or a sealed soil surface is considered (Mualem and Assouline, 1996; Smith 1990). This is an important characteristic of the infiltration process and the basis of the so-called time compression analysis for predicting the timing of ponding and runoff (Assouline et al., 2007; Brutsaert, 2005).

Numerical Solutions of Profile-Scale Infiltration Processes

While the empirical, analytical, and semi-analytical models discussed above provide descriptions of the infiltration process for relatively simple conditions (e.g., a homogeneous soil profile, constant initial saturation with depth, constant ponding at the soil surface), the quantitative analysis of real-world infiltration problems (e.g., a layered soil profile, variable initial saturation, time-variable rainfall, limited ponding) can be obtained only using numerical solutions of the water flow equation [i.e., Richards' equation (Eq. [3])]. The reason lies in the fact that the highly nonlinear eliptic parabolic Richards equation cannot be solved analytically, apart from for a very limited number of cases.

Since the 1960s soil water balance models have been developed that quantify and predict infiltration in soil by numerically solving the Richards equation for different BCs and resulted in a wide range of software tools such as HYDRUS (Šimůnek et al., 2008), COUP (Jansson, 2012), DAISY (Hansen et al., 2012), and SWAP (van Dam et al., 2008), among many others. By using such models based on the Richards equation along with sufficient vertical and temporal discretization, the infiltration rate and occurrence of ponding should be a direct outcome of the numerical solution in the spatiotemporal domain and do not have to be calculated "externally" using any of the introduced empirical or (semi-)analytical models above. Various simulations have been performed using HYDRUS-1D to demonstrate water infiltration into a one-dimensional soil profile under natural BCs (Šimůnek and van Genuchten, 2008; Šimůnek et al., 2008, 2016). The HYDRUS-1D model was selected for this purpose because it is one of the most widely used and verified codes for unsaturated flow and solute transport modeling (Scanlon, 2004), and the full set of simulations can be found at https://www.pc-progress.com/Downloads/Public_Lib_H1D/Using_HYDRUS-1D_to_Simulate_Infiltration.pdf.

Depending on the intensity of precipitation, discretization in both space and time need to be adapted to the rainfall flux, whereby most current models rely on a predefined vertical discretization and only the time discretization will be changed by an adaptive time stepping routine. In general, the typical size of the vertical discretization is often smaller than 1 cm close to the soil surface to adequately solve the Richards equation for rainfall events with high intensities. In some models, the upper BC can be automatically switched from a flux BC to a fixed pressure head (Dirichlet) BC during evaporation conditions to avoid the development of extreme pressure head gradients close to the soil surface. This approach stabilizes the numerical solution of the Richards equation. Additionally, the appropriate choice of temporal resolution of precipitation data is extremely important to capture the generation of excess water (Hortonian excess). Finally, using daily accumulated rainfall fluxes will lead to an underestimation of the generated excess water compared with the use of highly resolved rainfall data (Mertens et al., 2002).

Numerical Methods

Most early applications of numerical methods for solving variably saturated flow problems usually used the classical finite differences method (e.g., Bresler, 1973; Bresler and Hanks, 1969; Hanks et al., 1969; Rubin and Steinhardt, 1964). Integrated finite difference, finite volumes, and especially finite element methods became increasingly popular in the '70s and after (e.g., Huyakorn et al., 1986; Neuman, 1973; Paniconi and Putti, 1994; Šimůnek et al., 2008), accompanying the fast development of computers with increasing computational speed and memory. While finite difference methods are still used today in the majority of one-dimensional models, finite volume methods and/or finite element methods coupled with mass lumping of the mass balance term are usually used in two- and three-dimensional models (e.g., Healy, 2008; Pruess, 1991; Šimůnek et al., 2008). An overview of these developments with respect to infiltration prediction was given in the review of Assouline (2013).

Furthermore, a number of LSMs use semi-implicit numerical solutions to Richards' one-dimensional partial differential equation such as in Best et al. (2011), OLAM-SOIL (Walko and Avissar, 2008), ORCHIDEE (de Rosnay et al., 2002), and ISBA-SURFEX (Boone et al., 2000; Decharme et al., 2011). Conventional methods for solving this highly nonlinear equation inevitably lead to numerical and accuracy challenges that impact their hydrological performance.

Governing Flow Equations

In general, the Richards equation can be formulated, and thus solved numerically, in three different ways: water content (θ) based (often also denoted as the diffusivity form), pressure head (h) based, and in terms of a mixed formulation, when both θ and h appear simultaneously in the governing equation as shown in Eq. [3]. The most popularly used vadose zone flow models currently utilize the mixed formulation of the Richards equation and solve this equation using the mass-conservative method proposed by Celia et al. (1990).

Boundary Conditions

Infiltration rates for a point source infiltration process can be obtained by numerically solving the Richards equation for an appropriate upper (soil surface) BC. In general, two types of BCs can be used to simulate the infiltration process, i.e., the Dirichlet or Neumann BC. The Dirichlet (pressure head based) BC fixes the pressure head, h, at the soil surface ($z = 0$) to a value h_0 [L], which can be either constant or variable with time:

$$h(z,t) = h_0(t) \quad \text{at } z = 0 \qquad [14]$$

The value for h_0 can be either negative (e.g., for tension disk infiltration), zero, or positive (ponded infiltration). The majority of empirical, analytical, and semi-analytical models discussed above represent conditions with zero (or slightly positive) pressure head at the soil surface. The Neumann (flux-based) BC fixes the water flux (infiltration), q, at the soil surface to a required water flux, q_0 [L T^{-1}], which can again be either constant or variable with time:

$$-K\left(\frac{\partial h}{\partial z}+1\right)=q_0(t) \quad [15]$$

where q_0 is negative for infiltration and positive for evaporation when the z axis is defined positive upward if z is defined negative with depth. If water is allowed to build up on the soil surface after the onset of soil surface ponding, a "surface reservoir" BC may be applied (Mis, 1982; Šimůnek et al., 2008; van Dam et al., 2008):

$$-K\left(\frac{\partial h}{\partial z}+1\right)=q_0(t)-\frac{\mathrm{d}h}{\mathrm{d}t} \quad [16]$$

The flux q_0 in Eq. [16] is the net infiltration rate, i.e., the difference between precipitation and evaporation. Based on Eq. [16], the height $h(0,t)$ of the surface water layer (ponding height) increases due to precipitation and reduces because of infiltration and evaporation of the ponding layer.

Kollet and Maxwell (2006) closed the problem of variably saturated groundwater flow, infiltration, and surface water flow by applying flux and pressure continuity conditions at the top boundary, leading to a free-surface overland flow BC:

$$-K\left(\frac{\partial h}{\partial z}+1\right)=\frac{\partial \|h,0\|}{\partial t}-\nabla\mathbf{v}\|h,0\|+q_0(t) \quad [17]$$

where $\mathbf{v}$ is the depth-averaged velocity vector [L T^{-1}], which can be expressed in terms of Manning's equation (e.g., in Chow et al., 1988) to establish a flow depth–discharge relationship.

The Dirichlet (Eq. [14]) and Neuman (Eq. [15]) BCs are system-independent BCs for which prescribed quantities (i.e., pressure heads or water fluxes) do not depend on the conditions of the soil profile, its saturation status, or its infiltration capacity. These BCs thus may not properly describe real-world conditions in which infiltration or actual soil evaporation rates depend on the conditions of the soil profile and its saturation status, which may limit infiltration or evaporation. In many applications, neither the flux across nor the pressure head at a boundary is known a priori but follows from interactions between the vadose zone and its surroundings (e.g., the atmosphere). External meteorological conditions thus control only the potential water flux across the soil surface, while the actual flux also depends on the prevailing (transient) soil moisture conditions near the surface. This occurs, for example, when the precipitation rate exceeds the infiltration capacity of the soil, resulting in the accumulation of excess water on top of the soil surface and surface runoff, depending on soil properties and on topographic conditions (for two- and three-dimensional representation). Subsequently, the infiltration rate is no longer controlled by the precipitation rate but instead by the soil infiltration capacity.

Such conditions may be best described using system-dependent BCs, which take soil moisture conditions and the hydraulic conductivity of the soil near the soil surface into consideration. For example, in HYDRUS-1D, such a system-dependent BC is called an "atmospheric" BC. For these conditions, the soil surface BC may change from a prescribed flux to a prescribed head type condition (and vice versa). The numerical solution of Eq. [3] is then obtained by limiting the absolute value of the surface flux by the following two conditions (Neuman et al., 1974):

$$\left|-K\frac{\partial h}{\partial z}-K\right| \le i_\mathrm{p} \quad [18]$$

and

$$h_\mathrm{A} \le h \le h_\mathrm{S} \quad [19]$$

where i_p is the maximum potential rate of infiltration or evaporation under the current atmospheric conditions [L T^{-1}], and h_A and h_S are, respectively, minimum (i.e., for evaporation) and maximum (i.e., for infiltration) pressure heads at the soil surface allowed under the prevailing soil conditions [L]. When one of the endpoints of Eq. [19] is reached, a prescribed head BC will be used to calculate the actual surface infiltration or evaporation flux.

The value for h_A is determined from the equilibrium conditions between soil water and atmospheric water vapor (e.g., Feddes et al., 1974). The value of h_S is usually set equal to zero, which represents conditions when any excess water on the soil surface is immediately removed via runoff once ponding is reached. In this case, the Neumann BC (Eq. [15]) is switched internally in the model to the Dirichlet BC (Eq. [14]) with $h = 0$ once ponding is reached and then back to the Neumann BC once rainfall stops (during redistribution) and the pressure head decreases below zero. When h_S is allowed to be positive, it then represents a layer of water, which can form on top of the soil surface during heavy rains before the initiation of runoff. In such a case, the Neumann BC (Eq. [15]) needs to be switched to the Dirichlet BC (Eq. [14]) similarly as above, but the surface pressure head value h is calculated using the surface reservoir BC. Once rainfall stops, infiltration (calculated for a Dirichlet BC) continues until all water from the accumulated water layer has infiltrated, when the BC is switched back to the Neumann BC.

Vertical and Temporal Discretization

The numerical solution of the highly nonlinear Richards equation requires relatively fine spatial (on the order of centimeters) (Vogel and Ippisch, 2008) and temporal (on the order of minutes) discretization. Optimal spatial and temporal discretization depends strongly on the intensity of precipitation–evaporation–infiltration and the nonlinearity of the soil hydraulic properties, as well as on numerical stability criteria, involving hydraulic or thermal diffusivity (see, e.g., Best et al., 2005). Simulations with high flux rates and strong nonlinearity of soil hydraulic properties

require finer discretization in both space and time. Most current vadose zone, including land surface, models rely on a predefined vertical discretization, which is constant in time, while only the time discretization changes during simulations by an adaptive time stepping routine.

Spatial discretization should be made relatively small at locations where large hydraulic gradients are expected. Such a region is usually located close to the soil surface, where highly variable meteorological factors can cause rapid changes in soil water contents and corresponding pressure heads. Hence, it is generally recommended to use relatively thin soil layers (small discretization) near the soil surface and then to gradually increase their thickness with depth to reflect much slower changes in pressure heads at deeper depths.

Upscaling Approaches toward Larger Scales

Infiltration considered at larger scales is heavily affected by the heterogeneity of the soils and the land surface. Assouline and Mualem (2002, 2006) explicitly demonstrated the impact of heterogeneity, introduced by a combined effect of impervious areas and spatial variability in soil properties, on infiltration. Figure 5 shows the results in terms of the infiltration rate [$q(t)$] curves for a homogeneous and a heterogeneous field exposed to a constant rainfall rate.

Accounting for field spatial variability leads to shorter ponding times and to a more gradual decrease in the infiltration flux with time (Smith and Hebbert, 1979). Consequently, surface runoff will appear earlier in heterogeneous fields than in homogeneous ones. This results from the fact that part of the heterogeneous field has much lower hydraulic conductivity than that of the homogeneous one, and this generates the early runoff. As LSMs typically incorporate infiltration at grid sizes from meters to hundreds of kilometers, scaling approaches are necessary to account for subgrid heterogeneity at the model resolution. Also, parameters relevant for infiltration, as well as experiments for

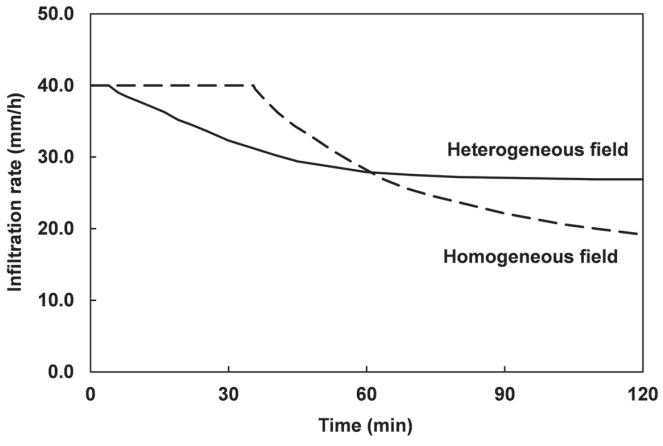

Fig. 5. Mean infiltration in a heterogeneous (solid line) vs. a homogeneous (dashed line) field.

direct infiltration measurements, are typically observed and performed at the point scale (see above). Therefore, scaling approaches are needed to translate the measurements to adequately address infiltration characteristics at larger scales. Two general strategies are discussed in the following: (i) the scaling of infiltration-related properties and (ii) the scaling of infiltration fluxes themselves. We have chosen this categorization rather than a scale-based categorization because several of the methods proposed below, such as, e.g., similarity scaling, aggregation, and Bayesian upscaling, can be applied at a range of scales. Figure 6 shows the different upscaling approaches to obtain effective parameters at the scale of LSMs. We distinguish four different categories: (i) the LSM upscaling approaches that either assign uniform soil properties to a dominant soil class or use probability density functions (pdfs) of parameters that reflect subgrid variability, (ii) parameter upscaling methods, (iii) similarity upscaling methods, and (iv) stochastic upscaling methods. The last three approaches have been mainly developed for upscaling from the field to catchment scale, while the first involves downscaling the parameters from grid to point scale before upscaling the resulting infiltration from point to grid scale. Within the LSM upscaling approaches, three main methods can be distinguished: (i) uniform upscaling assuming the soil hydraulic parameters are constant, (ii) empirical upscaling that use pdfs to define F_{sat} and the maximum infiltration rate, I_{max}, that are then further used to calculate grid-scale infiltration, and (iii) physical upscaling in which infiltration is calculated at the point scale and pdfs are used to upscale it to the grid scale.

Upscaling Spatially Heterogenous Parameters Relevant for Infiltration

Land surface models need input parameters at the grid scale, i.e., estimates of effective parameters to quantify hydrological and energy balance fluxes and to generate soil infiltration-related properties such as water storage at the grid cell level (see above). To adequately represent nonlinear relationships between model parameters and states and fluxes, it is generally agreed that spatial scaling ideally should take place after the model has been run. However, this is also a matter of computational resources, which are limited and generally do not afford simulations at the support scale, which is the area or volume over which a measurement is made or a state variable defined. Land surface models driven for global or continental applications typically require upscaling of information that is available at higher resolution to scales of a few to tens of kilometers. Here, a simplification of the landscape heterogeneity by dominant class selection (e.g., USDA soil classes) or simple parameter averaging typically does not account for nonlinear relationships of subgrid processes and may introduce important biases on specific LSM variables, including infiltration and runoff (Boone and Wetzel, 1999).

Another method proposed by Noilhan and Lacarrère (1995) consists in computing grid-scale land surface parameters according to observed soil textures (sand and clay) aggregated from the high resolution and using a continuous relationship derived from the

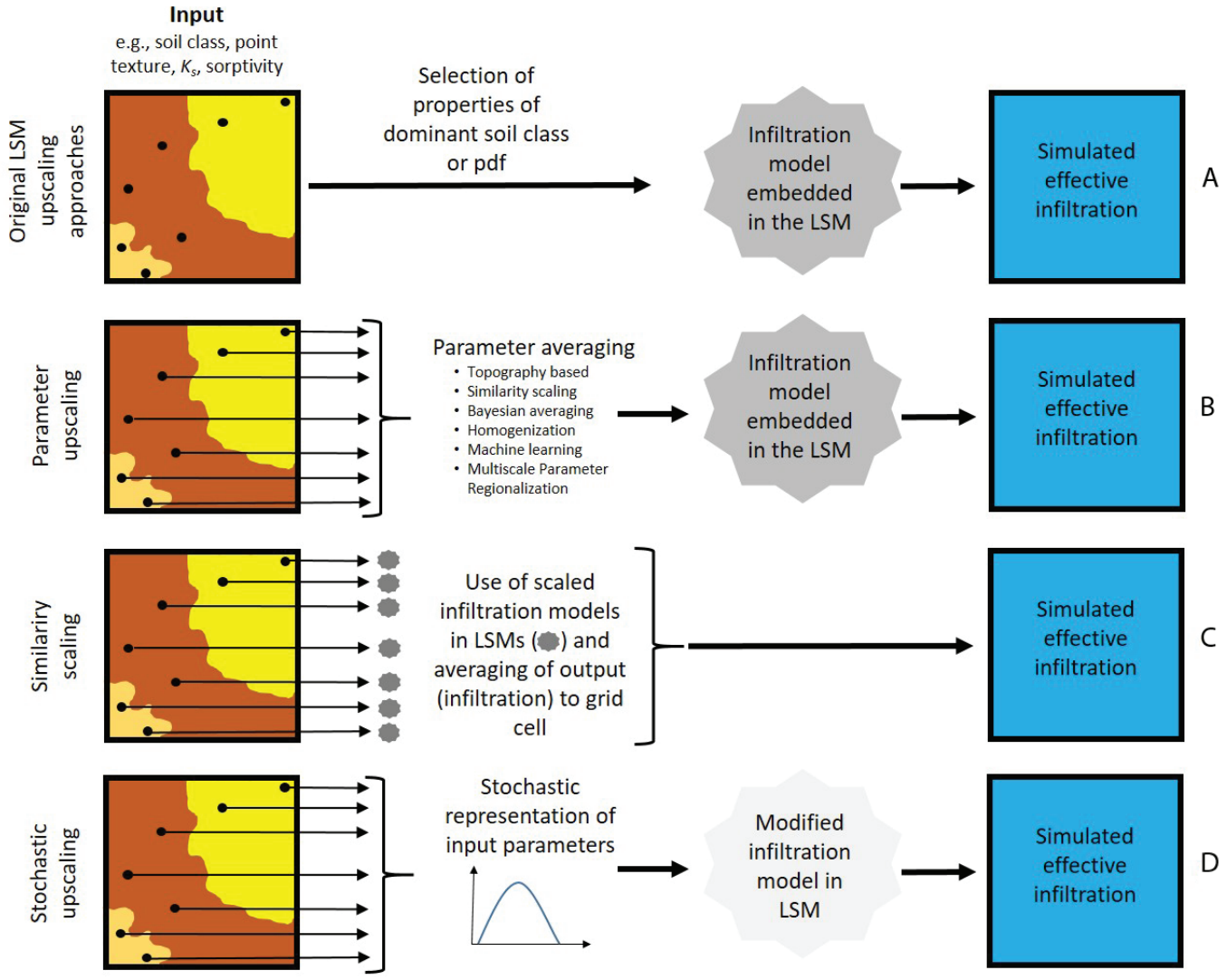

Fig. 6. Schematic overview of different upscaling methods of soil parameters (original land surface model [LSM] upscaling approach, parameter upscaling, similarity scaling, and stochastic upscaling) described in Infiltration Processes in Land Surface Models (A), Upscaling Spatially Heterogeneous Parameters Relevant for Infiltration (B), Similarity Scaling (C), and Stochastic Upscaling (D). Differences in the infiltration model used are indicated by different colors.

textural classification of Clapp and Hornberger (1978) or Cosby et al. (1984). The scaled effective parameters are often dependent on the spatiotemporal patterns of the unsaturated system at the smaller scale and are not simply a function of the average parameter values obtained from measurements.

General focus has been placed on upscaling soil hydraulic parameters because significant spatial variability of these properties was reported earlier by Nielsen et al. (1973), Warrick and Nielsen (1980), Peck (1983), and Logsdon and Jaynes (1996). In most of these cases, the field saturated hydraulic conductivity, K_s, was lognormally distributed (Reynolds and Eldrick, 1985; Russo et al., 1997; White and Sully, 1992). However, steady-state infiltration fluxes and soil surface water content are distributed either normally or lognormally (Cosh et al., 2004; Kutilek et al., 1993; Loague and Gander, 1990; Sisson and Wierenga, 1981; Vieira et al., 1981). Several studies have dealt with modeling the effect of the spatial variability of soil hydraulic properties on infiltration (Assouline and Mualem, 2002; Dagan and Bresler, 1983; Govindaraju et al., 2006; Milly and Eagleson, 1988; Sivapalan and Wood, 1986; Smith and Hebbert, 1979; Warrick and Nielsen, 1980; Woolhiser et al., 1996).

While heterogeneity in soil hydrology properties, parameters, and boundary conditions is ubiquitous, understanding of the sensitivity to different aggregation or upscaling methods is limited. Zhu and Mohanty (2002a, 2002b, 2003, 2004, 2006), Zhu et al. (2006, 2004), and Mohanty and Zhu (2007) investigated, in a series of studies, the suitability of various soil hydraulic parameter upscaling schemes by matching their prediction performances with ensemble vadose zone fluxes (infiltration and evaporation) under different hydroclimatic scenarios for horizontally and vertically heterogeneous soil systems. Their synthetic experimental results showed that soil texture, geological layering, groundwater depth,

surface and profile soil moisture status, vertical flux direction (infiltration vs. evaporation), hydraulic parameter statistics (correlations and spatial structures), root distribution in the soil profile, and topographic features and arrangements conjointly determine the "upscaled" pixel-scale soil hydraulic parameters for the equivalent homogeneous medium that delivers the same amount of flux (infiltration or evaporation) as the natural heterogeneous medium. Thus, different homogenization algorithms (rules) for different hydrologic scenarios and land attribute complexities were suggested for parameter upscaling. Several approaches have been proposed in the literature to upscale soil hydraulic properties from the point to larger scales to obtain effective properties (Vereecken et al., 2007), which are discussed in the following.

Topography-Based Aggregation

Expanding the power average operator of Yager (2001), Jana and Mohanty (2012a, 2012b, 2012c) coarsened the soil hydraulic parameters to the model grid scale in an attempt to study remote-sensing-based soil moisture distribution at the watershed scale (Little Washita). Two types of aggregating methods were combined in this topography-based aggregation technique. By combining the features of both mode-like and mean-type aggregating methods, the power average technique provided an ideal tool in scaling of soil hydraulic parameters for soil pedons. Power averaging operating across a number of spatial nodes uses a support function based on linear distances in different Cartesian coordinates, allowing data clustered around a particular value to combine nonlinearly while being aggregated. Generally, soil pedons clustered around a location tend to have similar properties; that correlation decreases as the distance between two points increases. In other words, the aggregating method considers the mutual support the pedons extend to each other when clustered.

Homogenization

Homogenization by spatially averaging the soil hydraulic parameters is a simple way of upscaling. Numerical studies such as those presented by Zhu and Mohanty (2002b) and Mohanty and Zhu (2007) and observational studies such as those of Jana and Mohanty (2012b) examined the impact of the areal heterogeneity of soil hydraulic parameters at the model grid scale on the ensemble response of hydrologic fluxes. In particular, arithmetic, geometric, and harmonic averages of the soil hydraulic parameters were tested with different parameter correlation structures. Findings of these studies suggested that different averaging schemes should be used for different soil hydraulic conductivity parameters and functional forms.

Similarity Scaling

Another method for scaling is based on the theoretical framework of geometric similarity for porous media introduced by Miller and Miller (1956). The basic idea is that porous media that are geometrically similar in their microscopic arrangement of particles differ only in terms of their characteristic length scale λ_{SC}. The underlying assumption is that the hydraulic behavior of a porous medium can be transformed into the behavior of a reference medium by scaling (Nielsen et al., 1998). This scaling factor, α_{SC}, is defined as the ratio between the characteristic length λ_{SC} of a geometrically similar soil and the characteristic length of the reference soil λ_r:

$$\alpha_{SC} = \frac{\lambda_{SC}}{\lambda_r} \quad [20]$$

This approach can also be used for spatial scaling of soil hydraulic properties (Mohanty, 1999; Shouse and Mohanty, 1998). Zhu and Mohanty (2006) used Miller–Miller scaling in combination with a one-dimensional infiltration equation based on the Haverkamp et al. (1990) model to derive effective hydraulic parameters at the grid scale of LSMs and global climate models (GCMs). The heterogeneity of soil hydraulic parameters was considered in the horizontal dimension, and the infiltration process was described using the concept of parallel stream tubes without lateral interaction. They found that the variability in Miller–Miller scaling factors had a stronger influence on the effective grid cell infiltration than the saturated water content and the ponding depth, which reflects microtopography. This approach was also implemented by Montzka et al. (2017) to generate an optimized soil hydraulic properties database at a coarse global grid resolution of 0.25° from the soil texture information system SoilGrids1km of Hengl et al. (2014). Further information about similarity and Miller–Miller scaling in terms of scaling infiltration processes is given below.

Bayesian Upscaling

Considered as a calibration method at the remote sensing footprint scale, the Markov chain Monte Carlo based upscaling algorithm introduced by Das et al. (2008) provides an alternative to derive the upscaled effective soil hydraulic parameters from a time series of soil moisture observations and stochastic information of the fine-scale soil hydraulic parameter variability. The Bayesian framework produces probability distributions of the effective (pixel-scale) soil hydraulic parameters, where preexisting knowledge about the local-scale soil parameters (e.g., from the Soil Survey Geographic [SSURGO] database) can be combined with dynamic hydrologic observations and model outputs.

Kim and Mohanty (2017) proposed a more general approach by accounting for the effects of mixed (weighted) physical controls (covariates) as well as the interactions between the controls on the soil moisture distribution and subsurface flow including lateral flow between grid cells. They used a Bayesian averaging scheme for effectively estimating the contributing ratios (weights) for the physical controls and their interactions. This scheme provides proper weights that show how the controls contribute to describing the spatial variability of soil moisture and thus effective soil hydraulic properties. This approach underpins the concept of hydrologic connectivity based on the probability of connected local pathways of surface and subsurface flow, by which emergent

catchment-scale behavior is depicted. The physical control based connectivity index approach can be easily adopted in land surface hydrologic and biogeochemical models, leading to an Earth System modeling framework, where geophysical attributes such as geology, ecotones, and topography are (or will be) the primary drivers for water, carbon, and energy cycles.

Machine Learning Based Upscaling

Pedotransfer functions (PTFs) have been used as inexpensive alternatives for estimating soil infiltration and hydraulic properties using soil textural and bulk density information at the local scale. Expanding the concept of the PTF to estimate landscape-scale soil hydraulic properties, Sharma et al. (2006) developed artificial neural networks based pedo-topo-vegetation transfer functions with good success by adding topographic and vegetation characteristics to soil textural and bulk density information. Advancing the idea within a Bayesian framework, Jana et al. (2008) and Jana and Mohanty (2011) developed multiscale Bayesian neural network (BNN) based PTFs. Using a BNN, they upscaled or downscaled soil hydraulic parameters using soil texture and structure data at one scale to simulate the key soil moisture contents related to soil water retention at another. In that study, training inputs to the BNN consisted of the percentage of sand, silt, and clay, the bulk density of the soil, and digital elevation map and vegetation data, while the targets were the soil water content at 0 (saturation), 33 (field capacity), and 1500 (wilting point) kPa. Using Markov chain Monte Carlo techniques, the BNN provides a distribution of the output parameter instead of a single deterministic value. Recently, Montzka et al. (2017) used PTFs to derive the effective spatial distribution of scaling factors and the mean soil hydraulic properties that can be used in LSMs to quantify the effect of spatial variability on infiltration fluxes.

Multiscale Parameter Regionalization

The multiscale parameter regionalization method proposed by Samaniego et al. (2010) is a two-step approach with initial regionalization and subsequent upscaling. The regionalization establishes a priori relationships between model parameters and distributed basin predictors at the fine scale, leading to linear or nonlinear transfer functions. These functions are used as global parameters to reduce overparameterization and ease transferability. Soil texture and land cover can be used as predictors for infiltration (Samaniego et al., 2010). The upscaling toward coarser scales is performed by a selection or combination of upscaling operators such as arithmetic mean, maximum difference, geometric mean, harmonic mean, and majority. With this approach, the subgrid variability is used for facilitating transferability toward ungauged and uncalibrated regions for improved model parameterization. Samaniego et al. (2017) analyzed the applicability of the multiscale parameter regionalization approach for several LSMs.

Other Parameter Scaling Approaches

Other parameter scaling methods are fractal approaches (e.g., Tyler and Wheatcraft, 1990) and the scaleway approach (e.g., Vogel and Roth, 1998). Although they have been used over small watersheds, they have strong limitations (Meng et al., 2006). Stochastic upscaling or aggregation methods statistically allow better accounting for landscape heterogeneity conditions. Stochastic upscaling makes use of geostatistical descriptors of spatial variables and quantify a probability distribution for each state variable at larger scales by stochastic perturbation rather than a deterministic quantity (see below).

Govindaraju et al. (2006) suggested a semi-analytical model to compute the space-averaged infiltration at the hillslope scale when spatial variability in both soil properties and rainfall intensity are accounted for. The soil spatial heterogeneity was characterized by a lognormal distribution of the saturated hydraulic conductivity, while the rainfall spatial heterogeneity was simulated by a uniform distribution between two extreme rainfall intensities (low and high). At each location, the soil K_s and the rainfall intensity was assumed to remain constant during the rainfall event. The main finding was that ponding time decreases with the increase in the coefficient of variation of K_s (see also Fig. 5).

Other researchers also developed and evaluated methods that are potentially applicable for transferring infiltration parameterizations across scales. Hailegeorgis et al. (2015) evaluated four regionalization methods for continuous streamflow simulation. Their regional calibration method uses the maximum weighted average of a performance measure such as the Nash–Sutcliffe efficiency to identify specific parameter sets per subpixel by the DREAM algorithm (Vrugt et al., 2009). Another method uses the regional median of each parameter for regionalization, where a limitation is that the correlation structure between parameters is lost. Scaling by the nearest neighbor approach includes the assumption that spatial proximity in terms of Euclidian distance explains parameter similarity. The physical similarity approach assumes that similarity of regions in physical attributes such as land use, cumulative distribution functions of terrain slopes, and/or soil types can explain their response in the hydrological variable.

The potential of most of these upscaling methods has not yet been tested in currently used LSMs. As highly resolved soil information becomes available that allows parameterization of subgrid variability, several of these methods may prove to be valuable in estimating effective soil properties controlling infiltration processes at the pixel scale of LSMs. First results using, e.g., the multiscale parameterization method and similarity approach show great potential in parameterizing key hydraulic properties at the grid scale of a LSM.

Upscaling Infiltration Processes

To upscale infiltration processes themselves rather than providing a method for the averaging of infiltration-related parameters as discussed above, besides scaling the Richards equation for infiltration (Sadeghi et al., 2012; Warrick and Hussen, 1993), the Miller–Miller similarity can be applied. The stochastic upscaling of infiltration is based on the frequency distribution

of infiltration-related parameters and allows the computation of effective infiltration fluxes using semi-analytical approximations.

Similarity Scaling

Besides providing a method for the averaging of infiltration-related parameters as presented above, similarity scaling can also be applied to reduce the number of parameters in the analytical or semi-analytical infiltration equations, which in turn also reduces the data requirement. Within the similarity scaling approach for infiltration, the infiltration data consists of a set of scaling factors, one for each location or grid cell, and an average infiltration function. In the following, mainly two examples of similarity scaling for infiltration are presented. The first example, Sharma et al. (1980), is based on the similarity scaling of cumulative infiltration Q [L], which is estimated over time t (Philip and de Vries, 1957):

$$Q(t) = S_{\mathrm{op},i} t^{1/2} + \mathrm{AC}_i t \qquad [21]$$

where $S_{\mathrm{op},i}$ and AC_i are the parameters fitted to each of the ith infiltration measurements within a region. Sharma et al. (1980) used two alternative approaches to realize the scaling of cumulative infiltration: either (i) by determination of two separate scaling factors for the sorptivity and steady-state infiltration, or (ii) by determination of a single optimized scaling factor. For the first approach, the two scaling factors $\alpha_{S\mathrm{op}}$ and α_{AC} (dimensionless), for sorptivity S_{op} [L T$^{-0.5}$] and steady-state infiltration AC [L T^{-1}], respectively, were calculated according to

$$\alpha_{S_{\mathrm{op},i}} = \left(\frac{S_{\mathrm{op},i}}{\langle S_{\mathrm{op}} \rangle} \right)^2 \qquad [22]$$

and

$$\alpha_{\mathrm{AC},i} = \left(\frac{\mathrm{AC}_i}{\langle \mathrm{AC} \rangle} \right)^{1/2} \qquad [23]$$

where $\langle S_{\mathrm{op}} \rangle$ and $\langle \mathrm{AC} \rangle$ represent the respective mean values of those fitted infiltration parameters. The scaling of the infiltration data was subsequently performed by

$$Q^* = \alpha Q \qquad [24]$$

and

$$t^* = \alpha^3 t \qquad [25]$$

where Q^* and t^* identify the scaled cumulative infiltration [L] and time [T], respectively, and the scaling factor α is either $\alpha_{S\mathrm{op}}$ or α_{AC}. At this point, both scaling factors α_{opt} and α_{AC} can be used to scale the cumulative infiltration data. However, both attempts, using either α_{opt} or α_{AC}, fail to arrange the scaled infiltration data near the reference cumulative infiltration curve $\langle Q \rangle$ defined by $\langle S_{\mathrm{op}} \rangle$ and $\langle \mathrm{AC} \rangle$. For the second scaling approach, a single scaling factor α_{opt} was derived by least-squares fitting (using Eq. [24] and [25]). The sum of squares, SS, between scaled cumulative infiltration and reference cumulative infiltration, given by

$$\mathrm{SS} = \sum_{t_i^*} \left(Q^*_{t_i^*} - \langle Q \rangle_{t_i} \right)^2 \qquad [26]$$

was minimized by adjusting α_{opt} based on the cumulative infiltration measurements available at each time step t_i for each of the multiple measurements. Finally, with this second scaling approach, all the measurements reasonably coalesced about the reference cumulative infiltration curve.

By using Eq. [26], Sharma et al. (1980) departed from the geometric similarity proposed by Miller and Miller (1956), which would require that $\alpha_{S\mathrm{op}}$ and α_{AC} are identical. A scaling methodology following the second approach (Eq. [26]) is empirical in nature and usually referred to as functional normalization (Tillotson and Nielsen, 1984). Nonetheless, it is still relevant because it provides a mathematical framework for the handling of Philips' infiltration in terms of spatial variability. Equations [24–26] can be used to account for the variability in infiltration when only the variance of the scaling factors and the mean infiltration curve are known. Furthermore, this approach provides an opportunity to lump both infiltration parameters AC_i and $S_{\mathrm{op},i}$ into a single scaling parameter $\alpha_{\mathrm{SC},i}$ for each soil. Yet, to the best of our knowledge, such an approach has not been implemented in any land surface or hydrological model. However, for the spatial scales of LSMs, it remains unclear how appropriate scaling parameters could be derived and implemented in practice.

The frequency distribution of α_{opt} determined by Sharma et al. (1980) had a mean of about 1, as expected, and a standard deviation of 0.58. The spatial distribution of α_{opt} did not show a distinct pattern, which was explained by Loague and Gander (1990) later on, as they determined a spatial autocorrelation length of <20 m for infiltration in the catchment under consideration. This, in turn, would support a purely stochastic approach to the variability of infiltration. However, this conclusion is based on the assumption of the occurrence of vertical fluxes only.

Hopmans (1989) simplified the scaling of Philips' infiltration suggested by Sharma et al. (1980) by substituting Eq. [22] and [23] into Eq. [21]. Accordingly, the scaled instantaneous infiltration q^* [L T^{-1}] yields

$$q^*(t) = \alpha_{\mathrm{SC}}^{1/2} \langle S_{\mathrm{op}} \rangle t^{-1/2} + \alpha_{\mathrm{SC}}^2 \langle \mathrm{AC} \rangle \qquad [27]$$

where q^* is the scaled infiltration rate [L T^{-1}], and $\langle S_{\mathrm{op}} \rangle$ [L T$^{-0.5}$] and $\langle \mathrm{AC} \rangle$ [L T^{-1}] represent the parameters of the reference infiltration curve, now determined by nonlinear regression to all infiltration measurements available. Hopmans (1989) also performed functional normalization according to Tillotson and Nielsen (1984) with the modified empirical three-parameter infiltration equation of Kostiakov (see Eq. [10]). Both scaling approaches were successful and Hopmans (1989) stressed that the attractiveness of this lies in the potential to lump the spatial variability of infiltration into a single parameter, which, for example, allows correlation with other environmental variables. Furthermore, it potentially removes any intercorrelations between the infiltration parameters.

Haverkamp et al. (1998) provided inspectional analyses of Miller–Miller similarity scaling for infiltration according to the theories provided by Green and Ampt (1911), Philip (1957), and

Talsma and Parlange (1972). However, the analyses presented by Haverkamp et al. (1998) remain at a theoretical level and were not tested in any practical application.

Stochastic Upscaling

A stochastic approach to upscale infiltration can be implemented via Monte Carlo simulations for any type of infiltration equation and any given distribution of relevant parameters. This has been demonstrated, e.g., by Smith and Hebbert (1979) and Sharma and Seely (1979). A sufficient number of random samples needs to be drawn from a given distribution of infiltration parameters and, after computation of every Monte Carlo model realization, the average and/or standard deviation of predicted infiltration can be obtained. However, due to the assumption that the infiltration process is ergodic, large sample sizes are usually required, resulting in a rather large computational demand, which in reality prohibits any practical application in large-scale studies involving hydrological models or LSMs. Notwithstanding, many semi-analytical solutions to infiltration problems are still validated against Monte Carlo results (e.g., Corradini et al., 2002; Craig et al., 2010; Govindaraju et al., 2001).

Starting with the infiltration theory according to Philip (1957), while making some considerable approximations, Sivapalan and Wood (1986) provided semi-analytical solutions to calculate average infiltration across a grid box for two cases. For the first case, a spatially constant rainfall rate and a lognormal distribution of saturated hydraulic conductivity K_s were assumed. In the second case, a spatially variable rainfall rate and spatially uniform distribution of K_s were considered. In both cases, run-on was not accounted for and the soil profiles were assumed to be vertically homogeneous. The approximations derived by Sivapalan and Wood (1986) were tested against Monte Carlo simulations, but an in-depth analysis of the uncertainties was not presented. Moreover, due to the mathematical complexity of the approximations, practical application was not feasible.

Smith and Goodrich (2000) simulated the ensemble behavior of infiltration according to Parlange et al. (1982) by making use of Latin hypercube sampling. They assumed that the lognormal probability density functions of K_s and the capillary parameter G were divided into n equal sub-areas, and infiltration was computed using the average of each sub-area. The areal average infiltration was then given as the equally weighted sum of all subdivisions. This method does not involve any analytical solution and has the advantage of a significantly reduced computational demand compared with the Monte Carlo technique. Govindaraju et al. (2001) assumed spatial autocorrelation of lognormally distributed saturated hydraulic conductivity and provided semi-analytical solutions to the Green–Ampt equation based on series expansion. As a follow-up, the semi-analytical solutions of Govindaraju et al. (2001) were combined by Corradini et al. (2002) with a kinematic wave expression to account for run-on effects.

Craig et al. (2010) provided approximations for the estimation of the average infiltration rate $\langle q \rangle$ [L T^{-1}] according to the Green–Ampt approach as a function of the precipitation rate J_w [L T^{-1}] and mean saturated hydraulic conductivity, $\langle K_s \rangle$, and standard deviation, σ_{Ks}, of a standard lognormal distribution, $f_k(K_s)$, of K_s. They estimated a dimensionless error term ε for J_w, K_s, and X, where X represents a dimensionless time parameter computed from time t, J_w, and α_{wf}, which is defined as the product of the absolute value of the wetting front suction head and the difference between saturated water content and initial water content at the beginning of the infiltration event. Finally, the averaged infiltration rate, q, is approximated by

$$q = \frac{J_w}{2}\operatorname{erfc}\left[\frac{\ln(J_w X) - K_s}{\sigma_{ks}\sqrt{2}}\right] + \frac{1}{2X}\exp\left(K_s + \frac{\sigma_{ks}^2}{2}\right)\operatorname{erfc}\left[\frac{\sigma_{ks}}{\sqrt{2}} - \frac{\ln(J_w X) - K_s}{\sigma_{ks}\sqrt{2}}\right] + J_w \int_0^{X(t)} \varepsilon\left(X(t),\, k_s\right) f_k(k_s)\, \mathrm{d}k_s \quad [28]$$

According to Craig et al. (2010), a comparison between the semi-analytical upscaling approach given in Eq. [28] with Monte Carlo simulations revealed errors of <3%, which appears to be acceptable for any practical purpose. They also provided approximations of infiltration for a given normal distribution of aggregate parameter α_{wf}. From Monte Carlo simulations, they concluded that the heterogeneity in K_s is of much greater relevance than the heterogeneity in α_{wf}.

Craig et al. (2010) upscaled the Green–Ampt equation to a basin or (LSM) grid cell. Thereby, the upscaled Green–Ampt equation is based on the information of the distributions of K_s and/or the initial soil water deficit of the basin or grid cell. Additionally, preferential flow, which is defined as the uneven and rapid movement of water through the soil, characterized by regions of enhanced flux, e.g., wormholes, root holes, and cracks, can also be incorporated by considering a bimodal distribution of K_s as

$$q = \int_0^\infty \int_0^\infty \left[X(t, \alpha_{GA}), K_s\right] f_{k\alpha_{GA}}(K_s, \alpha_{GA})\, \mathrm{d}\alpha_{GA}\, \mathrm{d}K_s \quad [29]$$

with

$$X = \frac{1}{1 + 1/(J_w/\alpha_{GA})t} \quad [30]$$

with $\alpha_{GA} = |h_f|(\theta_s - \theta_i)$, where h_f is the pressure head at the wetting front [L], θ_s is the saturated water content, and θ_i is the water content at the wetting front [L^3 L^{-3}]. The ponding time can be calculated as

$$t_p = \frac{\alpha_{GA} K_s}{J_w (J_w - K_s)} \quad [31]$$

This approach also allows calculating of the saturated land surface fraction in a basin or LSM grid cell. To our knowledge, none of the proposed methods related to stochastic upscaling have been tested or used in full LSMs or hydrological models.

Finally, Choi et al. (2007) developed a three-dimensional volume-averaged soil moisture transport model based on the Richards

equation to account for local-scale variation of topographic attributes such as elevation, slope, and curvature on subsurface soil moisture fluxes and thus also the infiltration flux. In this approach, the coordinate system $x_i \in \{x, y, z\}$ is replaced by $x_i^* \in \{x, y, z^*\}$, where z^* follows the terrain elevation, defined as

$$z^* = Z_g - z \quad [32]$$

where Z_g is the ground surface elevation [L]. The local terrain surface slopes, S_{xl}^*, are defined as

$$S_{xl}^* = \left(\frac{\partial Z_g}{\partial x} \frac{\partial Z_g}{\partial y} - 1 \right) \quad [33]$$

Second-order Taylor expansion of the hydraulic conductivity and diffusivity with respect to soil moisture were formulated and substituted in a diffusion, pressure-based Richards equation, and the soil water content and terrain slope at any point were approximated by a first-order perturbation approach. Scale-dependent functions are used to characterize subgrid variability, incorporating statistical properties that relate the dependence of soil moisture variability to terrain attributes. The covariance between soil water content and terrain slopes is defined as

$$\left\langle \theta' S_{xl}' \right\rangle = \rho \sigma_\theta \sigma_{S_{xl}} \quad [34]$$

where ρ is the correlation coefficient between the terrain slope and the soil water content. The correlation coefficient was expressed by Choi et al. (2007) as

$$\rho = \gamma_1 + \gamma_2 \left(\frac{\langle \theta \rangle}{\theta_s} \right) + \gamma_3 \left(\frac{\langle \theta \rangle}{\theta_s} \right)^2 \quad [35]$$

where γ_1, γ_2, and γ_3 are fitting parameters estimated from observations. Note that other approaches are available to estimate the variance of the soil water content (e.g., Choi et al., 2007; Qu et al., 2015; Vereecken et al., 2007).

Choi et al. (2007) combined this modeling approach with a one-dimensional diffusion wave model for surface overland flow, called it the conjunctive surface–subsurface flow model (CSSF), and proposed it for use in mesoscale climate simulations. The CSSF was tested through implementation in the common land model (CLM) (Oleson et al., 2008) using a set of offline simulations for catchment-scale basins around the Ohio Valley region. They showed that CSSF simulated a strong contribution of the effects of surface or overland flow depths of water on infiltration estimates that led to increased baseflow generation. In addition, a better representation of the surface–subsurface flow processes improved the representation of soil moisture spatial variability and may improve the partitioning of energy at the land surface.

Infiltration Processes in Land Surface Models

In the following, we provide an overview of how widely used LSMs represent infiltration processes at the global scale. Therefore, we selected 12 LSMs, namely: (i) OLAM-SOIL (Walko et al., 2000), (ii) ParFlow-CLM (Kollet and Maxwell, 2006, 2008a), (iii) ORCHIDEE rev4783 (d'Orgeval et al., 2008; Ducharne et al., 2017), (iv) Catchment Land Surface Model (CLSM) (De Lannoy et al., 2014; Ducharne et al., 2000; Koster et al., 2000), (v) ISBA-SURFEX (Boone et al., 2000; Decharme et al., 2011, 2016; Decharme and Douville, 2006), (vi) Noah-MP version 3.0 (Niu et al., 2011; Schaake et al., 1996), (vii) JULES version 4.6 (Best et al., 2011; Clark et al., 2011), (viii) CLM4.5 (Oleson et al., 2013), (ix) CABLE (Decker, 2015; Kowalczyk et al., 2013, 2006; Wang et al., 2011), (x) SSiB (Li et al., 2010; Sun and Xue, 2001; Xue et al., 1991, 1996; Zhan et al., 2003), (xi) CH-TESSEL (Balsamo et al., 2009; Entekhabi and Eagleson, 1989), and (xii) JSBACH version 3.0 (Hagemann and Stacke, 2015; Roeckner et al., 2003). All models are listed in Table 2 and the labeling is used throughout the appendix for consistency.

First, we review how these LSMs address the challenge of treating infiltration processes in a large grid cell and associated runoff generation. Second, we review how infiltration processes are treated numerically in different LSMs, considering approaches ranging from empirical to analytical equations or direct solution of the Richards equation with appropriate numerical schemes, boundary conditions, and vertical discretization. These approaches have been introduced above.

Grid-Scale Infiltration Processes

Here we focus on parameterization of infiltration and runoff generation processes and their definition at the grid scale. These include the maximum infiltration rate, the characterization of the soil water content distribution at the grid cell level, the characterization of grid cell heterogeneity with respect to infiltration controls, and the saturated surface fraction. Although most LSMs use a Richards type formulation to describe the soil water flow at the grid scale, it is used primarily to redistribute soil water vertically in the profile rather than for calculation of infiltration rates at each time step. This is justified by the computationally demanding solution of the pressure head at the land surface required for obtaining accurate and stable solutions of the Richards equation. This calculation is particularly demanding during high-intensity rainfall events, where accurate solutions require very small spatial and temporal discretization (see above) leading to very high computational demand. Various parametric approaches have been devised in LSMs to handle the process of infiltration efficiently within the constraints of data availability (e.g., spatially available K_s values) to avoid such a computational burden. However, the implementation of a Richards based solution for infiltration allows (i) direct calculation of excess water flux (e.g., rainfall) that cannot infiltrate, (ii) a physically based determination of the time to ponding, and (iii) direct accounting for the effect of variable soil properties on infiltration at the grid cell (when such information is available). Table 2 gives an overview of 12 different LSMs and their numerical treatment of infiltration processes. Four of the 12 LSMs derive infiltration rates directly from solving the Richards equation in its mixed form (ISBA-SURFEX, OLAM-SOIL, CLSM, and ParFlow-CLM) and thus appear below

Table 2. Overview of land surface models (LSMs) and their numerical treatment of the infiltration process.

No.	LSM	Key references†	Model time stepping	Vertical resolution of the first compartment	Temporal resolution of precipitation input	Form of Richards' equation used for 1D water movement	Infiltration rate from solution of Richards' equation	Is ponding allowed based on pressure head?	Impact of lower boundary (LB) on infiltration	Approaches to point-scale infiltration	Approaches to grid-scale infiltration
1	OLAM-SOIL	1	<1 d (~1 min–6 h)	2–5 cm	minutes	diffusivity form	yes	yes	LB of soil model is impermeable but >100 m deep; water table governed by Richards' equation	Richards' equation is coupled with surface water (ponding) upper boundary condition; infiltration occurs when infiltration capacity will be exceeded	uniform upscaling of infiltration
2	ParFlow-CLM	2, 3	variable	10 layers for first 3 m, additional 5 layers for next 100 m‡	variable	mixed form	yes	yes	Richards' equation is solved globally (saturated and variably saturated conditions); different types of BCs can be used (Dirichlet, Neumann, gravity drainage)	runoff occurs if precipitation exceeds K_s	uniform upscaling of infiltration
3	ORCHIDEE rev4783	4, 5	<1 d (30 min)	1-mm top layer, 11 layers total	30 min	diffusivity form	no	no	by controlling the soil moisture profile and therefore infiltration capacity	runoff occurs if precipitation exceeds K_s	exponential pdf on K_s
4	Catchment land surface model (CLSM)	6, 7, 8	<1 d (typically set to <1 h)	1 cm for Richards' equation in off-line simulations, 2–5 cm for catchment-scale simulations	hourly	mixed form	yes§	no	water table depth influences the soil moisture profile and therefore infiltration rates	runoff occurs if water table depth is above surface or precipitation exceeds infiltration capacity	Richards' equation combined with TOPMODEL formulations to derive parameters for catchment-scale vertical moisture transfer
5	ISBA-SURFEX	9, 10, 11, 12	<1 d (down to 5 min)	0.01 m (by default, but user can modify this)	max. 3 h but can be smaller depending on available data	mixed form	yes¶	no	default is free drainage (hydraulic conductivity in lowest model layer) except when ISBA is coupled to a groundwater model in which capillary rise can occur from groundwater	runoff occurs if precipitation exceeds K_s (Horton) or soil is saturated (Dunne)	F_{sat} based on reflected power pdf on soil moisture capacity (Dümenil and Todini, 1992) or TOPMODEL approach
6	Noah-MP version 3.0	13, 14	<1 d	four layers: 0.1, 0.3, 0.6, and 1.0 m	offline mode 30 min–1 h; in coupled mode down to seconds	diffusivity form	no	no	no impact due to free drainage LB	runoff occurs if precipitation exceeds K_s (Horton) or soil is saturated (Dunne)	exponential pdf on precipitation, and TOPMODEL approach for F_{sat}
7	JULES version 4.6	15, 16	<1 d (typically 1 h but set by user)	flexible, set by user; standard top layer = 10 cm	flexible but never >1 d; usually 1–6 h	diffusivity form	no	no	when TOPMODEL approach is used, there is an additional deep water store below the soil column, in which saturated conductivity is assumed to reduce exponentially with depth	runoff occurs if precipitation exceeds $I_{max} = \beta K_s$ (Horton) or soil is saturated (Dunne)	TOPMODEL approach for F_{sat}

continued on next page

Table 2. continued.

No.	LSM	Key references†	Model time stepping	Vertical resolution of the first compartment	Temporal resolution of precipitation input	Form of Richards' equation used for 1D water movement	Infiltration rate from solution of Richards' equation	Is ponding allowed based on pressure head?	Impact of lower boundary (LB) on infiltration	Approaches to point-scale infiltration	Approaches to grid-scale infiltration
8	CLM4.5	17	<1 d (30 min)	increasing layer thickness with depth, upper layer = 1.75 cm	3–6 h	(form is not provided)	no	yes	no impact of LB	runoff occurs if precipitation exceeds K_s (Horton) or soil is saturated (Dunne)	TOPMODEL approach for F_{sat}
9	CABLE	18, 19, 20, 21	fixed, depending on forcing data or coupling model time step	increasing layer thickness with depth; first layer 2.2 cm; soil thickness 4.6 m	depending on forcing data or coupling model time step	diffusivity form	no	no	infiltration depends on vertically averaged relative saturation over the grid cell, which includes the lowest soil layer.	air space in first three soil layers is filled from the top with infiltration water at the beginning of time step	gamma pdf on soil moisture
10	SSiB	22, 23, 24, 25, 26	<1 d	increasing layer thickness with depth, upper layer = 1.75 cm	30 min or hourly	diffusivity form	no	no	by interaction of baseflow and the overlying soil layers	runoff occurs if precipitation exceeds K_s	exponential pdf on precipitation
11	CH-TESSEL	27, 28	1 h or less	increasing layer thickness with depth, upper layer = 7 cm	flexible but never longer than 6 h offline; typically 3-hourly or hourly offline and ≤atmospheric time step when coupled	diffusivity form	no	no	no impact of LB	runoff occurs if soil moisture exceeds capacity	F_{sat} based on reflected power pdf on soil moisture capacity (Dümenil and Todini, 1992)
12	JSBACH version 3.0	29, 30	<1 d (hourly)	6.5 cm	hourly, daily	diffusivity form	no	no	no impact of LB	runoff occurs if soil moisture exceeds capacity	F_{sat} based on reflected power pdf on soil moisture capacity (Dümenil and Todini, 1992)

† 1, Walko et al. (2000); 2, Kollet and Maxwell (2006); 3, Kollet and Maxwell (2008a); 4, d'Orgeval et al. (2008); 5, Ducharne et al. (2017); 6, Koster et al. (2000); 7, Ducharne et al. (2000); 8, De Lannoy et al. (2014); 9, Boone et al. (2000); 10, Decharme and Douville (2006); 11, Decharme et al. (2011); 12, Decharme et al. (2016); 13, Niu et al. (2011); 14, Schaake et al. (1996); 15, Best et al. (2011); 16, Clark et al. (2011); 17, Oleson et al. (2013); 18, Kowalczyk et al. (2006); 19, Kowalczyk et al. (2013); 20, Wang et al. (2011); 21, Decker (2015); 22, Xue et al. (1991); 23, Xue et al. (1996); 24, Zhan et al. (2003); 25, Sun and Xue (2001); 26, Li et al. (2010); 27, Balsamo et al. (2009); 28, Entekhabi and Eagleson (1989); 29, Roeckner et al. (2003); 30, Hagemann and Stacke (2015).

‡ ParFlow-CLM vertical discretization is in general flexible and can be set by the user, the given example is used as the standard setting in TerrSysMP.

§ Parameters for catchment-scale vertical moisture transfer between surface and root zone, and root zone and catchment deficit, are derived from detailed Richards' equation simulations conducted off-line combined with TOPMODEL formulations.

¶ Calculation of infiltration rate from solution of Richards' equation is done only for small time steps. For large time steps and intense rain events, a Green–Ampt-based approach can permit infiltrated water to attain several layers during a time step.

only when dealing with specific issues of grid-scale parameterization of infiltration and runoff generation. Here it has to be noted that most reviewed LSMs (except OLAM-SOIL and Parflow-CLM) are designed to be used globally, with a typical grid cell size of 0.5° or more. These models first define uniform soil parameters at the grid cell scale (Table 3), used to calculate either infiltration or Hortonian and Dunne runoff at the point scale. In the latter case, grid-scale infiltration is defined as the incoming water that does not run off.

The Maximum Infiltration Rate in Land Surface Models

In LSMs, the maximum infiltration rate is used to partition the water flux reaching the land surface into infiltrable flux and excess water that generates surface runoff. We focus on infiltration of vegetated or bare land surfaces and exclude glaciers, lakes, and urban areas. An interesting example was provided by Entekhabi and Eagleson (1989), who used a Darcy-based approach to estimate the maximum infiltration rate or infiltrability for a heterogeneous grid cell in a LSM. They defined surface runoff, q_s, as the sum of Hortonian infiltration excess ($P_x - f^*$ for $P_x > f^*$ and $s < 1$, i.e., the first term on the right-hand side in Eq. [36]) and Dunne saturation excess (the second term on the right-hand side of Eq. [36]), where saturation excess is equal to P_x when $s \geq 1$:

$$q_s = \frac{1}{\kappa}\left[\int_0^1\int_{f^*}^{\infty}\left(P_x - f^*\right) f_{P_x}\left(P_x\right)\mathrm{d}P_x f_s\left(s\right)\mathrm{d}s + \int_1^{\infty}\int_0^{\infty}\left(P_x\right) f_{P_x}\left(P_x\right)\mathrm{d}P_x f_s\left(s\right)\mathrm{d}s\right] \quad [36]$$

Table 3. Overview of approaches used for the spatial distribution of saturated hydraulic conductivity, Ks, in the land surface models (LSMs).

LSM	Pedotransfer function to estimate for grid-scale K_s	Underlying soil maps to provide coverage of K_s	Use of soil structural information	K_s constant in grid cell	Variation of K_s with depth
OLAM-SOIL	Weynants et al. (2009) or de Boer (2016)	SoilGrids (Hengl et al., 2014)	yes	yes	yes
ParFlow-CLM	Schaap and Leij (1998) for first 10 soil layers; Gleeson et al. (2011) for deeper layers	FAO (1988) and Gleeson et al. (2011)	no	yes	yes
ORCHIDEE rev4783	lookup tables for van Genuchten soil parameters for each USDA class	Zobler (1986) at 1° is default soil texture map; other soil maps can be used: Reynolds et al. (2000) at 1/12° or SoilGrids1km (Hengl et al., 2014)	no	no†	yes
Catchment Land Surface Model (CLSM)	Campbell (1974) or Wösten et al. (2001)	Harmonized World Soil Database version 1.21 (FAO, 2009) and the State Soil Geographic (STATSGO2) database (De Lannoy et al. 2014)	no	yes	yes
ISBA-SURFEX	from Clapp and Hornberger (1978) or Cosby et al. (1984) (optional); for organic soils (Decharme et al., 2016)	Harmonized World Soil Database (FAO, 2009) at 1-km resolution	no	yes	yes
Noah-MP version 3.0	from Clapp and Hornberger (1978)	Harmonized World Soil Database (FAO, 2009) or Milovac et al. (2014)	no	yes	no
JULES version 4.6	from Clark and Gedney (2008); for organic soils, Chadburn et al. (2015b)	default configurations of JULES uses soil ancillaries based on sand, silt, clay fractions from the Harmonized World Soil Database using the function of Cosby et al. (1984)	no	yes	yes
CLM4.5	from Clapp and Hornberger (1978) and Cosby et al. (1984); for organic soils, Lawrence and Slater (2008)	based on IGBP soil dataset for mineral soils (IGBP, 2000), with organic soil described from ISRIC-WISE (Batjes, 2006) and the Northern Circumpolar Soil Carbon Database (Hugelius et al., 2013)‡	no	yes	yes
CABLE	same as horizontal	CABLE rev 2.0 uses Zobler soil class information (Zobler, 1986, 1999); Decker (2015) uses sand, clay, silt fractions from the Harmonized World Soil Database (FAO, 2009), calculating soil properties from the textures as in CABLE rev 2.0 from Zobler (1986)	no	yes	no
SSiB	from Clapp and Hornberger (1978) and Sellers et al. (1986)	Harmonized World Soil Database v.1.1 (FAO, 2009)	no	yes	no
CH-TESSEL	based on tabulated values for 7 textural classes including organic soils (Balsamo et al., 2009)	FAO (2003) soil texture map	no	yes	yes
JSBACH version 3.0	from Beringer et al. (2001)	based on improved FAO soil type dataset (Hagemann and Stacke, 2015)	no	yes	no

† Based on exponential pdf (see Table 3 and Appendix A, A2.6).
‡ The International Geosphere–Biosphere Program soil dataset (Global Soil Data Task, 2014) of 4931 soil mapping units and their sand and clay content for each soil layer were used to create a mineral soil texture dataset (Bonan et al., 2002). Soil organic matter data are merged from two sources. The majority of the globe is from ISRIC-WISE (Batjes, 2006). The high latitudes come from the 0.25° version of the Northern Circumpolar Soil Carbon Database (Hugelius et al., 2013). Both datasets report C down to 1-m depth.

where P_x [M L^2 T^{-1}] is the flux of water incident at the soil surface, f^* is the infiltrability of the first soil layer, s is effective relative saturation, κ is a scaling factor needed to redistribute the GCM grid-scale precipitation across the scale of precipitation events, and f represents the spatial pdf of the respective variables (rainfall and relative saturation). The first term on the right-hand side refers to the amount of point precipitation intensity that exceeds the infiltration rate of the soil, f^*, and therefore represents the maximum infiltration rate at that moment in time. The second term on the right-hand side refers to the rainfall that falls on saturated surfaces and cannot infiltrate.

Based on the Buckingham–Darcy equation, they derived f^* as

$$f^* = K_s v s + K_s (1 - v) \quad [37]$$

where

$$v = \frac{\mathrm{d}h}{\mathrm{d}s}\bigg|_{s=1} \frac{1}{\Delta z}$$

and h is the matric potential [L], Δz is the thickness of the first soil layer [L], s is the effective relative saturation (θ/θ_s), and K_s is the saturated hydraulic conductivity [L T^{-1}]. For gravitational flow, v = 0 and hence $f^* \approx K_s$. It is important to state that K_s is assumed to be uniform for a grid cell.

Other, more empirically based approaches have been implemented in LSMs to quantify the maximum infiltration rate to determine the excess water for surface runoff. Land surface models differ in the way they define this maximum infiltration rate and the input parameter needed to estimate the infiltration flux. An overview of the different equations used in LSMs to estimate I_{max} is given in Table 4. Appendix A2 provides a more detailed presentation of the concepts and equations. In general, all LSMs that use I_{max} require, in one way or another, information about the actual soil water status of the land surface. In Noah-MP and CLM, this is embedded in the saturated water fraction, F_{sat} (see below). H-TESSEL and CH-TESSEL require knowledge about the actual and maximum water content of the first 50 cm of the soil profile to calculate Hortonian infiltration. ORCHIDEE, JULES, and ISBA-SURFEX require information on the soil hydraulic conductivity to estimate I_{max}. CLSM does not use the concept of a maximum infiltration rate but assumes that the amount of water that can infiltrate in a certain time at the catchment scale is a function of the model's dynamically varying spatial moisture fields.

Based on the detailed description provided in Appendix A2 on how the maximum infiltration rate is estimated in LSMs, and the information provided in Table 2 on the numerical simulation of soil water flow at the grid cell scale, we conclude that currently used LSMs parameterize infiltration processes by (i) estimating the saturated area in a grid cell to calculate Dunne saturation excess—all precipitation that falls on the saturated surface fraction of a grid cell becomes immediately available for runoff and does not infiltrate into the soil profile, (ii) calculating the unsaturated land surface area available for Hortonian infiltration excess, and (iii) using different approaches to simulate the maximum amount of

Table 4. Overview of definition of parameters and properties affecting infiltration in the different land surface models (LSMs).

LSM	Distribution of soil moisture	Distribution of precipitation	Distribution of K_s	Saturated fraction of grid cell	Description or formulation of grid-scale I_{max}	Grid cell soil moisture variability equation used	b parameter
OLAM-SOIL	no	no	no	ponding is permitted, and the hydraulic head at the bottom of the pond is the Dirichlet upper boundary condition for Richards' equation in the soil layers; infiltration is the direct solution of Richards' equation	homogeneous within grid box	NA†	NA
ParFlow-CLM	no	no	no	no	no	NA	NA
ORCHIDEE rev4783	no	no	exponential pdf	no F_{sat}, i.e., no saturation-excess runoff, but ponding can occur because of infiltration-excess runoff (see Appendix A3, A3.3)	max. infiltration rate not imposed per se in model concept; it is the outcome K_s distribution and infiltration from top to bottom via a modified Green–Ampt model (see Appendix A2, A2.3)	not described for the horizontal variability	NA
Catchment Land Surface Model (CLSM)	amended TOPMODEL approach: grid cell soil moisture variability tied to the catchment water table depth distribution; moisture distribution shifted by root zone water in excess (or deficit) of equilibrium conditions	no	no	amended TOPMODEL approach: local water table depth related to local topographic index, mean topographic index, and mean water table depth; saturated fraction under equilibrium equals the land fraction with a water table above ground surface	max. infiltration rate not imposed per se in model concept; it is a complex outcome of off-line Richards' equation simulations, TOPMODEL formulations, and the model's dynamically varying spatial moisture fields (see Appendix A2, A2.4)	amended TOPMODEL approach: grid cell soil moisture variability tied to the catchment water table depth distribution; moisture distribution shifted by root zone water in excess (or deficit) of equilibrium conditions	NA

continued on next page

Table 4. continued.

LSM	Distribution of soil moisture	Distribution of precipitation	Distribution of K_s	Saturated fraction of grid cell	Description or formulation of grid-scale I_{max}	Grid cell soil moisture variability equation used	b parameter
ISBA-SURFEX	reflected power pdf or TOPMODEL approach	no	no	two options available: 1. F_{sat} based on a TOPMODEL type approach 2. Arno scheme following Dümenil and Todini (1992)	see Appendix A, A2.5	reflected power density function	can be set to 0.2 or 0.5 depending on model application
Noah-MP version 3.0	TOPMODEL approach	exponential pdf	no	$F_{sat}=(1-F_{frz})F_{max}e^{-0.5f_d(z_{wt}-z_{bot})}+F_{frz}$	$I_{max}=P_d\frac{D_x\left(1-e^{-kdt\Delta t}\right)}{P_d+D_x\left(1-e^{-kdt\Delta t}\right)}$	NA	NA
JULES version 4.6	modified TOPMODEL approach based on local topographic index	no	no	$F_{sat}=a_s\exp^{-c_s\lambda_{crit}}$	$I_{max}=(1-F_{sat})\beta_s K_s$	modified TOPMODEL approach based on local topographic index $\lambda_{local}=\ln\left[\frac{T(z_{local})}{T(z_\nabla)}\right]+\lambda_m$	NA
CLM4.5	TOPMODEL approach	no	no		$I_{max}=(1-F_{sat})K_s C_{ice}$	homogeneous within gridbox	NA
CABLE	Gamma pdf (Entekhabi and Eagleson, 1989)	no	no	$F_{sat}=1-\mathrm{erf}\left(\sqrt{\frac{K_p}{\lambda_s}}\right)$	NA	Entekhabi and Eagleson (1989) $f_s(s)=\frac{\lambda_s^{a_c}}{\Gamma(a_c)}s^{a_c-1}e^{-\lambda_s}$	NA
SSiB	no	exponential pdf	no	$F_{sat}=\frac{1}{b_{SSiB}}\log\left(\frac{K_s\Delta t}{P_{drop}a_{SSiB}}\right)-\frac{c_{SSiB}}{a_{SSiB}}$	NA	homogeneous within gridbox	constants based on different plant functional type (Xue et al., 1996)
CH-TESSEL H-TESSEL	reflected power pdf	no	no	$F_{sat}=1-\left(1-\frac{W}{W_{sat}}\right)^{b/(b+1)}$	$I_{max}=(W_{sat}-W)+\max\left(0,W_{sat}\left\{\left(1-\frac{W}{W_{sat}}\right)^{1/(b+1)}-\left[\frac{P_T+P_M}{(b+1)W_{sat}}\right]\right\}^{b+1}\right)$	reflected power density function	$b=\max\left(\frac{\sigma_{ov}-\sigma_{min}}{\sigma_{ov}+\sigma_{max}}\right)$
JSBACH version 3.0	reflected power pdf	no	no	Arno scheme following Dümenil and Todini (1992)	for each time step, infiltration is limited to the difference between water holding capacity of the root zone and water content of the root zone at the beginning of the time step	homogeneous within gridbox	NA

† NA, not applicable.

water that can enter the soil during a certain time step, any excess being Hortonian infiltration excess.

With respect to Hortonian infiltration excess, the majority of the LSMs use an empirical parameterization of I_{max}. The vertical redistribution of the amount of infiltrated water in most LSMs is based on a diffusion form of the Richards equation. A primary consideration in using the simplified infiltration parameterization presented above is the large computational burden of solving the more accurate pressure head based Richards equation. Such a direct approach, however, has the advantage of obviating the need for defining the maximum infiltration capacity, and that the amount of Hortonian infiltration excess and Dunne saturation excess are immediate outcomes of solving the Richards equation (albeit subgrid information and runoff–run-on processes must be represented). CLSM overcomes the computational burden of the mixed form of the Richards equation by running detailed Richards equation simulations solely off-line prior to LSM runs to derive parameters of catchment-scale vertical moisture transfer using an amended TOPMODEL approach. Also, Walko et al. (2000) developed a global LSM (part of OLAM-SOIL) capable of calculating infiltration processes using a pressure head based Richards equation and highly resolved spatial information of soil properties.

Spatial Heterogeneity in Soil Water Content Using Probability Densities

Characterization of subgrid soil moisture variability in LSMs is especially important to estimate the generation of Dunne saturation excess. We focus here on the different approaches used in LSMs to quantify heterogeneity in soil water content with respect to quantifying infiltration–runoff processes at the grid scale level. These approaches are based on the underlying assumption that spatial variability in soil water content and derived properties such as soil water storage or soil water deficit can be described by pdfs without considering their spatial patterns or specific locations. Different types of pdfs have been proposed and used in LSMs such as standard reflected power distribution functions, Gamma functions, and exponential functions.

Several researchers used standard reflection power distribution functions to describe the spatial variability of soil water content and soil water content dependent variables that affect infiltration. These functions are a special case of the more general β distribution function written as

$$f(x;\alpha_G,\beta_G)=\frac{\Gamma(\alpha_g+\beta_G)}{\Gamma(\alpha_G)\Gamma(\beta_G)}x^{\alpha_G-1}(1-x)^{\beta_G-1} \qquad [38]$$
$$0\le x\le 1;\ \alpha_G,\beta_G>0$$

where $\Gamma(...)$ is the Gamma function and α_G and β_G are the parameters of the Gamma function. Moore (1985) was among the first to propose the probability-distributed model (PDM) as a concept to characterize the spatial variability of soil water content related variables at the catchment scale. He used a standard reflected power cumulative distribution function to characterize the spatial variation of the storage capacity, c, written as

$$F(c)=1-\left(1-\frac{c}{c_{max}}\right)^b \qquad 0\le c\le c_{max};b>0 \qquad [39]$$

with the corresponding density function

$$f(c)=\frac{dF(c)}{dc}=\frac{b}{c_{max}}\left(1-\frac{c}{c_{max}}\right)^{b-1} \qquad [40]$$

where c is the water storage capacity at a certain location defined as the depth of water that can be stored [L], c_{max} is the maximum water storage capacity [L], and b controls the spatial variability of the storage capacity across the basin, whereby $b = 0$ indicates a constant value of the storage capacity and $b = 1$ means a capacity that follows a uniform distribution between 0 and c_{max}. Moore (1985) did not specify how to calculate the storage capacity from basic soil properties. Based on Eq. [40], we can derive the maximum water depth S_{max} [L] across the basin as

$$S_{max}=\int_0^{c_{max}}[1-F(c)]dc=\frac{c_{max}}{b+1} \qquad [41]$$

The concept proposed by Moore (1985) has been used in many LSMs using a bucket type of soil water model to characterize the spatial variability of infiltration and storage capacity such as in VIC (Liang et al., 1994), HD (Hagemann and Gates, 2003), or Richards equation based LSMs (e.g., JULES, H-TESSEL/CH-TESSEL). Clark and Gedney (2008) compared the PDM approach of Moore (1985) and a modified TOPMODEL approach in generating surface runoff using the MOSES (now JULES) LSM by comparing model output against the observed stream flows in three catchments. TOPMODEL performed best as it allowed a better response to subsurface flow contributing to peak flows but also capturing slower changes in recession times. PDM only improved the calculation of the surface runoff without improving subsurface flow. In Appendix A1 we briefly describe the PDM scheme of Moore (1985).

Rather than using a reflected power density function, Entekhabi and Eagleson (1989) proposed a two-parameter γ pdf to characterize the spatial heterogeneity of soil water content at the level of the grid cell:

$$f_s(s;\alpha_c,\lambda_s)=\frac{\lambda_s^{\alpha_c}}{\Gamma(\alpha_c)}s^{\alpha_c-1}\exp^{-\lambda s}, \qquad \alpha_c,\lambda_s,\ s>0 \qquad [42]$$

where s is the surface layer point soil water saturation defined by

$$s=\frac{\theta}{\theta_s} \qquad [43]$$

where θ is the actual and θ_s is the saturated volumetric soil water contents [$L^3\ L^{-3}$], respectively. The two-parameter Gamma distribution, Γ, in Eq. [42] is related to s via

$$\lambda=\frac{\alpha_c}{\langle s\rangle} \qquad [44]$$

where $\langle f(s) \rangle$ is the grid mean relative saturation of the surface soil layer [$L^3\ L^{-3}$]. This concept has been implemented, for example, in the CABLE model (Decker, 2015).

For the CLSM, the basic land element is the (irregularly shaped) hydrological catchment rather than the GCM grid cell. A number of these catchments lie within a given cell, and grid-cell fluxes are computed through areal weighting of the component catchment fluxes. Within an individual catchment element, CLSM simulates a dynamic water table depth of which the distribution is related to catchment topography characteristics using the TOPMODEL formulation (Eq. [A25]) (Beven and Kirkby, 1979). Each catchment is characterized by its topographic index distribution, which in effect is used to diagnose the spatial variability of soil moisture within the catchment from the catchment element's three bulk water prognostic variables: *catchment deficit* representing the catchment air-filled pore volume assuming hydrostatic equilibrium conditions for a given water table depth distribution, and *surface layer excess* and *root zone excess* representing the water in excess (or in deficit) of the corresponding hydrostatic equilibrium conditions. The information on soil moisture variability is used to define three distinct hydrological regimes: (i) the wilting area, (ii) the subsaturated-but-transpiring area, and (iii) the saturated fraction. The definition of these three regimes is key to CSLM because different evaporation and runoff physics are applied to each.

Representing Spatial Heterogeneity of Surface Properties that Control Infiltration in a Single Parameter

Several LSMs use a single parameter in combination with pdfs to characterize the spatial heterogeneity of infiltration processes. Many of these pdfs, presented above, can be derived from Eq. [38], which was used above. to describe the spatial variability of soil water content and related variables. The estimation of this exponent (denoted as B or b) in such pdfs remains an open question because it cannot be immediately derived from available soil properties. Please note that this exponent has sometimes received a different notation in some LSMs. Liang and Xie (2001) used the b notation to describe the variability of soil and grid cell properties affecting Dunne excess saturation in the VIC model and the B parameter to describe the variability of soil and grid cell properties affecting Hortonian infiltration excess in the VIC model. Three main approaches have been reported in the literature to determine this exponent, from here on referred to as the b parameter for simplicity.

In the first approach, the b parameter is obtained by model calibration to available hydrological time series. Huang et al. (2003) present a brief discussion of the literature dealing with the estimation of the b parameter in the VIC model. They showed that the calibration approach suffers from the problem of equifinality, as so many other LSM calibration exercises do. Furthermore, they did not manage to establish meaningful relationships between model parameters and physical characteristics of the catchment or regions.

In the second approach, the b parameter is derived from available soil and/or topographic information. For example, Dümenil and Todini (1992) suggested calculating the b parameter from the subgrid standard deviation of topography by

$$b = \max\left[\frac{\sigma_h - \sigma_{min}}{\sigma_h + \sigma_{max}}; 0.01\right] \quad [45]$$

where σ_h refers to the standard deviation of the topography within a model grid cell. Balsamo et al. (2009) stated that σ_h varies between 0.01and 0.5 and σ_{min} and σ_{max} can be set to values proposed by van den Hurk and Viterbo (2003). On the other hand, Habets et al. (1999), in this case for the ISBA model, assumed the b parameter to be constant.

The third option fits a pdf to the observed cumulative distributions of soil properties as a function of the occupied space in a grid cell or basin. Sivapalan and Woods (1995) fitted the so-called Xinanjiang distribution to data of soil profile depth to estimate the b parameter in

$$F_s(z^*) = 1 - \left(1 - \frac{Z}{Z_m}\right)^b \quad [46]$$

where F_s is the cumulative distribution function of the scaled infiltration capacity (scaled by its maximum value), Z is the soil profile depth to the bedrock [L], and Z_m is its maximum value of the bedrock depth within the grid cell [L]. Here, it is assumed that the available porosity is constant in space and time. To prove their concept, Sivapalan and Woods (1995) used a regionalized cumulative soil depth distribution for six landforms observed in the Serpentine catchment and obtained the best fit with a value of b = 4.03 and Z_m = 10 m.

Huang et al. (2003) used a method based on a self-organizing neural network map combined with a *K*-means clustering method to develop transfer functions that are able to transfer b values of data-rich to data-poor areas. The data-rich area was used to fit the relation to values of soil water capacity data derived from soil map information to the surface areas of catchments by

$$w = w_{max}\left[1 - (1 - A)^{1/b}\right] \quad [47]$$

where w and w_{max} are the point and maximum point soil water capacity, A is the area for which the soil water capacity is less than or equal to w, and b is defined as a soil water capacity shape parameter. In their study, Huang et al. (2003) used the STATSGO (Digital General Soil Map of the United States) database to represent the data-rich areas. Here, it has to be noted that appropriate soil information at resolutions <1 km is presently available, whereby the global SoilGrids1km 250-m database of Hengl et al. (2014) is only one example. These new developments will allow estimating the value of the b parameter at high resolution globally, without the need for applying transfer approaches as proposed by Huang et al. (2003). Additionally, such highly resolved global map information combined with PTFs would allow the b parameter to be directly related to the soil properties to be determined, as well as the subgrid

variability depending on the size of the grid cells used in LSMs. This is discussed below.

Estimating the Areal Saturation Fraction

Estimation of the areal saturation fraction, F_{sat}, as used for example in the equations listed in Appendix A2 (Eq. [A24], [A35], [A36], [A40], [A48], [A50], [A52], [A56]), is key in determining the contribution of Dunne saturation excess runoff and Hortonian infiltration excess runoff to the overall runoff generation of a grid cell in many LSMs. Here we discuss briefly the different approaches used in various LSMs. A correct representation of F_{sat} typically requires a good knowledge about subsurface properties like the depth to bedrock, the location of the groundwater table, soil porosity, and the actual state of the soil water content in the profile. One approach that is frequently used in LSMs is based on the assumption that the saturated fraction of a grid cell can be determined from topographical characteristics and the soil moisture status of a grid cell. This approach is closely related to the concept introduced in TOPMODEL and adopted in many studies of infiltration runoff generation. It has been used in LSMs such as CLM, JULES, Noah-MP, CSLM, and ISBA-SURFEX among others. Some LSMs require only information on the soil moisture distribution such as CABLE. ORCHIDEE does not use the concept of F_{sat} but introduces the notion of a ponded fraction, which serves as the opposite of F_{sat}. Instead of increasing runoff, it enhances infiltration since it allows the latter to develop over several time steps. JSBACH uses the Arno scheme to calculate surface runoff and infiltration and uses soil water capacity to determine F_{sat}. The equations used to calculate F_{sat} are listed in Table 4, and a more extensive description of the use of F_{sat} in various LSMs, including the concepts used in TOPMODEL, are presented in Appendix A2.

Characterizing the Surface Saturated Hydraulic Conductivity

The K_s is a key soil hydraulic property that controls soil water fluxes and thus the infiltration of water in soils. However, K_s is a scale-dependent parameter that strongly depends on the support size of the measurement (Ghanbarian et al., 2015), and it exhibits anisotropic behavior (Pachepsky and Hill, 2017). Despite its importance, point-scale K_s is a parameter that is still very difficult to estimate from PTFs that are typically based on simple basic soil information such a soil texture and bulk density. However, this information only partly explains the variability observed in point-scale K_s values. In the widely used ROSETTA software (Schaap et al., 2001), which contains soil hydraulic properties and basic soil information for various soils and is used to estimate soil hydraulic properties, the logarithmically transferred point-scale K_s value is estimated with a coefficient of determination (R^2) of 53.5% when using bulk density, sand, silt, and clay percentages. Including soil moisture content at field capacity and the wilting point, the R^2 increased to 64.7%. The HYPRES database of soil hydraulic properties for European soils developed by Wösten et al. (1999), which contains information on 1136 horizons for hydraulic conductivity, provided a PTF to estimate point-scale K_s with an R^2 of 19%. This function uses silt and clay content, bulk density, organic matter percentage, and whether the soil sample used to derive the properties originated from the topsoil or subsoil. A similar R^2 value was obtained by Vereecken et al. (1990) using clay, sand, and carbon content, as well as bulk density, for 127 undisturbed point-scale samples. To further increase the prediction of point-scale K_s, structural properties in addition to currently used soil properties need to be considered (Vereecken et al., 2010).

Currently, PTFs for point-scale K_s are based on relatively small sample volumes. In addition, point-scale K_s shows a high spatial variability as it is not only controlled by textural properties but also by soil structural properties and by the management of soils (Strudley et al., 2008; Van Looy et al., 2017). Some of these aspects are elaborated in more detail below. Here we review the different approaches that currently are being used in LSMs to estimate K_s and to represent its spatial distribution at the grid scale.

Spatial Distribution of the Saturated Hydraulic Conductivity. Table 3 provides an overview of the approaches used to quantify grid-scale K_s in 12 different LSMs. It must be stressed that these estimations of grid-scale K_s are based on PTFs (using the textural class as input for prediction), although the support scale for the development of these PTFs is in all cases the point scale.

In all models studied in the analysis except for ORCHIDEE and ISBA-SURFEX, K_s is considered horizontally uniform across the grid cell. ORCHIDEE considers an exponential distribution of the infiltrability across the grid cell and with depth. Infiltrability is defined as the arithmetic mean of K_s in the deepest fully saturated layer and the hydraulic conductivity in the topmost unsaturated layer. ISBA-SURFEX also considers an exponential distribution of K_s within a grid cell but only for Hortonian runoff (Decharme and Douville, 2006). As already mentioned above, heterogeneous soil surfaces will generate runoff earlier than homogeneous soil surfaces, which is partly caused by the heterogeneity in K_s.

With respect to the vertical heterogeneity, JSBACH, Noah-MP, and CABLE assume a constant K_s value with depth. CLSM, JULES, ISBA, ORCHIDEE, and OLAM-SOIL allow for both constant and depth-variable K_s values. Vertical heterogeneity of K_s in CLM is derived directly from vertical heterogeneity in soil texture. In ORCHIDEE, K_s decreases exponentially with depth using the K_s value defined at the 30-cm depth as a reference value. The extent of the exponential decrease depends on an extinction factor. Furthermore, the K_s profile may be modified depending on root density. For example, CLSM differentiates between surface and root zone layer hydraulic properties (including K_s) in the Richards equation simulations that are used in the derivation of time-scale parameters of catchment-scale vertical moisture transfer. For subsurface runoff, CLSM uses a TOPMODEL based approach with a depth-dependent K_s. ISBA can consider up to 14 soil layers with a varying K_s value.

Estimators for the Saturated Hydraulic Conductivity. In all LSMs, the estimation of grid-scale K_s is typically based on soil textural information but using classical PTFs developed for the point scale (details on these PTFs are provided in Appendix A4). These estimations are often completed with specific estimation functions for organic-rich soils (e.g., CLM 4.5, ISBA, JULES, see details below and Table 3).

Rahmati et al. (2018) compared the K_s values for the point scale provided by Clapp and Hornberger (1978) with K_s estimates derived from field-scale infiltration experiments using the global soil infiltration database SWIG. The K_s derived from these experiments did not show a dependence on soil textural properties. Only for sand and loamy sand were the values of Clapp and Hornberger (1978) and the SWIG data on the same order of magnitude. For all other textural classes, SWIG values were larger by a factor of two to a factor of >1000. Weynants et al. (2009) pointed out that improved estimates of point-scale K_s may be obtained by including structure-related information such as pedologic data and information about land use and crop management, which strongly affect surface soil properties as a result of tillage, root growth, soil trampling by cattle, etc. (see below).

A notable advance is offered by OLAM-SOIL (Walko and Avissar, 2008; Walko et al., 2000), which uses the PTFs developed by Weynants et al. (2009) or de Boer (2016) to estimate K_s. The PTFs of Weynants et al. (2009) are based on a dataset of 182 point-scale samples of Belgian soils (Vereecken et al., 1989, 1990). They estimated the texture-dependent K_s value by extrapolating the unsaturated soil hydraulic conductivity data to saturation and then calculated the ratio between the textural-dependent K_s and the measured K_s value, which was also available. This ratio is a measure of the effect of related structural properties on the measured K_s and was shown to depend on the sand fraction in the soil.

Use of Soil Maps to Estimate the Saturated Hydraulic Conductivity. The previous section shows that the basic soil information that is used to derive the soil properties needed to estimate point-scale K_s differs among the models. Importantly, each LSM, in particular when used for weather forecasting or GCM studies, can use different soil maps to inform the model on soil hydraulic parameters (so-called *ancillary data*). For example, CABLE uses the Zobler soil class information (Zobler, 1986). The version used by Decker (2015) uses the soil texture from the Harmonized World Soil Database (FAO, 2009), and so does JULES. OLAM-SOIL uses the SoilGrids data published by Hengl et al. (2014, 2017). The SoilGrids databases provide information on basic soil properties at seven depths in the soil profile up to 2 m. They also provide estimates of the depth to bedrock and the distribution of soil classes. The gridded predictions were based on ~150,000 soil profiles and remotely sensed data. The input data used to estimate the soil hydraulic properties by CLSM or ISBA-SURFEX are obtained from the Harmonized World Soil Database version 1.21 (HWSD1.21) and the State Soil Geographic (STATSGO2) project (De Lannoy et al., 2014). PARFLOW-CLM uses the UNESCO soil map of the world (FAO, 1988) to provide a global coverage of K_s values.

The default soil texture map used in ORCHIDEE is the map presented by Zobler (1986) at 1°, and it is used in the currently ongoing CMIP6 simulations. CMIP6 refers to the Coupled Model Intercomparison Project Phase 6 that aims to address (i) how the Earth system is responding to forcing, (ii) the origins and consequences of systematic model biases, and (iii) the assessment of future climate change in the context of internal climate variability, predictability, and scenario uncertainty (Eyring et al., 2016). ORCHIDEE can also use two other soil texture maps. The first one is the map developed by Reynolds et al. (2000) at 1/12° and the second is the surface SoilGrids maps at 1 km (Hengl et al., 2014). All these maps are used to define the dominant texture at the model resolution using the USDA texture classification.

CLM 4.5 uses the soil dataset produced by the International Geosphere–Biosphere Program (Global Soil Data Task, 2014) that comprises 4931 soil mapping units and contains the textural composition (sand and clay content). These data were used by Bonan et al. (2002) to create a global soil map of mineral soil textural data. The global data on soil carbon content are obtained from ISRIC-WISE (Batjes, 2006), whereas the soil carbon content for the higher latitudes are obtained from the Northern Circumpolar Soil Carbon Database (Hugelius et al., 2013).

Saturated Hydraulic Conductivity and Infiltration in Organic Soils. Four models listed in Table 3 adjust the calculation of K_s for soils rich in organic matter because these soils typically show higher K_s than mineral soils. Organic soils mostly refer to soils in the northern latitudes and tropical areas and include permafrost and peat soils. The first few centimeters of these soils typically have a soil organic C content of up to 100% (Lawrence and Slater, 2008). CLM 4.5 uses the approach proposed by Lawrence and Slater (2008) to calculate K_s:

$$K_{s,i} = \left(1 - f_{sc,i}\right) K_{s,\min,i} + f_{sc,i} K_{s,sc,i} \quad [48]$$

where $f_{sc,i}$ is the soil C density of a soil normalized by the soil C density of peat in the ith layer, $K_{s,sc,i}$ is the saturated hydraulic conductivity [L T^{-1}] of the organic C fraction in the ith layer, $K_{s,\min,i}$ is the saturated hydraulic conductivity of the mineral fraction [L T^{-1}], whereby $K_{s,\min}$ is obtained from the point-scale PTFs of Clapp and Hornberger (1978) and Cosby et al. (1984) and given by

$$K_{s,\min,i} = 0.0070556 \times 10^{-0.884 + 0.0153(\%\text{sand})_i} \quad [49]$$

Values for $K_{s,sc}$ were given by Letts et al. (2000).

In JULES and ISBA-SURFEX, a geometric average of the point-scale K_s is used to account for the effect of soil C following the approach of Chadburn et al. (2015b) and Decharme et al. (2016), respectively, with

$$K_s = K_{s,\min}^{(1-f_{sc})} K_{s,sc}^{f_{sc}} \quad [50]$$

For CLM 4.5, soil organic matter data are obtained from the Harmonized World Soil Database, except for the northern

high latitudes, which come from the Northern Circumpolar Soil Carbon Database (Hugelius et al., 2013). In ISBA, the soil organic C content is determined from two soil horizons (0–30 and 30–100 cm) of the HWSD1.21.

In JSBACH, three additional classes are added to the 11 soil textural classes, namely peat, moss, and lichen, each with an average value of K_s according to Beringer et al. (2001).

In CLSM, soils are stratified into four levels of organic C content (De Lannoy et al., 2014), with the highest one (>8.72% C, i.e., >15% organic matter) representing peat. Peat parameters were taken from the point-scale information provided by Wösten et al. (2001) that represents highly decomposed peat. In a recently developed peatland module for CLSM, parameters and model structure were further revised, accounting for the high macropore fraction of undecomposed peat by allowing direct infiltration to the water table when the topsoil layer becomes saturated, i.e., effectively turning off the Hortonian runoff mechanism over peatlands (Bechtold et al., 2019).

Numerical Treatment of Infiltration in Land Surface Models

The precipitation simulated in LSMs either infiltrates into the soil or becomes runoff when the soil is saturated (Dunne overland flow) or if the precipitation rate exceeds the infiltration capacity of the soil (Hortonian runoff). As discussed above, various modeling approaches have been developed to describe infiltration and the transition to surface runoff. In the following, we provide an overview of the numerical treatments used by the LSMs listed in Table 2.

The version of ORCHIDEE described here (Ducharne et al., 2017) solves water infiltration and redistribution based on the diffusivity form of the Richards equation, using an 11-layer vertical discretization (de Rosnay et al., 2002). Since d'Orgeval et al. (2008), point (profile) scale infiltration is no longer calculated based on the Richards equation; instead, it invokes a piston-like wetting front inspired by the Green and Ampt (1911) formulation to simplify the boundary conditions under time-varying rainfall rates and soil moisture profiles. In ORCHIDEE, the speed of the wetting front propagation is simplified in two ways, which both tend to reduce infiltration compared with the classical Green and Ampt formulation: (i) the suction at the front is neglected, and (ii) the hydraulic conductivity at the wetting front is not the soil K_s but an arithmetic mean of K_s in the lowest fully saturated layer and $K(\theta)$ in the topmost unsaturated layer (the resulting value is termed K_i). An iterative procedure is used to account for saturation of one soil layer after the other, and infiltration-excess (Hortonian) runoff results when the rainfall rate cannot infiltrate during a single ORCHIDEE time step of 30 min. In this framework, infiltrability depends on the profiles of K_s and $K(\theta)$, which itself depends on K_s and θ based on the Mualem–van Genuchten model (Eq. [7] and [8]). The value of K_s at the 30-cm depth is taken from Carsel and Parrish (1988) for the 12 USDA soil textural classes, but K_s exponentially decreases with depth following Beven and Kirkby (1979).

In the original JULES version listed in Table 2, soil water fluxes are calculated by numerically solving the diffusivity form of the Richards equation for the soil water content increment $\Delta\theta$, where $K(\theta)$ and $h(\theta)$ are given by either Brooks–Corey (Eq. [4–6]) or van Genuchten (Eq. [7–8]) parametric models. The choice of parametric model is set by the user. Note that currently the JULES van Genuchten scheme uses parameters (h_c and n_{vg}) that are directly derived from the Brooks–Corey soil ancillary parameters as used for the Cosby et al. (1984) $K(\theta)$ and $h(\theta)$ equations, rather than using the van Genuchten-specific PTFs given by Wösten et al. (1999), for example. The numerical scheme uses an implicit "forward time step weighting" for numerical stability, in which the water fluxes are first calculated as a first-order finite difference scheme using Eq. [3], but then the moisture increments are recalculated with K and h given by the water contents after the time step, effectively solving (see Best et al. [2011] for details)

$$\frac{\partial\theta}{\partial t}=\frac{\partial}{\partial z}\left[K\left(\theta+\delta\theta\right)\frac{\partial h\left(\theta+\delta\theta\right)}{\partial z}+1\right] \quad [51]$$

The vertical discretization in JULES is flexible and set by the user. For the standard operational configurations and current Earth system model, only four soil layers are used, with thicknesses of 0.1, 0.25, 0.65, and 2 m. For greater numerical accuracy, a finer discretization has been applied (e.g., Chadburn et al., 2015b). Model time stepping in JULES is typically <1 h but is also set by the user. Recently, Haverd et al. (2016) and Cuntz and Haverd (2018) implemented a new soil (Haverd and Cuntz, 2010) and snow model with physically accurate freeze–thaw processes within CABLE, which solved the Richards equation in the mixed form.

In JSBACH (Hagemann and Stacke, 2015; Roeckner et al., 2003), the diffusive form of the Richards equation is used with hourly model time stepping. The soil profile is discretized in the first compartment with 6.5-cm layer thickness, and vertical infiltration is calculated based on the ARNO scheme according to Dümenil and Todini (1992), whereby water will infiltrate while precipitation is below the difference between the local storage capacity and the initial water content within the root zone. In JSBACH, no ponding is allowed and the lower boundary has no impact on the infiltration rate.

In SSiB (Sun and Xue, 2001; Xue et al., 1991; Zhan et al., 2003), the water flow is solved by the diffusivity form of the Richards equation, whereby the soil is discretized nonuniformly, with smaller layer thicknesses close to the surface (upper layer = 1.75 cm). Time stepping is <1 h, and runoff will occur if precipitation exceeds K_s. No ponding of water is allowed at the soil surface.

Noah-MP (Niu et al., 2011; Schaake et al., 1996), JULES (Best et al., 2011), and CABLE (Decker, 2015; Kowalczyk et al., 2013, 2006) also solve the Richards equation in its diffusivity form, and none of these models calculate the infiltration rate directly from the Richards equation. Vertical discretization varies between 2.2 cm (CABLE) and 10 cm (Noah-MP and JULES) for the upper layer, and time stepping is < 1 d for all models (see Table 2). No ponding is allowed for any of these three models, and for

Noah-MP and JULES the lower boundary does not affect infiltration, whereas for CABLE the infiltration will be modified by changes in the soil moisture profile due to groundwater influence.

Another set of LSMs solve the Richards equation in its mixed form such as Parflow-CLM (Kollet and Maxwell, 2006, 2008b), OLAM-SOIL (Walko et al., 2000), ISBA (Boone et al., 2000; Decharme and Douville, 2006), CLSM (Ducharne et al., 2000; Koster et al., 2000), and CABLE enhanced by Haverd et al. (2016) and Cuntz and Haverd (2018). Because these models solve the Richards equation in the mixed form, the infiltration rate can be directly computed from solving the Richards equation. Nevertheless, ponding is only allowed in OLAM-SOIL, Parflow-CLM, and the enhanced CABLE.

In CLSM, infiltration rates are not solely an outcome of the Richards equation simulations. They are one component of an overall catchment-scale model concept, with other processes affecting infiltration rates. CLSM uses a non-traditional framework that strongly emphasizes the subgrid horizontal variability of the land surface hydrological processes. The results of the one-dimensional Richards equation simulations are combined with TOPMODEL formulations that control the varying water table depth and moisture fields at the catchment scale. From this combination, time-scale parameters of catchment-scale vertical moisture transfer are derived. It is to be emphasized that in this approach the spatial water table depth distribution is an important factor influencing catchment-scale infiltration rates.

Sensitivity of Infiltration–Runoff Process to Model Parameters

Most sensitivity studies that have been performed with LSM models with respect to infiltration–runoff processes have focused more on the analysis of runoff and river discharge (e.g., Huang et al., 2017; Materia et al., 2010; Zhang et al., 2016) and less on the sensitivity of the infiltration process to model parameters. Here we review the results from sensitivity studies on LSMs that provide information on key parameters controlling infiltration processes and thus ultimately the whole water and energy balance.

One of the first studies to analyze the sensitivity of LSMs to infiltration processes was conducted by Dirmeyer and Zeng (1999). They analyzed the sensitivity of infiltration to the treatment of convective precipitation and the choices made with respect to the vertical resolution of the soil profile and soil properties. They found that the choice of the thickness of the surface soil layer impacts the simulation of infiltration, with thinner surface layers causing infiltration excess to be more likely because the thinner surface layer has a much smaller capacity. Basic information about the impact of the vertical discretization of the hydrological components is also provided above. Unfortunately, in most LSMs the discretization is predefined and often fairly coarse. In addition, Dirmeyer and Zeng (1999) found that a "realistic" distribution of convective rainfall in space and time at the grid cell scale is needed to adequately represent the infiltration and thus surface runoff. In addition, evaporation of intercepted canopy water will be overestimated if "unrealistic" distributions of convective rainfall are assumed. They also analyzed in detail the impact of having a depth-dependent soil porosity (they used three layers for the SSiB model), with a higher porosity for shallow soil layers and lower porosity (more compaction) for deeper ones. By doing so, they modeled larger infiltration amounts and reduced gravitational drainage. Finally, thinner soil layers (2 instead of 5 cm) were found to generate more infiltration excess, i.e., higher surface runoff, during high insensitivity rainfall events and soil melt.

Soet et al. (2000) analyzed different conceptualizations of the land surface scheme and parameter values for three sites with contrasting soils and climate using the ECMWF TESSEL LSM developed by Viterbo and Beljaars (1995). A sensitivity analysis, set up to explore the impact of using standard parameter values instead of site-specific ones, found that implementing site-specific soil hydraulic properties had a significant effect on runoff and infiltration at all three sites. On the other hand, the use of standard soil parameters led to a systematic underestimation of evapotranspiration and biases in surface runoff that differed in sign for the three different locations.

The sensitivity of the infiltration shape parameter b in the VIC model (see above) as well as the exponent in the Brooks–Corey equation (Eq. [4–6]) were found to be key for correct representation of the hydrological system and the partitioning of rainfall between infiltration and runoff under dry soil conditions (Demaria et al., 2007). Ducharne et al. (1998) found a similar sensitivity to the b parameter for the bucket model version of ORCHIDEE. On the other hand, the impact of these parameters on surface runoff generation and stream flow simulations in wet regions was not significant. Shi et al. (2014) analyzed the sensitivity of the catchment outlet discharge rate to soil properties in the Pennsylvania State University model Flux PIHM and found an important impact of the van Genuchten parameters h_c and $n_{vg}\alpha$ and n (see Eq. [7] and [8]) on both discharge rate and soil water content. Runoff simulations of 10 state-of-the-art hydrological and land surface models including H-TESSEL, JULES, and ORCHIDEE were compared by Beck et al. (2017), and they argued for the need to better calibrate, parameterize, and regionalize the parameters of these macroscale models. Most models were found to generate snowmelt runoff that occurred too early, due to either the underestimation of precipitation or incorrect descriptions of input snowfall, snow physics, and meltwater infiltration into the soil (Bierkens, 2015). Getirana et al. (2014) calibrated river routing parameters and stated that one of the most important aspects to getting the runoff timing (by 1 or 2 mo!) and runoff volumes right was the specification of the soil water threshold when runoff occurs (using the Habets and Saulnier [2001] option for runoff in ISBA). Getirana et al. (2017) extended the study to a large group of LSMs including those presented here (e.g., CLSM, ISBA, H-TESSEL, JULES, ORCHIDEE) and found that this was also the case for most of the other LSMs in the ALMIP2 (AMMA Land Surface Model Intercomparison Project 2; https://www.umr-cnrm.fr/amma-moana/amma_surf/almip2/index.html) ensemble analysis.

In another study, Gudmundsson et al. (2012) compared nine large-scale LSMs including H-TESSEL/CH-TESSEL, JULES, and ORCHIDEE to predict observed runoff percentiles of 426 small catchments throughout Europe and found that the differences in performance among the models became more pronounced for low runoff percentiles. They concluded that this might be explained by the uncertainty associated with the representation of hydrological processes, such as the depletion of soil moisture storage by root water uptake. It is likely that differences in the treatment of infiltration and calculation of hydraulic properties will also have played a role. The performance of three LSMs was analyzed by Sahoo et al. (2008), including HySSiB, Noah, and CLM, and they found substantial differences in the prediction of surface and subsurface runoff for the Little River experimental watershed, Georgia, United States, which was caused by differences in the partitioning of the precipitation into infiltration, surface runoff, and evaporation. An extensive analysis was presented by Zhou et al. (2012), who compared a set of 14 LSMs (including VISA, CABLE, ISBA, CLMTOP, and Noah) and six Budyko-type models against the observed mean annual runoff from 150 large basins. They showed that the LSM biases in the prediction of the simulated mean annual runoff were caused by errors in forcing data and model parameterizations but also by structural model errors. The largest biases between the LSM estimates and observed runoff were found in regions with low mean annual runoff, which corresponds with the findings of Gudmundsson et al. (2012).

Hogue et al. (2006) evaluated the model performance and parameter sensitivity for varying levels of LSM complexity across four different biomes using five LSMs including Noah-MP. They found a large variability among porosity, K_s, and the b parameter used in these models. Based on the impact of these parameters on the simulation results, they advocate either a rigorous calibration or the development and integration of improved vadose zone water flow models. Especially, calibration of these parameters at different experimental sites led to differences with respect to the standard values. A study in the same direction was performed by Cuntz et al. (2016), who analyzed the role of hard-coded model parameters (i.e., providing the user with no option to change values) on the hydrological fluxes in Noah-MP. They found that the total runoff was sensitive to both plant and soil parameters (e.g., soil porosity) and that therefore these parameters should be considered for calibration. They also stated that surface runoff is affected by subsurface runoff, which is dependent on available soil water in the soil profile.

Yang and Niu (2003) compared three different schemes of topography-based runoff production for the LSM VISA (which is based on the LSM of Bonan, 1998) and analyzed their sensitivities to key parameters using two catchments. They found that the decay factor, f, which controls the timing and partitioning of subsurface runoff by rescaling K_s with depth, is a highly important parameter controlling water table depth and the saturated fraction of the grid cell. Shellito et al. (2016) compared calibrated soil hydraulic parameters in Noah using in situ soil moisture network data and surface soil moisture from SMOS satellite observations obtained from seven sites in the United States. Most calibrated simulations led to higher surface runoff than simulations based on hydraulic parameters estimated from textural information using a PTF. The calibrated soil hydraulic parameters included pore size distribution index, saturated soil water content, K_s, and the saturated matric potential (or air-entry value, h_c) in the Brooks–Corey equations (Eq. [4–6]). Finally, Yang et al. (2005) concluded that the characterization of the vertical soil hydraulic heterogeneity is highly important to correctly describe soil water and soil temperature at the land surface and thus indirectly infiltration and surface runoff. Based on numerical simulations and experimental data, they concluded that it was not possible to replace vertical soil heterogeneity by a homogeneous soil with effective parameters.

In conclusion, there is relatively little information provided in the literature on how well the infiltration process and the generation of Dunne or Hortonian overland flow are modeled using different LSMs and which model parameters mostly impact the infiltration process. In addition, this literature review indicates that it is difficult to identify sources of errors in handling infiltration estimation due to the complexity and the different ways in which the infiltration process is being described. One approach to address comparisons of different approaches was proposed by Clark et al. (2015), who advocated the development of models that include different parameterizations of the infiltration process so that parameters and parameterizations can be evaluated in a controlled manner.

Improving the Infiltration Process in Land Surface Models

The balance between parameterization of a complex heterogeneous soil structure and exogenic processes that affect infiltration with the operational performance to compute infiltration–runoff processes that are embedded within LSMs requires an understanding of the trade-off of adding more complex physics to describe the infiltration–runoff process and the reality of the technical aspects of computing land surface processes and the determination of related parameters. Also, infiltration and runoff are just two of many processes impacting the land–atmosphere interaction. We therefore aim here to provide an overview to contextualize the complexity of the derivation of soil hydraulic parameters rather than to point out the shortcomings of LSMs in terms of modeling infiltration and runoff.

In general, there are many soil characteristics broadly related to soil composition and structure (including macro- and biopores) and also to exogenic processes, including water repellency, wetting and drying, swelling and shrinkage, air entrapment, freeze–thaw, thermal gradients, impermeable layers, and anthropogenic perturbations (e.g., tillage, harvesting) that impact infiltration and runoff at the point scale (see Young and Crawford [2004] and Hannes et al. [2016], for example).

Most of these are presently not considered in most hydrological and land surface models, or not in enough detail, and there is little ongoing work in this sense such as the implementation of soil structure in the OLAM-SOIL model (see Table 3) by the use of a dual-porosity model. Unfortunately, the main challenge in implementing soil structure into the LSMs lies in the lack of PTFs considering, e.g., soil structure explicitly and also the temporal change in soil structure.

In the following, we provide an overview of these processes and features and discuss the impact on infiltration and runoff generation briefly.

Soil Structure

The physical soil structure is formed by the combination of the size, shape, and arrangement of voids and solids, which ultimately affect water infiltration and runoff, mainly through the soil hydraulic properties (water retention and hydraulic conductivity curves) that are part of most LSMs and hydrological models. In general, the amount of water that infiltrates into a soil is dependent on the available void space (represented by the model soil layer porosity), which is the cross-sectional area of flow. Greater soil aggregation and pore connectivity increase bypass or preferential flow, therefore increasing the hydraulic conductivity and movement of water to deeper soil layers (e.g., Franzluebbers, 2002; Nissen and Wander, 2003). However, the process has not been implemented in most LSMs (Le Vine et al., 2016), apart from the efforts described by Rahman and Rosolem (2017). The formation of aggregates and the stability of the intra-aggregate void spaces is dependent on the rearrangement, flocculation, and cementation of soil and is mediated by soil organic C, soil biota, ionic bridging, soil clay content, and carbonates. Additionally, macroorganisms facilitate soil porosity, infiltration, and aggregate stability by ingestion of soil (Brown et al., 2000). Factors affecting soil aggregation are summarized in Fig. 7. Macropores, defined as large continuous openings formed by macroorganisms (e.g., earthworm burrows, old root channels)

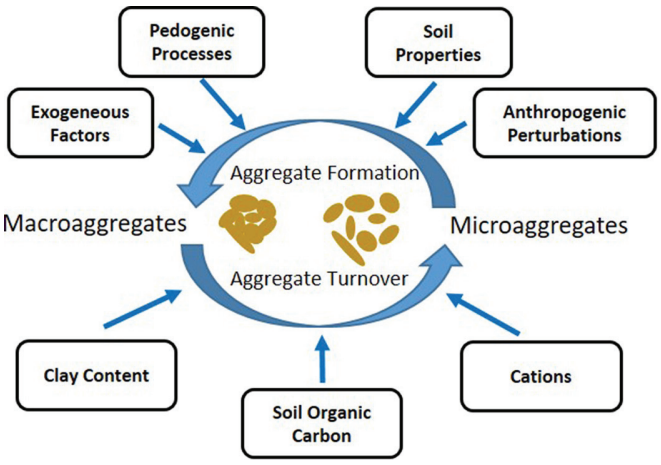

Fig. 7. Factors affecting soil aggregation (modified from Bronick and Lal, 2005).

also have an important influence on infiltration and subsurface storm flows as reviewed by Beven and Germann (1982) and for snowmelt infiltration by Mohammed et al. (2018).

Growing vegetation modifies the soil matrix, affecting soil hydraulic conductivity and soil water storage. Roots alter the pore size distribution and the connectivity between pores as they push into the soil matrix, and they also release complex organic compounds into the soil (Bengough, 2012). The continuous network of branched roots that permeate the soil, with new roots frequently forming while old ones decay, causes hydrological processes to change. Root length distribution is a key property that controls connectivity and preferential flow pathways within the rooting zone and thus impacts infiltration (Lange et al., 2009).

Hysteresis in the Soil Water Retention Curve and Thermal Effects on Hydraulic Properties

Many LSMs assume that the difference between the soil water retention behavior between wetting and drying phases in unsaturated soils (hysteresis) can be ignored and that the soil can be considered as having one unique soil water retention curve, which is used to solve the Richards equation (Eq. [3]).

However, hysteresis can play a crucial role in the accurate description of the flow processes within a soil profile (Glass et al., 1989; Hanks et al., 1969; Ibrahim and Brutsaert, 1968; Scott et al., 1983). Hysteresis is a process that describes the nonidentical nature of equilibrium soil water content in relationship to matrix potential during the wetting or drying phases. The relationship between actual soil water content and matric potential can be obtained in desorption, i.e., drying of wet soils, or sorption, i.e., gradual wetting of dry soil. The resulting desorption–sorption curves are generally not identical because equilibrium soil water content is greater at a given suction during drying than during wetting. The relationship of actual water content and matrix potential has been extensively studied by Haines (1930), Everett (1955), Poulovassilis (1962), Topp (1971), Mualem (1974), Mualem and Dagan (1975), Parlange (1976), Hogarth et al. (1988), Nimmo (1992), Bachmann and van der Ploeg (2002), Huang et al. (2005), and Mualem and Beriozkin (2009).

Thermal gradients also induce significant changes in the estimated water fluxes because temperature affects soil hydraulic properties (Ben Neriah et al., 2014; Gardner, 1955; Grant and Bachmann, 2002; Grant and Salehzadeh, 1996; Hopmans and Dane, 1986; Nimmo and Miller, 1986; Parlange et al., 1998; Philip and de Vries, 1957; She and Sleep, 1998). For example, increasing water temperature decreases water viscosity, causing an increase in hydraulic conductivity (Levy et al., 1989) and thermal swelling of solid particles that change soil pore characteristics and the solid–liquid interface between soil particles (Gao and Shao, 2015).

The advancement of innovative modeling that includes the hysteretic nature of the soil water retention curve was reviewed and further developed by Nuth and Laloui (2008), but it has to be mentioned that for large-scale LSMs the inclusion of hysteretic complexity requires greater computing capability and the

knowledge of input parameters from observations and databases or availability of appropriate PTFs.

Soil Water Repellency

Soil water repellency (SWR) or hydrophobicity reduces the affinity of soils to infiltrating water such that they resist wetting for periods ranging from a few seconds to hours or even weeks (e.g., Doerr and Thomas, 2000; King, 1981). Additionally, soil water repellency is spatially and temporally very variable (Regalado and Ritter, 2008; Ritsema and Dekker, 1998; Täumer et al., 2005). Soil water repellency is mostly caused by the coating of the soil particles by hydrophobic substances, whereby different organic compounds derived from living or decomposing plants or microorganisms can be responsible for SWR. Soils below particular vegetation types (such as needle leaf trees), soils with higher soil C content, coarse-textured soils, as well as areas with frequent wildfire are more prone to SWR than others. A review of factors affecting SWR was given by Doerr et al. (2000). As mentioned, SWR will reduce the soil infiltration capacity (e.g., Imeson et al., 1992; van Dam et al., 1990) and therefore will increase overland flow (e.g., Crockford et al., 1991; McGhie and Posner, 1981; Witter et al., 1991). Topsoil SWR may cause Hortonian overland flow (runoff) even during precipitation events with rates much smaller than the saturated hydraulic conductivity. In LSMs where K_s is derived from PTFs and where water repellency is not included, this may lead to overestimation of infiltration for SWR-prone soils. In some areas, water-repellent layers underlie highly permeable hydrophilic surface layers, and here, the infiltrating water may pond above the water-repellent layer; subsequently, the infiltration water can be stored above this hydrophobic layer and be used for evapotranspiration.

This process can also cause saturated excess overland flow if the permeable layer becomes fully saturated, can cause lateral water flow either through structural gaps or along the slope of the hydrophilic layer, or the water can move downward through the hydrophilic layer along preferential flow paths (Doerr et al., 2000). A schematic illustration of the possible hydrological responses caused by top- and subsoil hydrophobicity is provided in Fig. 8. According to our knowledge, SWR has not yet been implemented in any LSM.

Compaction, Swelling, and Shrinkage

Compaction is the process of reducing the volume of voids in a soil, mainly those filled with air, by packing the soil particles closer together. It can result from natural processes such as soil overburden or from anthropogenic causes, such as the use of cultivation machinery or cattle grazing. Compaction is often characterized by an increase in soil bulk density. This has often been considered as an appropriate independent variable to quantify the decrease in the soil saturated hydraulic conductivity (Ahuja et al., 1989; Assouline and Or, 2008; Laliberte et al., 1966; Or et al., 2000) or changes in the soil hydraulic functions (Ahuja et al., 1998; Assouline, 2006a, 2006b; Stange and Horn, 2005) following compaction. These estimates can thus be applied to evaluate the impact of soil compaction on infiltration. Soil swelling during wetting and shrinking during drying induces dynamic changes in porosity with changing water content of the soil and changes in the hydraulic properties, which consequently affect infiltration (Giraldez and Sposito, 1985; Philip, 1970; Raats and Klute, 1969; Smiles, 1974; Sposito, 1975). In general, the macroporosity, and to a lesser extent the microporosity, of swelling and shrinking soils is affected by their shrinkage and swelling behavior (Alaoui et al., 2011), whereby exactly these voids in the pore system are highly important for rapid water infiltration into the soil and the separation between infiltration and runoff. Electrolyte concentration of the applied water also can have a significant impact on soil hydraulic properties and on the infiltration process. The way the soil structure responds to electrolyte concentration depends on pedogenic processes and the

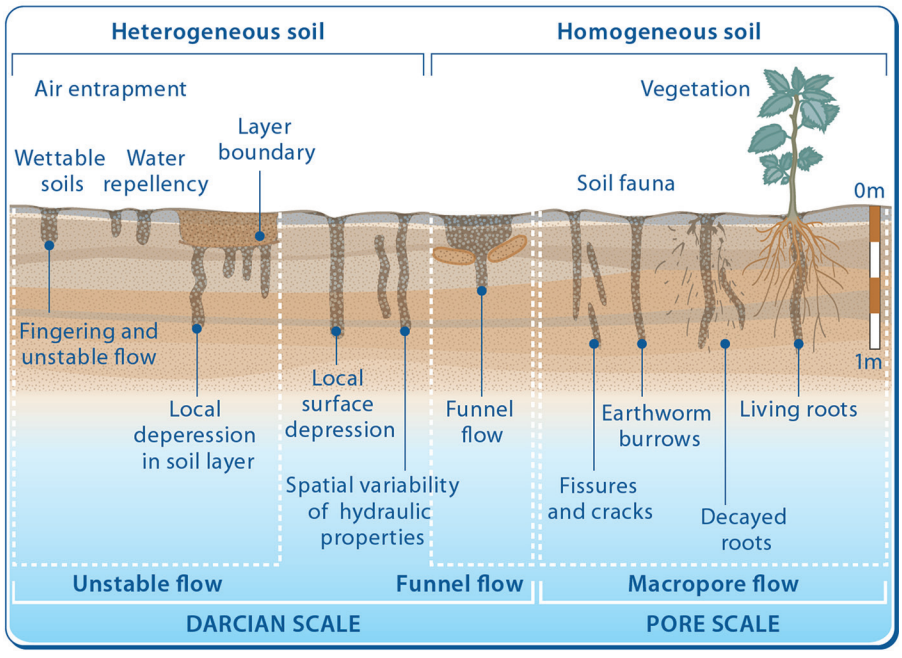

Fig. 8. Schematic illustration of possible hydrological responses of the soil under wettable and water-repellent soils, layer bounds, spatial variability of soil hydraulic properties, and macropore flow induced by soil fauna and vegetation. (From Or et al. class notes with permission.)

nature of the parent material. For example, a high proportion of Na^+ ions relative to other cations weaken the bonds between soil particles, decreasing hydraulic conductivity (Frenkel et al., 1978; McNeal and Coleman, 1966; Quirk, 1994; Rengasamy and Olsson, 1991). This process and its impacts on soil physical and chemical properties has been described in several studies (Assouline and Narkis, 2011; Assouline et al., 2016; Bresler et al., 1982; Greene and Hairsine, 2004; Jury et al., 1991; Kim and Miller, 1996; Quirk and Schofield, 1955; Russo, 2005).

Additionally, expansive soils, including peat, can adsorb large quantities of water during rainfall and therefore reduce surface runoff. According to the USDA soil classification, clayey soils with clay content >30% (often Vertisols) cover around 320 million ha globally and are sensitive to swelling and shrinkage (Dinka and Lascono, 2012). Several studies have looked at the dynamics of shrinking and swelling and associated crack changes for the purpose of improving hydrological models (e.g., Arnold et al., 2005; Bronswijk, 1991; Kishné et al., 2010) but not for LSMs. An extensive review of these models was provided by Adem and Vanapalli (2015). Unfortunately, the shrink–swell properties of Vertisols vary also as a function of soil properties, climate, topography, vegetation, cropping management, and management practices (Davidson and Page, 1956; Lin et al., 1998; Thomas et al., 2000; Vaught et al., 2006), which complicates representation in hydrological and land surface models.

Freeze and Thaw

Many soils at higher elevation or latitudes freeze and thaw seasonally, impacting the soil physical properties and therefore substantially affecting water movement in the landscape. The main effect of freeze–thaw cycles (FTCs) on soil properties lies in their impact on the soil structure, which, as shown above, regulates infiltration and runoff to a large extent (e.g., Chamberlain and Gow, 1979; Fouli et al., 2013; Qi et al., 2006). Freezing and thawing processes induce uneven stress within the soil, but the conclusions in the literature about the effects on soil structure and water flow are not unanimous. There are indications that FTCs decrease soil stability (Edwards, 1991; Kværnø and Øygarden, 2006), whereas Lehrsch (1998), Lehrsch et al. (1991), and Park et al. (2011) observed increasing stability after a few FTCs, while an increased number of FTCs caused a decrease in soil stability, leading to changes in soil hydraulic parameters over time. On the other hand, there seems to be more consensus that the effect of FTCs on clayey soils is much larger than on coarse-textured soils (Bisal and Nielsen, 1967; Kværnø and Øygarden, 2006). Unger (1991) additionally stated that FTCs decrease soil bulk density.

It is also known that the hydraulic conductivity of frozen soil decreases rapidly as the temperatures fall (Williams and Burt, 1974), and some models do take this into account (e.g., CLM, Noah-MP, SSiB, SURFEX, CABLE, OLAM-SOIL, ORCHIDEE). Additionally, even water in the liquid phase is impacted by temperature changes as the viscosity of the pore water increases significantly with decreasing soil temperatures (Hillel, 1998), leading to lower fluidity and water percolation even before freezing. Finally, if the freezing front is near the soil surface, ponding is likely to occur at the soil surface after a precipitation event, resulting in runoff because the amount of liquid water-filled pathways has been reduced. Most LSMs take this effect into account. Also, as the freezing front moves down the soil profile, soil water will migrate toward the freezing front, leaving a drier soil behind, resulting in a larger matric potential gradient pulling the water toward the freezing front (Jame, 1977). Even though some LSMs account for the direct impact of freezing on K_s, temporal changes in the hydraulic parameters due to structural changes induced by FTCs have not been implemented yet. This might be problematic for regions where FTCs might become more frequent under future climate change, as stated by Eigenbrod (1996).

Impermeable Soil Layers

Impermeable layers, or more precisely soil horizons with extremely low saturated hydraulic conductivity, frequently occur in natural or managed soils. Often these layers are denoted as hardpans, hard layers, or compacted horizons located at either the surface or subsurface (Busscher, 2011). These layers can be caused by traffic, tillage practices, trampling of livestock, or soil-forming properties that result in layers with high density or cemented soil particles (Hamza and Anderson, 2005; Silva et al., 2000). For example, the extent of compacted soil is estimated worldwide at 68 million ha of land from vehicular traffic alone (Flowers and Lal, 1998). Some of these compacted or extremely dense soil layers are relatively thin and are therefore often neglected in soil maps at coarser scales. Additionally, changes in the saturated hydraulic conductivity due to soil compaction is often not accounted for in PTFs if bulk density is not used for the prediction of the hydraulic parameters (Van Looy et al., 2017). Nevertheless, these layers are of utmost importance because they control the infiltration of water into the soil and its redistribution to greater depth. In general, the presence of impermeable soil layers will lead to the same hydrological response as shown for the hydrophobic layers depicted in Fig. 8, generating more overland flow (runoff) and subsurface flow events.

Impermeable layers complicate the naturally occurring soil vertical heterogeneity, where generally successive distinct layers of soil with different hydraulic properties occur. Several studies have proposed solutions for infiltration into layered soil systems (Childs and Bybordi, 1969; Colman and Bodman, 1945; Hanks and Bowers, 1962; Miller and Gardner, 1962; Philip, 1967; Raats, 1973; Warrick and Yeh, 1990; Zaslavsky, 1964). Chu and Marino (2005) presented a solution for determining ponding conditions and simulating infiltration into a layered soil profile based on the Green and Ampt approach for unsteady rainfall. Beven (1984) and Selker et al. (1999) also extended the Green and Ampt model for infiltration into soil profiles where pore size varied with depth. A review of the applications of the Green and Ampt model to vertically heterogeneous conditions was provided by Kale and Sahoo (2011).

A special case of a layered soil profile occurs when a seal layer or crust develops on the soil surface, resulting from the destructive

action of raindrop impacts on the soil, which alters the soil structure and soil hydraulic properties, especially K_s. This process and its impacts on physical and chemical properties was described by Quirk and Schofield (1955), Bresler et al. (1982), Jury et al. (1991), Kim and Miller (1996), Greene and Hairsine (2004), Russo (2005), and Assouline et al. (2015). A review of the approaches proposed to model infiltration into sealed (or crusted) soils can be found in Mualem and Assouline (1992), Mualem and Assouline (1996), and Assouline (2004). The direct effect of the presence of the impeding seal layer at the soil surface is to reduce ponding time and the infiltration rate during rainfall (Römkens et al., 1986a, 1986b). Hillel and Gardner (1969, 1970) first addressed the problem of infiltration in the case of sealed soils. They presumed that a sealed soil can be modeled as a uniform soil profile capped with a saturated thin layer of low permeability with constant prescribed physical properties such as the saturated hydraulic conductivity. Their simplified solution was based on the Green and Ampt model, assuming a constant water content (or suction) at the interface between the seal and the soil beneath. It was further applied in different studies (Ahuja, 1974, 1983; Moore, 1981a; Parlange et al., 1984). Variations and extensions of this basic approach included the simulation of infiltration with time-dependent seal hydraulic conductivity functions (Ahuja, 1983; Brakensiek and Rawls, 1983; Chu et al., 1986; Farrell and Larson, 1972; Moore, 1981b; Vandervaere et al., 1998; Whisler et al., 1979). An additional conceptual model, based on the model of Corradini et al. (1997), was suggested by Smith et al. (1999). Römkens and Prasad (1992) applied the solution of Prasad and Römkens (1982) based on the spectral series approach to solve the infiltration equation in soils topped by a constant or transient crust.

Note that in all these studies the hydraulic properties of the seal layer were arbitrarily chosen. Mualem and Assouline (1989) as well as Baumhardt et al. (1990) have addressed the problem of infiltration into sealed and sealing soils by attributing to the seal layer hydraulic functions that evolved from those of the undisturbed soil and that were related to the specific rainfall kinetic energy and intensity involved in the seal formation. The impact of soil surface sealing on infiltration is illustrated in Fig. 9, which depicts that soil surface sealing reduces the ponding time and the infiltration rates into the soil profile, including the final quasi-steady rate. As a result, much more runoff is formed by a given rainfall event when the soil surface sealing is accounted for.

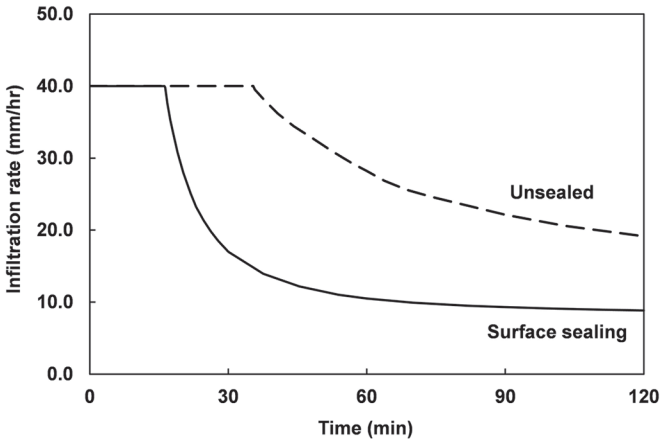

Fig. 9. The impact of soil surface sealing on infiltration.

Instability of Different Flow Regimes

Wetting front instability occurring under certain flow regimes can also significantly affect the infiltration process (DiCarlo, 2004; Jury et al., 2003; Or, 2008; Parlange and Hill, 1976; Philip, 1975; Raats, 1973). Wetting front instability refers to a splitting up of the infiltration front into several fingers along which water is rapidly transported downward. Because a part of the soil pore volume is bypassed by the infiltration through fingers, wetting front instability leads to considerably deeper infiltration than in the case of stable wetting fronts. Raats (1973) explained that an increase of soil water pressure with depth above the wetting front in general leads to instabilities of the wetting front. Entrapment of air, the presence of layers with higher water-entry values, water repellency, but also the reversal of pressure gradients during redistribution just after infiltration at the soil surface has ceased can cause such an increase in pressure above the wetting front that leads to unstable wetting fronts (Wang et al., 1998, 2003a, 2003b). Another process, which originates at the pore scale and which can explain the persistence of individual fingers due to pressure increase or pressure overshoot above the wetting front of a single finger, is the dynamic pressure–water content relation that results from a rapid filling of larger pores and a subsequent redistribution (DiCarlo, 2013).

Solution of Numerical Issues

Rainfall of different intensity also affects infiltration depths and runoff ratios (Frauenfeld and Truman, 2004). For example, varying intensity rainfall simulations yield larger runoff ratios and peak runoff rates than uniform rainfall simulations (Dunkerley, 2012). Using Horton equations, predicted runoff rates were significantly improved during intra-event time variation of fluctuating rainfall simulations (Dunkerley, 2017).

Conventional solution methods to the highly nonlinear Richards one-dimensional partial differential equation used in LSMs inevitably lead to numerical and accuracy issues, which impact their hydrological performance. Land surface models may consider the implementation of alternative, one-dimensional, unsaturated zone flow solution methods (such as those provided by Ogden et al., 2015). The Ogden Soil Moisture Velocity Equation (SMVE) approach uses the hodograph method to transform Richards' equation into a differential equation for a velocity and uses a discretization of the resulting equation in the form of "bins" containing values of the water content. The scheme is computationally efficient, although the explicit time steps are limited by stability considerations because there are no convergence limits as imposed by implicit schemes. Ogden et al. (2015) considered the transport of three regimes of soil water in detail, namely infiltration, wetting fronts disconnected from the surface, and groundwater recharge. The SMVE method offers accuracy comparable to, or in some cases

exceeding, that of the numerical solution of the Richards partial differential equation method but without the numerical complexity and in a form that is robust, continuous, and suitable for use in models of coupled climate and hydrology at a range of scales.

Summary and Conclusion

Infiltration processes are at the core of LSMs, representing the complex and highly dynamic coupling between precipitation and land surface properties where soil, vegetation, initial soil conditions, and topography interact. Although the formulation of infiltration representation for the soil profile scale is well established and tested by the soil physical community, there are still issues that need resolving with regard to the parameterization of infiltration in LSMs. In particular, the extension of the concepts to the catchment and global grid cell scales remains challenging and is in some cases tentative, and with various different solutions that are currently in use. In this perspective, we reviewed and analyzed the different approaches used in current LSMs to predict soil infiltration processes. Specific attention was given to the underlying physical principles and concepts used to predict infiltration at the point and grid scales and the approaches used to describe spatial heterogeneity and upscaling of key parameters controlling the infiltration process in LSMs. We identified several topics and processes that warrant further attention in advancing the prediction of infiltration processes.

First, there is the prediction of K_s, a key parameter in describing infiltration. Currently, K_s estimates in LSMs are derived from PTFs that are typically based on the textural composition of soils but do not consider the impact of soil structure on the infiltration process in general. Recently, Rahmati et al. (2018) published a global database of infiltration measurements that clearly shows that K_s derived from field experiments cannot be predicted from soil texture alone. Therefore, research needs to be directed toward the development of PTFs that consider the effect of structural properties on K, e.g., using land use and tillage treatment as proxies (Jorda et al., 2015). This might be even more important as a recent study of Hirmas et al. (2018) indicated that drier climates induce the formation of greater soil macroporosity than do more humid ones and that such climate-induced changes occur across shorter timescales than have previously been considered. Translation of the effects of these different, largely exogenic, processes to time-varying hydraulic properties (currently hydraulic properties in LSMs are kept constant in time) is one of the greatest challenges in current land surface modeling. For example, the increase in high-frequency rainfall events under future climate conditions will make crust formation for certain soil types more likely, which will cause a decrease in infiltration and increase in surface runoff. Ignoring these aspects will add further uncertainties to predictions of future land–atmosphere interactions. This issue needs to be addressed urgently and in a coherent fashion whereby other soil properties (e.g., thermal properties) and vegetation parameters that depend on, or affect, soil properties (such as rooting depth) are changed concurrently. Additionally, numerical simulations are needed to quantify the effect of K_s estimates considering the role of soil structure on the energy, water, and matter cycles.

Second, due to the availability of spatially highly resolved soil map information at the global scale with a spatial resolution of 250 m or even less, quantification of the subgrid variability is now within reach. The use of this information in combination with PTFs allows direct estimation of b, a lumped parameter used in several LSMs to describe the spatial variability of infiltration capacity. In addition, this highly resolved spatial information can be used to derive effective soil hydraulic parameters such as the Mualem–van Genuchten parameters, which are used in the solution of the Richards equation. The increasing availability of highly resolved spatial data poses questions about how to effectively and efficiently represent subgrid soil and landscape information in LSMs. The strengths and weaknesses as well as the validity and applicability of the methods presented here with respect to modeling land surface processes at the continental and global scales still has not been addressed.

The requirement to correctly represent Hortonian infiltration but also redistribution processes of water in the subsurface (e.g., due to root water uptake or capillary rise) is best fulfilled by using a Richards-equation-based approach. Stochastic analyses of water flow in spatially heterogeneous soil fields (Mantoglou and Gelhar, 1987a, 1987b; Vereecken et al., 2007) have shown that the upscaled Richards equation at the field or larger scale has a form similar to the local-scale equation. However, the spatial variability of soil hydraulic properties introduces a hysteretic behavior of the larger scale system, as the effective hydraulic conductivity is a function of the hydraulic gradient and of its history reflecting nonequilibrium conditions. How far this nonequilibrium behavior is relevant for grid-scale infiltration processes needs to be further studied. The definition of the effective parameters in the upscaled Richards equation, however, requires detailed knowledge of the spatial statistics of local-scale hydraulic parameters. The availability of highly resolved soil maps in combination with PTFs opens up new opportunities to define subgrid variability of hydraulic parameters and thus to quantify effective hydraulic parameters at the scale of LSMs. Also for heterogeneous porous media, the solution of the Richards equation for an infiltration problem remains stable (Egorov et al., 2003). To represent the impact of soil structure, macropores, cracks, or other well-connected structures on water infiltration in soils, several modifications ranging from changing the typically used unimodal pore size distribution to a dual or multimodal pore size distribution to introducing an extra flow equation that represents the infiltration in the macropore pore network and that is coupled with the flow equation in the soil matrix have been proposed (see reviews of Jarvis [2007] and Šimůnek et al. [2003]). These well-connected and highly conductive structures could also be represented in three-dimensional Richards models (e.g., Vogel et al., 2006). But even for such media, the solution of the Richards equation leads eventually to relatively stable infiltration profiles that could be represented fairly well by an upscaled

Richards equation with effective parameters (e.g., Schlüter et al., 2012). It must be noted, though, that the local water fluxes above the infiltration front can be very heterogeneous (but the wetting front is relatively homogeneous). However, the Richards equation cannot reproduce unstable infiltration fronts that are observed at the local scale as a consequence of pore-scale dynamic effects. Phenomena like finger development in gravity-dominated flow, which can have an important impact on the vertical distribution of the infiltrated water and how it varies with the infiltration rate at the soil surface are therefore not represented by the Richards equation. Several approaches to account for these dynamic and nonequilibrium processes by adding additional terms to the continuum Richards equation have been proposed (Cueto-Felgueroso and Juanes, 2009; DiCarlo, 2013; Eliassi and Glass, 2002). Although these approaches describe experimentally observed non-uniform infiltration fronts, it still requires further investigation how the upscaled unstable infiltration can be described by a continuum model and what its consequences are for the water distribution during an infiltration event at the LSM grid scale.

Also, correct representation of Hortonian infiltration requires consideration of the vertical heterogeneity of soil hydraulic parameters, a vertically variable discretization with the finest discretization near the surface, and the use of a pressure-head-based Richards equation. Recently, LSMs such as Parflow/CLM, ISBA, CLSM, and OLAM-SOIL have developed approaches that allow these requirements to be fulfilled. Introducing similar approaches in other LSMs automatically avoids the need to define a maximum infiltration capacity of soils, leading to a more physically consistent description of infiltration.

We observed a disparity between the approaches used at the field or small catchment scale and the approaches applied at the grid scale in LSMs. This, of course, is a result of having two different scientific communities working predominantly at different spatial scales. The soil physics community mainly focuses on the field scale and typically uses semi-analytical solutions or full implementations of the Richards equation to explicitly solve for infiltration flux. This in general requires fine vertical discretization (approximately millimeters near the surface boundary) and short time steps (seconds) to calculate infiltration fluxes. Modeling of infiltration in LSMs is performed at a much larger scale, which usually does not allow a fine spatial and temporal discretization to keep the models computationally efficient. The majority of the LSM community has therefore taken the approach of parameterizing the infiltration process at the land surface and using the Richards equation, mainly in the diffusive form, to redistribute infiltrated water in the soil profile. The common basis for both approaches is the Richards equation, even though for different reasons. It is, however, the goal of this review to foster the cooperation and the exchange of ideas between the two communities. As a first step, the work of Montzka et al. (2017) provides a global concept of subgrid variability of soil hydraulic properties along with the methods of similarity scaling. As the need increases to account for subgrid variability in LSMs, these above-mentioned methods provide options for incorporating this uncertainty.

Furthermore, there is a large diversity among the analyzed LSMs in estimating key properties such as soil moisture capacity and in the treatment of the heterogeneity of soil moisture at the grid scale. In the case of soil moisture heterogeneity, three mathematical formulations have been used: (i) reflection power distribution functions, (ii) γ distributions, and (iii) exponential distributions with a variable number of parameters (two or three). In some cases, LSMs also use different approaches to derive the saturated fraction (F_{sat}) of a grid cell, which is used to partition between Dunne saturation excess and Hortonian infiltration excess. Besides differences in concepts used to formulate the saturated fraction, there is a large divergence in the way the saturated fraction of the land surface within a pixel, F_{sat}, is being parameterized.

Differences include whether or not the groundwater depth is explicitly simulated, and if so, how, and the treatment of the storage capacity of the soil between the land surface and the bedrock or groundwater table depth.

In addition, our analysis showed that basic soil information that is used to obtain spatial coverage of key soil hydraulic properties differs strongly among LSMs but also among the various versions of one single LSM. The impact of using different spatial soil maps combined with the wide range of approaches used to estimate K_s and other soil hydraulic properties is not yet known. Further research is needed in this direction to quantify the impact of this input variability.

Also, many LSMs use a prescribed parameterization of the maximum infiltration capacity to partition precipitation between infiltrable water and runoff (exceptions being Parflow/CLM, ISBA-SURFEX, ORCHIDEE, CLSM, and OLAM-SOIL). These approaches have been heavily tuned by each LSM to ensure that they fit with runoff observations. The lack of a general framework for this central hydrological process leaves a serious gap in the present LSM parameterizations and hinders simple and transparent updating of soil information when it becomes available.

Moreover, re-infiltration, called run-on, is ignored in most LSMs; runoff production that occurs at sites where the infiltration capacity is exceeded may re-infiltrate in the grid cell due to soil and land surface heterogeneity so that not all of the runoff that is generated at a grid cell needs to be routed out of the cell or to a receiving water body. A classic example is the run-on in vegetation patches or bands (strips) in semiarid regions (Assouline et al., 2015). Roots can increase the local infiltration capacity so that runoff from sealed, unvegetated areas can infiltrate in vegetated areas (Nimmo et al., 2009). In addition, run-on leads to a scaling behavior of rainfall–runoff relations, with generally less runoff produced at a larger scale than what would be derived from smaller scale rainfall–runoff relations. A crucial property that defines the rainfall–runoff relations at larger scales is the connectivity of regions that generate runoff (Herbst et al., 2006).

Finally, several processes that control infiltration and thus impact the soil water balance, and ultimately the energy balance

and related land–atmosphere interactions, at the grid cell scale require more attention. This includes the role of vegetation in the infiltration process, the role of the runoff–run-on process at the grid cell scale, and the dynamics of soil structural properties. Correct representation of the runoff–run-on process will need spatially distributed information about parameters controlling Hortonian infiltration excess generation and the formulation and parameterization of redistribution mechanisms within the grid cell. The role of vegetation is related to the effect it exerts on the structural status of the vadose zone, leading to soil properties that are changing over time. In addition, changes in land use and management may affect the structural status of the vadose zone and thus affect water infiltration into soils. One way forward would be to develop PTFs that consider time-dependent soil properties. This, however, requires a basic understanding of how vegetation and management practices change soil hydraulic properties of soils, suggesting the need for greater integration of soil physics, plant science, and land management. There is increasing evidence that spatial variability in water infiltration may also be attributed to dynamics of vegetation-driven spatial heterogeneity (Archer et al., 2012, 2013; Puigdefábregas, 2005) leading to increased infiltration capacity of soils. These processes that may lead to a decrease in Hortonian infiltration have not yet been introduced in LSMs.

Currently, activities have been initiated between ISMC SoilMIP, and the Global Energy and Water Exchanges (GEWEX) project (https://soil-modeling.org/activities/events/the-gewex-soilwat-initiative-first-planning-workshop-for-scope-and-interactions-advancing-integration-of-soil-and-subsurface-processes-in-climate-models) to advance the implementation of high-quality soil information and the description of soil processes in LSMs. These improved LSMs, in turn, will feed into Earth system models for global prediction and closure of water, energy, and carbon budgets. This review is a part of this initiative and one of the first outcomes of this joint activity based on a workshop held in Leipzig, Germany, in 2016. Further activities are presently ongoing, such as the analysis of the effect of incorporating soil structure on the soil water balance of the terrestrial system, and new ones are being initiated and developed.

List of Symbols

a fraction of surface runoff
a_r fitting parameter in CLSM
a_s fitting parameter for each grid box to estimate F_{sat} (JULES)
a_{SSiB} constant in Eq. [A54]
A fraction of an area for which the soil moisture capacity is £I
AC_i steady-state infiltration at the ith location [L T^{-1}]
A_f fitting parameter
A_{gf} grid box fraction of soil water capacity
A_1 fitting parameter [L T^{-1}]
b parameter that reflects the grid cell heterogeneity
b_{BC} parameter in the Brooks–Corey equation (Clapp and Hornberger, 1978)
b_r fitting parameter in CLSM
b_{SSiB} constant in Eq. [A54]
B potential infiltration rate shape parameter—a measure of the spatial variability of the potential infiltration rate, defined as the maximum infiltration rate of each point when the surface is ponded (Liang and Xie, 2001)
B' parameter related to the Brooks–Corey exponent of the water retention characteristic
B_{TW} exponent of the tension water capacity distribution curve
c water storage capacity at a certain location [L]
c_{max} maximum water storage capacity [L]
c_s fitting parameter for each grid box to estimate F_{sat} (JULES)
c_{SSiB} constant in Eq. [A54]
C fraction of an area for which the potential infiltration rate is less than or equal to f (Liang and Xie, 2001)
C_{ice} ice impedance factor
C_v tunable parameter
d_o maximum local water deficit [L]
d_x length of the grid cell (km)
$\langle d_2 \rangle$ depth of the root zone [L]
D_b spatially averaged soil moisture storage deficit
D_{bmax} maximum soil water storage [L]
D_x soil water storage [L]
D_{sm} local soil moisture deficit [L]
D_t mean water storage deficit [L]
D_θ the amount of water stored between surface and groundwater [L]
f pdf of the respective variables
f point potential infiltration rate [L T^{-1}]
f^* infiltrability of the first soil layer [L T^{-1}]
f_c final infiltration capacity [L T^{-1}]
f_d decay factor [L^{-1}]
f_{h20sfc} fraction of the area that is inundated
f_H Hortonian infiltration capacity at time t [L T^{-1}]
f_m maximum potential infiltration rate [L T^{-1}]
f_{mm} average potential infiltration rate [L T^{-1}]
f_{sno} fraction of the grid cell covered by snow
$f_s(s)$ gamma function of the mean surface layer point soil water saturation
$f_{sc,i}$ fraction of soil carbon in the ith layer
$f_{unf,i}$ pdf representing the spatial variability of the local maximum infiltration rate in a grid cell
f_0 initial infiltration capacity [L T^{-1}]
$F(c)$ standard reflected power cumulative distribution function of the spatial variation of the storage capacity c
F_{frz} fractional impermeable area as a function of soil ice content of the surface soil layer cumulative distribution of mean infiltrability (ORCHIDEE)
F_{max} fraction of pixels in a grid cell whose topographic index is ^{3} the grid cell mean topographic index
$F_s(z^*)$ cumulative distribution function of the scaled infiltration capacity (Eq. [46])
F_{sat} saturated fraction of the catchment or grid cell in a LSM
h_{sat} pressure head at air-entry value [L]
h matric potential [L]
h_A minimum (i.e., for evaporation) pressure head at the soil surface allowed under the prevailing soil conditions [L]
h_c matric potential at air entry [L]
h_f capillary pressure at the wetting front [L],
$h_o(t)$ matric potential at the soil surface at time t [L]
h_S maximum (i.e., for infiltration) pressure heads at the soil surface allowed under the prevailing soil conditions [L]
H total water head [L]
i point soil moisture capacity [L]
$i^*(t)$ scaled infiltration rate [L T^{-1}]
i_c infiltration capacity [M L^2 T^{-1}]
i_p maximum potential rate of infiltration or evaporation under the current atmospheric conditions [L T^{-1}]
I spatially averaged actual infiltration [L T^{-1}]
I^* scaled cumulative infiltration [L]
$I_{c,t}$ cumulative infiltration capacity at time t [L]
$\langle I_m \rangle$ mean maximum infiltration rate over the grid cell
I_{max} maximum infiltration rate [M L^2 T^{-1} or L T^{-1}] or maximum soil moisture capacity [L]
I_r infiltration rate for the whole soil column [L T^{-1}]
I_{roff} normalized runoff in SSiB [L T^{-1}]
$I_{unf,i}$ local maximum infiltration rates for unfrozen soil [L T^{-1}]
J Darcian water flux [L T^{-1}]
J_w precipitation rate [L T^{-1}]

K_{dt} constant parameter set equal to 3.0
K_i^{int} average of hydraulic conductivity at the wetting front and the deepest saturated node [L T^{-1}]
K_i^{int*} scaled K_i^{int} [L T^{-1}]
K_o hydraulic conductivity of the soil surface layer [L T^{-1}]
K_{ref} reference K value (2 ′10^{-6} m s^{-1}) [L T^{-1}]
K_s saturated hydraulic conductivity [L T^{-1}]
$K_{s,min,i}$ saturated hydraulic conductivity of the mineral phase of the ith layer [L T^{-1}]
$K_{s,sc,i}$ saturated hydraulic conductivity of the organic soil carbon of the ith layer [L T^{-1}]
l tortuosity index in the Mualem model
m fitting parameter in the van Genuchten model
m pore size distribution index in van Genuchten model
M_{se} surface layer excess [L]
n_{vg} fitting parameter in the Kostiakov equation
P_{drop} precipitation reaching surface after canopy interceptrion in SSiB [L T^{-1}]
P_M snowmelt [L, M L^2 T^{-1}, or L T^{-1}]
P_R rainfall rate [L T^{-1}]
P_T throughfall precipitation [L, M L^2 T^{-1}, or L T^{-1}]
P_x flux incident at the soil surface [M L^2 T^{-1}]
q_{cap} infiltration capacity of the soil [L T^{-1}]
$q(t)$ infiltration flux [L T^{-1}]
$q^*(t)$ scaled infiltration rate [L T^{-1}]
q_D Dunne saturation excess runoff [L T^{-1}]
$q_{evapo.soil}$ water loss due to evaporation [L T^{-1}]
q_f final (constant) infiltration rate [L T^{-1}]
q_H Hortonian excess infiltration runoff [L T^{-1}]
q_i initial infiltration rate [L T^{-1}]
$q_{in,soil}$ infiltration rate of water into the soil [L T^{-1}]
$q_{in,surface}$ surface moisture flux remaining after surface runoff has been removed [L T^{-1}]
$q_{liq,o}$ moisture input into the grid cell [L T^{-1}] and is the sum of liquid precipitation reaching the surface and snowmelt
q_{re} recharge rate [L T^{-1}]
q_s surface runoff (ML^{2}T^{-1}) or [L T^{-1}]
q_u downslope subsurface flow rate per unit contour width [L T^{-1}]
$Q(t)$ cumulative infiltration at time t [L]
Q_{wat} input of water (rainfall, snowfall, dew) [L T^{-1}]
$r(t)$ water supply rate [L T^{-1}]
r_o amount of water that needs to infiltrate (throughfall, snowmelt, and ponded water) [L T^{-1}]
$R(i)$ mean infiltration excess runoff [L T^{-1}]
s water content expressed as saturation
$\langle s \rangle$ grid mean surface layer soil water saturation
S grid cell mean storage
S_e effective saturation
S_g surface gradient
Sl mean slope in the grid cells
Sl_{max} maximum threshold slope
S_{max} maximum water depth across the basin [L]
S_o minimum storage below which there is no surface saturation [L]
$S_{op,i}$ soil sorptivity at the ith location[L T^{-2}]
SW equilibrium root zone wetness index
SW_o minimum value of the soil wetness index distribution
SWI soil water index
S_{xl}^* local terrain surface slope
t time [T]
t^* scaled time [T]
tanβ local surface topographic slope
t_f time needed to infiltrate a certain amount of water [T]
t_p time to ponding [T]
T transmissivity [L T^{-1}]
T_o transmissivity of the soil profile [L T^{-1}]
$T(z_\nabla)$ transmissivity in Eq. [A38]
$\bar{\mathbf{v}}$ depth averaged velocity vector [L T^{-1}]
v_K parameter describing the decrease of saturated hydraulic conductivity with depth
w_{act} subgrid water content that corresponds to the fractional saturation
w_{min} minimal local subgrid soil water capacity
w_{max} maximum local soil water capacity
W vertically integrated soil water content (over the first 50 cm of the soil profile) [L]
W_{sat} vertically integrated saturated soil water content (over the first 50 cm of the soil profile) [L]
$\bar{x}$ mean catchment value of ln(a/tan$b$)
X dimensionless time
z_{bot} middle point of the bottom layer (1.5 m) [L]
$z(i)$ thickness of the ith soil layer [L]
z_l local water table depth [L]
z_{pdm} depth over which soil moisture is considered [L]
z_{wt} water table depth [L]
z_∇ mean water table depth [L]
Z soil profile depth to bedrock [L]
Z_g ground surface elevation [L]
Z_m maximum value of profile depth to bedrock [L]
α_{AC} Miller–Miller scaling factor for final infiltration capacity
α_G parameter in the Gamma distribution
α_{GA} parameter proportional to the matric potential at the wetting front
α_K decay constant in Kostiakov equation
α_{opt} single Miller–Miller scaling factor for infiltration
α_s shape parameter in the spatial distribution function of soil wetness
α_{sc} Miller–Miller similarity scaling factor
α_{Sop} Miller–Miller scaling factor for sorptivity
α_T upstream area that contributes flow through a unit contour positioned at the point or specific catchment area
α_{wf} product of the absolute value of wetting front suction head and the difference between saturated water content and initial water content at the beginning of the infiltration event
β parameter depending on grid resolution
β_G parameter in the Gamma distribution
β_K fitting parameter in the Kostiakov equation
β_s correction parameter for K_s
β_T slope parameter
γ parameter related to topography
γ_f fraction of surface runoff
$\gamma_{1,2,3}$ fitting parameters
δ_t model time step [L]
ε dimensionless error
θ volumetric soil water content
θ_i initial water content
θ_{ice} the content of ice
θ_l the content of liquid water
θ_r residual moisture content
θ_{rz} mean diagnosed root zone moisture content
θ_s saturated soil water content
θ_{wilt} water content at wilting point
κ scaling factor needed to redistribute the GCM grid scale precipitation over the scale of precipitation events
κ_p related to the standard deviation of the subgrid slope
λ wetness index
λ_{crit} critical topographic index
λ_m mean topographic or wetness index
λ_p dimensionless pore size distribution index
λ_r characteristic length of Miller–Miller scaling reference soil [L]
λ_s subgrid heterogeneity of soil
λ_{sc} characteristic length of a Miller-Miller similar porous medium [L]
ρ correlation coefficient between the terrain slope and the soil water content
σ_{Ks} standard deviation of saturated hydraulic conductivity [L T^{-1}]

σ_{max}	maximum standard deviation of the orography
σ_{min}	minimum standard deviation of the orography
σ_{or}	standard deviation of the orography
σ_{slope}	standard deviation of the subgrid slope variability
σ_{Sxl}	standard deviation of local surface slopes
σ_{θ}	standard deviation of soil water content
τ	time scale of transfer of surface layer moisture into the root zone [T]

Appendix A1

The Probability Distributed Model of Moore (1985)

In the PDM-based scheme (Moore, 1985) for calculating Dunne runoff, F_{sat} was described as

$$F_{sat} = 1 - \left(1 - \frac{S - S_0}{S_{max} - S_0}\right)^{b/(b+1)} \quad [A1]$$

where S is the grid cell mean water storage [L], S_0 is the minimum water storage below which there is no water saturation at the surface [L], S_{max} is the maximum possible grid cell water storage [L], and b is a shape parameter proposed by Moore (1985) that reflects the heterogeneity in a lumped manner (see also Eq. [40]). Parameters b and S_0 were obtained from model calibration using catchment data, and S_{max} was obtained from available data and calculated from

$$S_{max} = \theta_{sat} z_{pdm} \quad [A2]$$

where z_{pdm} [L] is the soil depth throughout which the soil water content is considered for PDM modeling. Clark and Gedney (2008) assumed z_{pdm} to be 1 m.

Appendix A2

Description of Maximum Infiltration Rate in Different Land Surface Models

Note that only those models using the maximum infiltration rate in their concept are described here and that the last number of the label (e.g., A2.**3**) refers to the number given in Table 2 to facilitate reading. Additionally, I_{max} depends on F_{sat} for those models relying on the F_{sat} approach.

A2.3 ORCHIDEE

ORCHIDEE (Ducharne et al., 2017) includes a subgrid distribution of infiltration, which reduces the effective infiltration rate into each successive layer of the wetting front. In practice, the mean infiltrability of a layer over the grid cell is spatially distributed using an exponential pdf, then compared locally to the amount of water that needs to infiltrate (called r_0 and comprised of throughfall, potentially increased by snowmelt and ponded water). As a result, infiltration-excess runoff is produced over the fraction of the grid cell where r_0 [L T^{-1}] is larger than the local K_i^{int} [L T^{-1}] defined by the exponential distribution of mean saturated hydraulic conductivity $\langle K_i^{int} \rangle$, applying the following cumulative distribution function:

$$F\left(K_i^{int}\right) = 1 - \exp\left(-\frac{K_i^{int}}{\left\langle K_i^{int} \right\rangle}\right) \quad [A3]$$

The K_i^{int} value is calculated as the average of the actual hydraulic conductivity at the wetting front and the deepest saturated node. A spatial integration is conducted for each soil layer that becomes saturated when the wetting front propagates, giving the mean infiltration excess runoff, $R_{e,i}$, produced from the saturation of each ith soil layer:

$$R_{e,i} = r_0 - K_i^{int}\left[1 - \exp\left(-\frac{r_0}{K_i^{int}}\right)\right] \quad [A4]$$

By reducing the effective conductivity,

$$K_i^{int*} = K_i^{int}\left[1 - \exp\left(-\frac{r_0}{K_i^{int}}\right)\right]$$

compared with the uniform case ($K_i^{int*} = K_i^{int}$), this subgrid distribution increases surface runoff, given by the sum of R_i from all the layers saturated during the time step. The model also considers the mean slope of the grid cell, with a reinfiltration of excess water possible only at low slopes. This subgrid distribution can be seen as opposite to the parameterization of Warrilow et al. (1986) because the actual hydraulic conductivity, K, rather than the precipitation rate is spatially distributed within the grid cells.

A2.4 CLSM

The Catchment Land Surface Model (CLSM) (Koster et al., 2000), the land model component of the NASA Goddard Earth Observing System (GEOS-5) coupled Earth system model, does not impose a priori a maximum infiltration rate in its formulation. The amount of water that can infiltrate within a certain time at the catchment scale is a function of the model's dynamically varying spatial moisture fields. Infiltration in CLSM is considered here in two steps: (i) precipitation throughfall into the near-surface soil layer (2 or 5 cm), and (ii) the subsequent transfer of this soil water into the root zone. It is important to recognize that CLSM is designed to emphasize a description of horizontal moisture variability that is linked to the simulation of a spatially variable dynamic water table depth. This is discussed in more detail above. In effect, the land surface area in CLSM is divided into distinct (and dynamically changing) hydrological regimes. Regarding the throughfall into the near-surface layer, all rainwater runs off the surface in the "saturated fraction" regime, effectively as Dunne runoff and without infiltration. In recent versions of CLSM, the other two regimes (the "subsaturated-but-transpiring" and the "wilting" regimes) allow all precipitation water in a given time step to infiltrate and thereby increase the surface soil moisture, although if the layer becomes fully saturated, the excess does run off the surface, effectively as Hortonian runoff.

The transfer of surface layer moisture into the root zone is controlled by a time scale, τ [T], computed as

$$\tau = \frac{a_r}{\left(\theta_{rz} + b_r M_{se}\right)^3} \quad [A5]$$

where a_r and b_r are fitted parameters, θ_{rz} is the mean diagnosed root zone moisture content [$L^3\ L^{-3}$], and M_{se} is the surface layer excess [L] (see above). With this timescale defined, the water transferred from the surface layer to the root zone, ΔM_{se} [L], is

$$\Delta M_{se} = \frac{-M_{se}\Delta t}{\tau} \quad [A6]$$

The empirical equation for the timescale τ was fitted to results from high-resolution (1-cm) solutions of the vertical one-dimensional Richards equation, conducted off-line prior to running climate or land surface simulations. The simulations behind these off-line solutions used a comprehensive set of values for the CLSM's water prognostic variables (see Ducharne et al., 2000) appropriately downscaled to 1-cm vertical resolution, and a comprehensive set of soil classes parameterized by the Campbell (1974) equations, with corresponding hydraulic parameters based on lookup tables or using the PTFs of Wösten et al. (2001) (De Lannoy et al., 2014).

In CLSM, the catchment-scale infiltration rate decreases by two mechanisms in which the actual groundwater level is crucial: (i) the unsaturated area into which rainfall can infiltrate at the catchment scale decreases for rising water levels, i.e., higher areal fractions of the saturated regime, and (ii) the hydraulic gradient between surface and root zone in the unsaturated area decreases when the root zone fills up due to infiltration and rising water levels. The combination of both mechanisms results in a dynamic prediction of catchment-scale maximum infiltration rates into the surface layer that range from high values (larger than K_s) under deep water level conditions to values that drop below K_s under shallow water level conditions.

A2.5 ISBA-SURFEX

In ISBA-SURFEX (Decharme and Douville, 2006), the local maximum infiltration rates for unfrozen soil are given by

$$I_{unf,i} = K_{s,i}\left[\frac{b_{BC} h_c}{\Delta z}\left(\frac{\theta}{\theta_s} - 1\right) + 1\right] \quad [A7]$$

where h_c is the matric potential at air entry [L], θ_s is the soil porosity or saturated water content [$L^3\ L^{-3}$], b_{BC} is the pore size distribution index from the Brooks–Corey equation (dimensionless) (see Eq. [4]), Δz is the top layer soil thickness of 0.1 m, and $K_{s,i}$ is the saturated hydraulic conductivity at the ith location [$L\ T^{-1}$]. The variable $I_{unf,i}$ comes from the equation presented in the study by Abramopoulos et al. (1988) for calculating infiltration and evapotranspiration in global climate models, whereby the maximum infiltration was defined as

$$I_{max} = K_{s,i}\left[\left.\frac{dh_i}{d\theta_i}\right|_{\theta_i=\theta_s}\left(\frac{\theta_i - \theta_s}{z_i}\right) + 1\right] \quad [A8]$$

where i refers to the top soil layer ($i = 1$), θ_i is the volumetric soil water content of the top soil layer [$L^3\ L^{-3}$], and z_i is the thickness of this layer [L]. The mean maximum infiltration rate, I_{max}, is used to calculate the surface runoff generated by Hortonian overland flow as

$$q_{HH} = \mu\left[\int_0^1 \int_{f^*}^{\infty} \left(P_{x,i} - I_{unf,i}\right) f_{P_{x,i}}\left(P_{x,i}\right) dP_{x,i}\, f_{unf,i}\left(I_{unf,i}\right) dI_{unf,i}\right] \quad [A9]$$

where P_x is the incident flux reaching the soil surface and

$$f_{unf,i}\left(I_{unf,i}\right) = \frac{1}{I}\exp\left(\frac{-I_{max,i}}{I_{max}}\right) \quad [A10]$$

where I_{max} is the mean maximum infiltration rate across the grid cell [$L\ T^{-1}$]. Here $f_{unf,i}(I_{unf,i})$ represents the spatial variability of the local maximum infiltration rate in a grid cell.

The parameter μ in Eq. [58] is given by

$$\mu = 1 - \exp\left(-\beta P_x\right) \quad [A11]$$

where β is a parameter depending on the grid resolution according to

$$\beta = 0.2 + 0.5\exp\left(-0.01 dx\right) \quad [A12]$$

where dx is the length of the grid cell in kilometers.

Combining all equations, we obtain

$$q_{HH} = \frac{P_x}{1 + I_{unf}\left(\mu / P_x\right)} \quad [A13]$$

Overall, the infiltration rate is calculated from the difference between the throughfall rate and surface runoff, whereby the throughfall rate has three components, namely interception, snowmelt, and dripping from the interception reservoir.

A2.6 Noah-MP

Wang et al. (2016) defined the maximum infiltration rate, I_{max} [$L\ T^{-1}$], for a grid cell in Noah-MP as

$$I_{max} = \frac{P_x D_x\left[1 - \exp\left(-kdt\,\delta_t\right)\right]}{P_x + \left[1 - \exp\left(-kdt\,\delta_t\right)\right]} \quad [A14]$$

where δ_t is the model time step [T], D_x is incorrectly termed by Wang et al. (2016) as soil water diffusivity, when in fact it is simply the soil water storage in length units [L], calculated as

$$D_x = \sum_{i=1}^{4} \Delta z_i \left(\theta_s - \theta_i\right) \quad [A15]$$

and

$$kdt = kdt_{ref}\frac{K_s}{K_{ref}} \quad [A16]$$

where P_x is the precipitation rate [$L\ T^{-1}$], K_s is the saturated hydraulic conductivity [$L\ T^{-1}$], θ_s and θ_i are the volumetric saturated water content and the actual water content [$L^3\ L^{-3}$] at the ith time step, respectively, kdt is a parameter in Eq. [A14], kdt_{ref} is a constant parameter set equal to 3.0 (dimensionless), and K_{ref} is a reference K value (2×10^{-6} m s^{-1}).

In Noah-MP (Niu et al., 2005, 2011), I_{max} is used to calculate Hortonian excess infiltration as

$$q_s = F_{sat} Q_{wat} + (1 - F_{sat}) \max\left[0, \left(Q_{wat} - I_{max}\right)\right] \quad [A17]$$

where F_{sat} is calculated from TOPMODEL (see below), Q_{wat} [L T^{-1}] is the input of water (rainfall, snowfall, dew), and I_{max} is the maximum soil infiltration capacity calculated according to Entekhabi and Eagleson (1989), where it is defined as infiltrability.

A2.7 JULES

In the JULES model (Best et al., 2011), the maximum surface infiltration rate is defined as $I_{max} = \beta_s K_s$, where β_s is the enhancement factor (dimensionless), generally set equal to 0.5 for bare soil, whereas larger values are used for vegetated grid cells (4 for trees, 2 for grasses and shrubs), to account for infiltration enhancing factors such as root macropores, and K_s is the saturated hydraulic conductivity [L T^{-1}]. This approach may lead to an underestimation of the infiltration rate because sorptivity forces are not taken into account and essentially all the water reaching the soil surface will infiltrate. Hortonian runoff is calculated as the difference between throughfall plus snowmelt and infiltration. Runoff can increase under certain configurations to avoid supersaturation of the upper soil layer—thus explicitly representing Dunne runoff at the point scale. If the "large-scale hydrology" scheme is used, Dunne runoff is calculated in addition to Hortonian runoff, based on the surface saturated fraction, F_{sat} (see Appendix A3), according to

$$q_{dunne} = F_{sat} q(t) \quad [A18]$$

where $q(t)$ is the infiltration rate [L T^{-1}], which is multiplied by $1 - F_{sat}$ to account for this additional runoff term. Note, that ponding is not simulated.

A2.8 CLM

The Community Land Model (CLM) version 4.5 (Oleson et al., 2013) calculates the maximum soil infiltration capacity as

$$I_{max} = (1 - F_{sat}) K_s C_{ice} \quad [A19]$$

where K_s is the saturated hydraulic conductivity [L T^{-1}] and C_{ice} is an ice impedance factor (dimensionless). Hortonian excess infiltration runoff, q_H [L T^{-1}], is generated as

$$q_H = \max\left[q_{in,\,soil} - (1 - f_{h20sfc}) I_{max}, 0\right] \quad [A20]$$

where f_{h20sfc} is the fraction of the area where ponded water exists and thus equals F_{sat}. Note that Hortonian excess infiltration runoff is only generated and ponded water only occurs on the diagnosed unsaturated fraction ($1 - F_{sat}$) of the soil column. The variable $q_{in,soil}$ refers to the infiltration rate of water into the soil, defined as

$$q_{in,soil} = (1 - f_{h20sfc}) q_{in,surface} - q_H - (1 - f_{sno} - f_{h20sfc}) q_{evapo,soil} \quad [A21]$$

and

$$q_{in,surface} = (1 - F_{sat}) q_{liq,o} \quad [A22]$$

where $q_{liq,o}$ is the water input into the grid cell [L T^{-1}], which is the sum of liquid precipitation reaching the surface and snowmelt, $q_{evapo,soil}$ [L T^{-1}] is the water loss due to evaporation, $q_{in,surface}$ [L T^{-1}] is the surface water flux after surface runoff has been removed, and f_{sno} is the fraction of the grid cell covered by snow.

A2.11 H-TESSEL and CH-TESSEL

In H-TESSEL (Balsamo et al., 2009) or in the more recent CH-TESSEL, both based on the same hydrological principles (Boussetta et al., 2013), the maximum infiltration rate is calculated to determine Hortonian overland flow as

$$I_{max} = (W_{sat} - W) + \max\left(0, W_{sat}\left\{\left(1 - \frac{W}{W_{sat}}\right)^{1/(b+1)} - \left[\frac{P_T + P_M}{(b+1) W_{sat}}\right]\right\}^{b+1}\right) \quad [A23]$$

where P_T is the throughfall precipitation [L], P_M is the snowmelt [L] leading to P_x as the total water reaching the surface ($P_x = P_T + P_M$ [L]), and W and W_{sat} [L] are the vertically integrated soil water contents (equivalent to θ and θ_s, albeit with different units) over the first 50 cm of the soil profile. The b parameter reflects the grid cell heterogeneity (see above). In H-TESSEL and CH-TESSEL, $q_s = P_x - I_{max}$, where q_s is surface runoff (defined as R in Balsamo et al., 2009). Notice that the units of I_{max} are length, although it is defined as a rate in Balsamo et al. (2009).

Appendix A3

Description of the Saturated Water Fraction

Note that only those models using the maximum infiltration rate in their concept will be described here and that the last number of the label (e.g., A3.**3**) refers to the number given in Table 2 to facilitate reading. Because the TOPMODEL concept to calculate F_{sat} is embedded in several LSMs presented in this appendix, we briefly present the basic equations and ways to calculate basic properties.

A3.0 TOPMODEL

In the TOPMODEL approach (Niu et al., 2005), F_{sat} can be defined as

$$F_{sat} = \int_{\lambda \geq (\lambda_m + f_d z_\nabla)} \mathrm{pdf}(\lambda) \mathrm{d}\lambda \quad [A24]$$

where f_d is the decay factor [L^{-1}], which is a measure of the decline of K_s with increasing depth, z_∇ is the mean water table depth (positive for values below the ground surface), and the local water table depth z_l is given by

$$z_l = z_\nabla - \frac{1}{f_d}(\lambda_m - \lambda) \quad [A25]$$

where λ_m is the mean topographic (wetness) index and λ is the local topographic index, defined as

$$\lambda = \ln\left(\frac{\alpha_T}{\tan\beta_T}\right) \quad [A26]$$

where α_T is the specific catchment area and $\tan\beta_T$ is the local surface topographic slope.

To calculate the average water table depth, Chen and Kumar (2001) proposed an iterative procedure where D_θ is the amount of water stored between surface and groundwater:

$$D_\theta = \int_0^{z_\nabla} [\theta_s(z) - \theta(z)]\,dz \quad [A27]$$

where the water contents $\theta_s(Z)$ and $\theta(Z)$ denote the catchment or basin average [$L^3\ L^{-3}$]. Further, D_θ is calculated from

$$D_\theta = \sum_{i=1}^{NLAYERS} [\theta_s - \theta(z)_i]\Delta z_i \quad [A28]$$

The water content $\theta(z)$ is calculated using, e.g., the Brooks–Corey equation (Eq. [4–6]) and the assumption that the soil water content profile is an equilibrium with the groundwater by

$$\theta(z) = \theta_s \left[\frac{h_c - (z_\nabla - z)}{h_c}\right]^{-1/B'} \quad [A29]$$

$$\theta(z) = \theta_s(z) \left[\frac{h_c - (z_\nabla - z)}{h_c}\right]^{-1/B'} \quad [A30]$$

where B' is related to the Brooks–Corey exponent of the water retention characteristic and h_c is the pressure head at air entry (cm). This approach was used by Niu et al. (2005) to develop a runoff scheme for global climate models, and it has also been implemented in CLM (see below)

A3.3 ORCHIDEE

The ORCHIDEE model does not use F_{sat} to generate surface runoff, which is the complement of upscaled local infiltration rates (see above). In contrast, it uses the concept of the ponded fraction to reduce the surface and enhance infiltration. A fraction of surface runoff, γ_f, is allowed to pond in flat areas, and it is kept to be infiltrated at the following time step with throughfall and snowmelt to account for the effect of ponding on infiltration (d'Orgeval et al., 2008). This fraction γ is constant over time but varies spatially, based on the mean slope Sl in the grid cells and a threshold slope Sl_{max} (with a default value of 0.5%), such that the ponding fraction decreases from 1 when Sl = 0 to 0 when $Sl \geq Sl_{max}$:

$$\gamma_f = 1 - \min(1, Sl/Sl_{max}) \quad [A31]$$

This leads to grid-scale surface runoff reduced by γ_f.

A3.4 Catchment Land Surface Model

In the Catchment Land Surface Model (CLSM), the saturated land fraction under equilibrium conditions is effectively computed as the fraction of the area for which the water table depth lies "above" the ground surface, based on the TOPMODEL framework. The strategy for calculating the saturated land fraction was described above.

A3.5 ISBA-SURFEX

In the ISBA-SURFEX model, the saturation excess runoff can also be computed using the TOPMODEL assumption instead of using the Arno scheme, so only Dunne runoff is affected by F_{sat} (Decharme and Douville, 2006). It is described according to a corrected approach of the original TOPMODEL framework proposed by Saulnier and Datin (2004) and written as

$$q_D = P_x F_{sat} \quad [A32]$$

where F_{sat} is defined as the saturation fraction of a grid cell, being inversely proportional to the mean water storage deficit, D_t, of the grid cell, whereby D_t can be written as

$$D_t = (\theta_s - \theta) d_2 \quad [A33]$$

The value of D_t is bounded between 0 and d_o, the maximum local water deficit, defined by

$$d_o = (\theta_s - \theta_{wilt}) d_2 \quad [A34]$$

where θ_s and θ are the saturated and mean volumetric water content averaged across the depth d_2 [L] at grid scale [$L^3\ L^{-3}$] that can be, optionally, the depth of the entire root zone (Decharme and Douville, 2006) or the depth of the layer in which the cumulated root profile reached 90% (Decharme et al., 2013), and θ_{wilt} is the water content at the wilting point [$L^3\ L^{-3}$]. Here, D_t will be d_o when $F_{sat} = 0$ or vice versa.

A3.6 Noah, Noah-MP

We briefly describe the way infiltration is handled in Noah and then present Noah-MP and the approaches used to calculate F_{sat}.

In the Noah model (Schaake et al., 1996), the spatially averaged actual infiltration rate, I_r, depends on the cumulative infiltration capacity ($I_{c,t}$) at a certain moment in time t; $I_{c,t}$ is expressed as

$$I_{c,t} = D_b [1 - \exp(-K_{dt} \Delta t)] \quad [A35]$$

where Δt is the model time step, K_{dt} is a constant, and D_b represents the spatially averaged soil water storage for the whole soil column. The value of D_b in each soil layer is computed by

$$D_b(i) = D_{bmax}(i) \left(1 - \frac{\theta_l(i) + \theta_i(i) - \theta_{wilt}(i)}{\theta_s(i) - \theta_{wilt}(i)}\right) \quad [A36]$$

where $D_{bmax}(i)$, $\theta_l(i)$, $\theta_i(i)$, $\theta_{wilt}(i)$, and $\theta_s(i)$ are the maximum soil water storage, the content of liquid water and ice, the wilting point, and soil porosity or saturated water content, respectively, in the ith soil layer; $D_{bmax}(i)$ is defined by

$$D_{bmax}(i) = -z(i)[\theta_s(i) - \theta_{wilt}(i)] \quad [A37]$$

where $z(i)$ is the thickness of the ith soil layer.

Then, the infiltration rate for the whole soil column is given by

$$I_r = \frac{P_R I_{c,t} / (P_R + I_{c,t})}{\Delta t} \quad [A38]$$

where P_R is the precipitation input into the whole column.

Soil freezing has a significant effect on the permeability of soils because ice impedes the infiltration rate. Noah computes the impermeable area factor FC to consider the influence of freezing on soil infiltration following Koren et al. (1999).

Noah-MP is an improved version of Noah, whereby Noah-MP (Niu et al., 2011) offers four options for computing infiltration and surface–subsurface runoff. Option 1 is the TOPMODEL-based runoff scheme with the simple groundwater scheme (Niu and Yang, 2007) implemented by Cai et al. (2014), where the fraction of the gridbox that is saturated, F_{sat}, is given by

$$F_{sat} = (1 - F_{frz}) F_{max} \exp\left[-0.5 f_d \left(z_{wt} - z_{bot}\right)\right] + F_{frz} \quad [A39]$$

where z_{bot} is the soil profile thickness (default = 2.0 m), z_{wt} (L) is the water table depth, F_{max} is set to a global mean value of 0.38, and F_{frz} is the fraction of impermeable area as a function of soil ice content of the surface soil layer. For urban areas, F_{frz} is set to 0.95. The runoff decay factor, f_d, in Eq. [A39] equals 6 m^{-1}.

Option 2 is a simple TOPMODEL-based runoff scheme with an equilibrium water table (Niu et al., 2005). As in Option 1, this scheme parameterizes both surface and subsurface runoff as functions of the water table depth but with a sealed bottom of the soil column (zero-flux lower boundary condition) in accordance with one of the TOPMODEL assumptions, i.e., the exponential decay of saturated hydraulic conductivity; F_{sat} is calculated as

$$F_{sat} = (1 - F_{frz}) F_{max} \exp(-0.5 f_d z_{wt}) + F_{frz} \quad [A40]$$

where f_d is set to 2.0 m^{-1}.

Option 3 is an infiltration-excess-based surface runoff scheme with a gravitational free-drainage subsurface runoff scheme as used in the original Noah (Schaake et al., 1996). Surface runoff (R) is computed as the excess of precipitation (P_d) not infiltrated into the soil ($R = P_d - I_{max}$). The maximum infiltration rate, I_{max}, is computed as

$$I_{max} = P_d \frac{D_x \left[1 - \exp(-kdt \Delta t)\right]}{P_d + D_x \left[1 - \exp(-kdt \Delta t)\right]} \quad [A41]$$

with

$$D_x = \sum_{i=1}^{N} \Delta z_i \left(\theta_s - \theta_i\right) \quad [A42]$$

and

$$kdt = kdt_{ref} \frac{K_s}{K_{ref}} \quad [A43]$$

where Δt is the time step [T], K_s [L T^{-1}] is the saturated hydraulic conductivity, which depends on soil texture and is prescribed in a lookup table, and N is the number of layers. The parameters $kdt_{ref} = 3.0$ and $K_{ref} = 2 \times 10^{-6}$ m s^{-1} were determined in the framework of the PILPS 2(c) experiments for the Red–Arkansas River basins in the Southern Great Plains region of the United States (Wood et al., 1998).

Finally, Option 4 is the BATS runoff scheme, which parameterizes surface runoff as a fourth power function of the top 2-m soil wetness (expressed as degree of saturation) and subsurface runoff as gravitational free drainage (Yang and Dickinson, 1996), described by

$$F_{sat} = (1 - F_{frz}) \left(\frac{\theta_{tot}}{\theta_s}\right)^4 + F_{frz} \quad [A44]$$

with

$$\theta_{tot} = \frac{1}{z_{bot}} \sum_{i=1}^{N} \Delta z_i \theta_i \quad [A45]$$

A3.7 JULES

There are two options in JULES to account for the spatial heterogeneity of soil water content and thus determine F_{sat}. The first option is based on a modified form of TOPMODEL (Beven and Kirkby, 1979), described by Gedney and Cox (2003), where the assumption of an exponential decay of K_s with depth (leading to Eq. [A24–A25]) is relaxed. Grid box mean water table depth, z_∇, is calculated using the approach described for A3.0 TOPMODEL (Eq. [A27–A29]). This is used to estimate a critical topographic index λ_{crit} using the relation

$$\lambda_{crit} = \ln\left[\frac{T(0)}{T(z_\nabla)}\right] + \lambda_m \quad [A46]$$

where transmissivity $T(z_\nabla)$ is given by

$$T(z_\nabla) = \int_z^\infty K_s(z) dz \quad [A47]$$

The value of F_{sat} is then calculated as the fraction of the grid box for which $\lambda > \lambda_{crit}$, assuming λ follows a γ distribution with mean (λ_m) and standard deviation read in from observational datasets. To speed up the computation, the integral over the probability distribution of λ is calculated for a range of mean water table depths during model initialization and approximated by an exponential function as

$$F_{sat} = a_s \exp\left(-c_s \lambda_{crit}\right) \quad [A48]$$

where a_s and c_s are fitted to approximate the full integral (i.e., Eq. [A24]). Recently, this scheme has been modified to account for the impact of frozen water in the soil by replacing K_s in Eq. [A47] by $(1 - \theta_f)^{2b+3} K_s$ (where b is the Brooks–Corey parameter and θ_f is the frozen water content) and additionally correcting the grid box mean water table depth (z_∇) to account for the fact that the profile of soil moisture above the water table will not follow the same equilibrium profile (assumed in Eq. [A29]) when ice is present. The second option for calculating F_{sat} is the use of the probability distributed model of Moore (1985) (see Eq. [38]).

A3.8 CLM 4.5

In CLM 4.5 (Lawrence et al., 2011; Oleson et al., 2013), the fraction of the saturated area, F_{sat} is calculated as

$$F_{sat} = F_{max}\exp(-0.5 f_d z_\nabla) \quad [A49]$$

where F_{max} is the maximum value of F_{sat} and f_d is the decay factor [L^{-1}]; F_{max} is defined as the fraction of subgrid cells from a high-resolution digital elevation map in a grid cell whose topographic index (the ratio of the upstream area to the slope; Niu et al., 2005) is larger than or equal to the grid cell mean topographic index. It is the value of the discrete cumulative distribution function of the topographic index when the grid cell mean water table depth is zero.

A3.9 CABLE

The original CABLE model (version 2, Kowalczyk et al., 2013) generates surface runoff from excess infiltration only when the first three soil layers are at least 95% saturated. There is no other surface runoff generation process. However, Decker (2015) implemented subgrid-scale soil water content variability, explicit runoff generation, and groundwater in CABLE. The fraction of the saturated area, F_{sat}, follows Entekhabi and Eagleson (1989) and is defined as

$$F_{sat} = \int_{\kappa_p}^{\infty} f(s)\mathrm{d}s \quad [A50]$$

where $f(s)$ is the Gamma distribution of Eq. [42], and κ_p is defined by Eq. [A53]. One can solve this integral assuming a constant α_c in Eq. [42], which then links $s = (\theta - \theta_r)/(\theta_s - \theta_r)$, the mean of the vertically averaged relative saturation over the grid cell, with λ_s due to the properties of the Gamma distribution (Eq. [42]):

$$\lambda_s = \frac{1}{2s} \quad [A51]$$

For $\alpha_c = 1/2$,

$$F_{sat} = 1 - \mathrm{erf}\left(\sqrt{\frac{\kappa_p}{\lambda_s}}\right) \quad [A52]$$

Finally, κ_p is parameterized by an empirical formulation as

$$\kappa_p = C_v \sigma_{slope} \quad [A53]$$

with C_v as a fitting parameter and σ_{slope} as the standard deviation of the subgrid slope.

Haverd et al. (2016) and Cuntz and Haverd (2018) recently implemented a new soil (Haverd and Cuntz, 2010) and snow model with physically accurate freeze–thaw processes within CABLE, which is currently combined with the developments of Decker (2015).

A3.10 SSiB

In the SSiB model, the normalized runoff I_{roff} is spatially distributed as a function of the fractional area of grid area x ($0 < x < 1$) (Sato et al., 1989):

$$I_{roff}(x) = a_{SSiB}\exp(-b_{SSiB}x) + c_{SSiB} \quad [A54]$$

where a_{SSiB}, b_{SSiB}, and c_{SSiB} are constants. This distribution has also been applied to the convective precipitation. The constants (a, b, and c) were obtained by comparison with the observational data and are normalized so that

$$\int_0^1 I_{roff}(x)\mathrm{d}x = 1 \quad [A55]$$

Based on the above two spatial distributions, the saturation fraction, F_{sat}, could be obtained (Sato et al., 1989) as

$$F_{sat} = \frac{1}{b_{SSiB}}\log\left(\frac{K_s \Delta t}{P_{drop} a_{SSiB}}\right) - \frac{c_{SSiB}}{a_{SSiB}} \quad [A56]$$

where K_s is the saturated hydraulic conductivity [$L\ T^{-1}$], Δt is the time interval [T], and P_{drop} is the precipitation reaching the surface after interception by the canopy [$L\ T^{-1}$]. The spatial distribution of convective precipitation has also been applied to obtain the value of P_{drop} (Sellers et al., 1996).

A3.12 JSBACH

JSBACH uses the original Arno scheme (Dümenil and Todini, 1992) to determine surface runoff and infiltration. Accordingly, the saturated fraction is estimated for the grid box fraction for which the soil water capacity of the root zone is less than or equal to the grid box mean root zone soil moisture. The shape parameter b is determined using Eq. [45].

Appendix A4

Use of Pedotransfer Functions for the Estimation of Saturated Hydraulic Conductivity

For soils with low organic C content, Noah-MP and CLM 4.5 use the PTFs developed at point scale by Clapp and Hornberger (1978) and Cosby et al. (1984) to estimate K_s. In ISBA-SURFEX, K_s is related to the soil textural properties (clay and sand) using the Noilhan and Lacarrère (1995) continuous relationships derived from theses PTFs. These PTFs are basically class PTFs (Van Looy et al., 2017) that give average values of Brooks–Corey parameters and the measured K_s for each textural class of the USDA classification and are also developed at point scale.

Soil classes in CLSM are parameterized by Campbell (1974) equations, and the corresponding hydraulic parameters including K_s are based on lookup tables for 12 different soil textural classes or using the PTFs of Wösten et al. (2001), which are both developed at the point scale. Campbell's method used the Brooks–Corey parameterization of the soil water retention curve and a single point measurement of K at a given water content to calculate the complete hydraulic conductivity function.

None of the models directly considers the effect of soil structure on saturated hydraulic conductivity. Only OLAM-SOIL considers implicitly the impact of structural properties on K_s by linearly interpolating between the measured K_s value and the value of the hydraulic conductivity obtained at a pressure head of about −6 cm as proposed by Weynants et al. (2009). Based on the work of Jarvis (2007), this value was considered to delineate the saturation range that is controlled by structural properties.

In JSBACH, K_s values are assigned to 11 textural classes based on data presented by Beringer et al. (2001). However, the origin of the tabulated K_s values, which appear to be mean measured values for a specific textural class, is not clear. Most likely, they were derived from the dataset of Clapp and Hornberger (1978).

JULES uses sand and clay content to estimate the K_s for the main soil column. Below the soil column is an additional "deep water store," within which K_s decreases exponentially with depth, with a dampening factor set equal to 3 as proposed by Clark and Gedney (2008). The K_s values can also be defined for each soil layer and can account for the presence of soil organic matter (Chadburn et al., 2015a). Rahman and Rosolem (2017) incorporated the effect of preferential flow into JULES (but note that this has not yet been adopted in the current "official" UKMO version of JULES) to allow simulation of highly fractured unsaturated chalk soils. Their bulk hydraulic conductivity (BC) model introduces only two additional parameters (namely the macroporosity factor and the soil wetness threshold parameter for fracture flow activation) and uses the K_s from the chalk matrix. The BC model was implemented into JULES and applied to a study area encompassing the Kennet catchment in the southern UK, and the model performance at the catchment scale was evaluated against independent datasets (e.g., runoff and latent heat flux). The results demonstrated that the inclusion of the BC model in JULES improved the simulations of land surface water and energy fluxes across the chalk-dominated Kennet catchment. This simple approach to account for soil structure has potential for large-scale land surface modeling applications. ORCHIDEE uses van Genuchten soil parameters (K_s, n, α, θ_r, and θ_s) for each USDA class. In addition, a decay of K_s with depth is imposed (as also in JULES), as described above. With respect to the horizontal variability, ORCHIDEE uses an exponential PDF to describe horizontal heterogeneity.

Acknowledgments

This review emerged from discussions among the GEWEX-SoilWat community held at the workshop in Leipzig (Germany) in 2016 and is a product of the International Soil Modeling Consortium (ISMC) effort. We would like to thank Randal Koster (NASA-GMAO) for discussion of CLSM parts.

References

Abramopoulos, F., C. Rosenzweig and B. Choudhury. 1988. Improved ground hydrology calculations for global climate models (GCMs): Soil water movement and evapotranspiration. J. Climate 1:921–941. doi:10.1175/1520-0442(1988)001<0921:ighcfg>2.0.co;2

Adem, H.H., and S.K. Vanapalli. 2015. Review of methods for predicting in situ volume change movement of expansive soil over time. J. Rock Mech. Geotech. Eng. 7:73–86. doi:10.1016/j.jrmge.2014.11.002

Ahuja, L.R. 1974. Applicability of the Green–Ampt approach to water infiltration through surface crust. Soil Sci. 118:283–288. doi:10.1097/00010694-197411000-00001

Ahuja, L.R. 1983. Modeling infiltration into crusted soils by the Green–Ampt approach. Soil Sci. Soc. Am. J. 47:412–418. doi:10.2136/sssaj1983.03615995004700030004x

Ahuja, L.R., D.K. Cassel, R.R. Bruce, and B.B. Barnes. 1989. Evaluation of spatial distribution of hydraulic conductivity using effective porosity data. Soil Sci. 148:404–411. doi:10.1097/00010694-198912000-00002

Ahuja, L.R., F. Fiedler, G.H. Dunn, J.G. Benjamin, and A. Garrison. 1998. Changes in soil water retention curves due to tillage and natural reconsolidation. Soil Sci. Soc. Am. J. 62:1228–1233. doi:10.2136/sssaj1998.03615995006200050011x

Alaoui, A., J. Lipiec, and H.H. Gerke. 2011. A review of the changes in the soil pore system due to soil deformation: A hydrodynamic perspective. Soil Tillage Res. 115-116:1–15. doi:10.1016/j.still.2011.06.002

Anwar, S.A., A.S. Zakey, S.M. Robaa, and M.M. Abdel Wahab. 2018. The influence of two land-surface hydrology schemes on the regional climate of Africa using the RegCM4 model. Theor. Appl. Climatol. doi:10.1007/s00704-018-2556-8

Archer, N.A.L., M. Bonell, N. Coles, A.M. MacDonald, C.A. Auton, and R. Stevenson. 2013. Soil characteristics and landcover relationships on soil hydraulic conductivity at a hillslope scale: A view towards local flood management. J. Hydrol. 497:208–222. doi:10.1016/j.jhydrol.2013.05.043

Archer, N.A.L., J.N. Quinton, and T.M. Hess. 2012. Patch vegetation and water redistribution above and below ground in south-east Spain. Ecohydrology 5:108–120. doi:10.1002/eco.210

Arnold, J.G., K.N. Potter, K.W. King, and P.M. Allen. 2005. Estimation of soil cracking and the effect on surface runoff in a Texas Blackland Prairie watershed. Hydrol. Processes 19:589–603. doi:10.1002/hyp.5609

Assouline, S. 2004. Rainfall-induced soil surface sealing: A critical review of observations, conceptual models, and solutions. Vadose Zone J. 3:570–591. doi:10.2136/vzj2004.0570

Assouline, S. 2006a. Modeling the relationship between soil bulk density and the hydraulic conductivity function. Vadose Zone J. 5:697–705. doi:10.2136/vzj2005.0084

Assouline, S. 2006b. Modeling the relationship between soil bulk density and the water retention curve. Vadose Zone J. 5:554–563. doi:10.2136/vzj2005.0083

Assouline, S. 2013. Infiltration into soils: Conceptual approaches and solutions. Water Resour. Res. 49:1755–1772. doi:10.1002/wrcr.20155

Assouline, S. and M. Ben-Hur. 2006. Effects of rainfall intensity and slope gradient on the dynamics of interrill erosion during soil surface sealing. doi:10.1016/j.catena.2006.02.005

Assouline, S. and Y. Mualem. 2002. Infiltration during soil sealing: The effect of areal heterogeneity of soil hydraulic properties. Water Resour Res 38(12):1286. doi:10.1029/2001WR001168

Assouline, S., and Y. Mualem. 2006. Runoff from heterogeneous small bare catchments during soil surface sealing. Water Resour. Res. 42:W12405. doi:10.1029/2005WR004592

Assouline, S., and K. Narkis. 2011. Effects of long-term irrigation with treated wastewater on the hydraulic properties of a clayey soil. Water Resour. Res. 47:W08530. doi:10.1029/2011WR010498

Assouline, S., K. Narkis, R. Gherabli, and G. Sposito. 2016. Combined effect of sodicity and organic matter on soil properties under long-term irrigation with treated wastewater. Vadose Zone J. 15(4). doi:10.2136/vzj2015.12.0158

Assouline, S., and D. Or. 2008. Air entry–based characteristic length for estimation of permeability of variably compacted earth materials. Water Resour. Res. 44:W11403. doi:10.1029/2008WR006937

Assouline, S., and D. Or. 2013. Conceptual and parametric representation of soil hydraulic properties: A review. Vadose Zone J. 12(4). doi:10.2136/vzj2013.07.0121

Assouline, S., J.S. Selker, and J.-Y. Parlange. 2007. A simple accurate method to predict time of ponding under variable intensity rainfall. Water Resour. Res. 43:W03426. doi:10.1029/2006WR005138

Assouline, S., S.E. Thompson, L. Chen, T. Svoray, S. Sela, and G.G. Katul. 2015. The dual role of soil crusts in desertification. J. Geophys. Res. Biogeosci. 120:2108–2119. doi:10.1002/2015JG003185

Bachmann, J., and R.R. van der Ploeg. 2002. A review on recent developments in soil water retention theory: Interfacial tension and temperature effects. J. Plant Nutr. Soil Sci. 165:468–478. doi:10.1002/1522-2624(200208)165:4<468::AID-JPLN468>3.0.CO;2-G

Balsamo, G., A. Beljaars, K. Scipal, P. Viterbo, B. van den Hurk, M. Hirschi, and A.K. Betts. 2009. A revised hydrology for the ECMWF model: Verification from field site to terrestrial water storage and impact in the integrated forecast system. J. Hydrometeorol. 10:623–643. doi:10.1175/2008JHM1068.1

Barry, D.A., J.-Y. Parlange, R. Haverkamp, and P.J. Ross. 1995. Infiltration under ponded conditions: 4. Explicit predictive infiltration formula. Soil Sci. 160:8–17. doi:10.1097/00010694-199507000-00002

Barry, D.A., J.-Y. Parlange, L. Li, D.-S. Jeng, and M. Crapper. 2005. Green Ampt approximations. Adv. Water Resour. 28:1003–1009. doi:10.1016/j.advwatres.2005.03.010

Barry, D.A., J.-Y. Parlange, M.-C. Liu, G.C. Sander, M.B. Parlange, D.A. Lockington, et al. 2007. Infiltration and ponding. In: J.A. Filar, editor, Encyclopedia of life support systems: Mathematical sciences. Mathematical modeling. Vol. II. EOLSS Publ., Oxford, UK.

Batjes, N.H. 2006. ISRIC-WISE derived soil properties on a 5 by 5 arc-minutes global grid. Rep. 2006/02. ISRIC World Soil Inf., Wageningen, the Netherlands.

Baumhardt, R.L., M.J.M. Römkens, F.D. Whisler, and J.-Y. Parlange. 1990. Modeling infiltration into a sealing soil. Water Resour. Res. 26:2497–2505. doi:10.1029/WR026i010p02497

Bear, J. 1972. Dynamics of fluids in porous media. Elsevier, New York.

Bechtold, M., G.J.M. De Lannoy, R.D. Koster, R.H. Reichle, S. Mahanama, W. Bleuten, et al. PEAT-CLSM: A specific treatment of peatland hydrology in the NASA Catchment Land Surface model. J. Adv. Model. Earth Syst. doi:10.1029/2018MS001574

Beck, H.E., A. van Dijk, A. de Roo, E. Dutra, G. Fink, R. Orth, and J. Schellekens. 2017. Global evaluation of runoff from 10 state-of-the-art hydrological models. Hydrol. Earth Syst. Sci. 21:2881–2903. doi:10.5194/hess-21-2881-2017

Bengough, A. 2012. Water dynamics of the root zone: Rhizosphere biophysics and its control on soil hydrology. Vadose Zone J. 11(2). doi:10.2136/vzj2011.0111

Ben Neriah, A., S. Assouline, U. Shavit, and N. Weisbrod. 2014. Impact of ambient conditions on evaporation from porous media. Water Resour. Res. 50:6696–6712. doi:10.1002/2014WR015523

Beringer, J., A.H. Lynch, F.S. Chapin, M. Mack and G.B. Bonan. 2001. The representation of arctic soils in the land surface model: The importance of mosses. J. Climate 14:3324–3335. doi:10.1175/1520-0442(2001)014<3324:Troasi>2.0.Co;2

Best, M.J., P. Cox, and D. Warrilow. 2005. Determining the optimal soil temperature scheme for atmospheric modeling applications. Boundary-Layer Meteorol. 114:111–142. doi:10.1007/s10546-004-5075-3

Best, M.J., M. Pryor, D.B. Clark, G.G. Rooney, R.L.H. Essery, C.B. Menard, et al. 2011. The Joint UK Land Environment Simulator (JULES), model description: 1. Energy and water fluxes. Geosci. Model Dev. 4:677–699. doi:10.5194/gmd-4-677-2011

Betson, R.P., and J.B. Marius. 1969. Source areas of storm runoff. Water Resour. Res. 5:574–582. doi:10.1029/WR005i003p00574

Beven, K. 1984. Infiltration into a class of vertically non-uniform soils. Hydrol. Sci. J. 29:425–434. doi:10.1080/02626668409490960

Beven, K., and P. Germann. 1982. Macropores and water flow in soils. Water Resour. Res. 18:1311–1325. doi:10.1029/WR018i005p01311

Beven, K.J. and M.J. Kirkby. 1979. A physically based, variable contributing area model of basin hydrology. Hydrol. Sci. Bull. 24:43–69.

Bierkens, M.F.P. 2015. Global hydrology 2015: State, trends, and directions. Water Resour. Res. 51:4923–4947. doi:10.1002/2015WR017173

Bisal, F., and K.F. Nielsen. 1967. Effect of frost action on the size of soil aggregates. Soil Sci. 104:268–272. doi:10.1097/00010694-196710000-00006

Bonan, G.B. 1998. The land surface climatology of the NCAR Land Surface Model coupled to the NCAR Community Climate Model. J. Climate 11:1307–1326. doi:10.1175/1520-0442(1998)011<1307:Tlscot>2.0.Co;2

Bonan, G.B., K.W. Oleson, M. Vertenstein, S. Levis, X.B. Zeng, Y.J. Dai, et al. 2002. The land surface climatology of the Community Land Model coupled to the NCAR Community Climate Model. J. Climate 15:3123–3149. doi:10.1175/1520-0442(2002)015<3123:Tlscot>2.0.Co;2

Boone, A., V. Masson, T. Meyers, and J. Noilhan. 2000. The influence of the inclusion of soil freezing on simulations by a soil–vegetation–atmosphere transfer scheme. J. Appl. Meteorol. 39:1544–1569. doi:10.1175/1520-0450(2000)039<1544:TIOTIO>2.0.CO;2

Boone, A., and P.J. Wetzel. 1999. A simple method for modeling sub-grid soil texture variability for use in an atmospheric climate model. J. Meteorol. Soc. Jpn. 77:317–333. doi:10.2151/jmsj1965.77.1B_317

Boussetta, S., G. Balsamo, A. Beljaars, A.-A. Panareda, J.-C. Calvet, C. Jacobs, et al. 2013. Natural land carbon dioxide exchanges in the ECMWF integrated forecasting system: Implementation and offline validation. J. Geophys. Res. Atmos. 118:5923–5946. doi:10.1002/jgrd.50488

Bouwer, H. 1964. Unsaturated flow in ground-water hydraulics. J. Hydraul. Eng. 90(HY5):121–144.

Brakensiek, D.L., and W.J. Rawls. 1983. Agricultural management effects on water processes: II. Green and Ampt parameters for crusting soils. Trans. ASAE 26:1753–1757. doi:10.13031/2013.33838

Bresler, E. 1973. Simultaneous transport of solutes and water under transient unsaturated flow conditions. Water Resour. Res. 9:975–986. doi:10.1029/WR009i004p00975

Bresler, E., and R. Hanks. 1969. Numerical method for estimating simultaneous flow of water and salt in unsaturated soils. Soil Sci. Soc. Am. J. 33:827–832. doi:10.2136/sssaj1969.03615995003300060013x

Bresler, E., B.L. McNeal, and D.L. Carter. 1982. Saline and sodic soils: Principles–dynamics–modeling. Springer, Berlin. doi:10.1007/978-3-642-68324-4

Bronick, C.J., and R. Lal. 2005. Soil structure and management: A review. Geoderma 124:3–22. doi:10.1016/j.geoderma.2004.03.005

Bronswijk, J.J.B. 1991. Relation between vertical soil movements and water-content changes in cracking clays. Soil Sci. Soc. Am. J. 55:1220–1226. doi:10.2136/sssaj1991.03615995005500050004x

Brooks, R., and A. Corey. 1964. Hydraulic properties of porous media. Hydrol. Pap. 3. Colorado State Univ., Fort Collins.

Brown, G.G., I. Barois, and P. Lavelle. 2000. Regulation of soil organic matter dynamics and microbial activity in the drilosphere and the role of interactions with other edaphic functional domains. Eur. J. Soil Biol. 36:177–198. doi:10.1016/S1164-5563(00)01062-1

Brutsaert, W. 2005. Hydrology: An introduction. Cambridge Univ. Press, Cambridge, UK. doi:10.1017/CBO9780511808470

Buckingham, E. 1907. Studies on the movement of soil moisture. Bureau of Soils Bull. 38. US Gov. Print. Office, Washington, DC.

Busscher, W. 2011. Hardpan soils: Management. Springer, Dordrecht, the Netherlands.

Cai, X.T., Z.L. Yang, Y.L. Xia, M.Y. Huang, H.L. Wei, L.R. Leung, and M.B. Ek. 2014. Assessment of simulated water balance from Noah, Noah-MP, CLM, and VIC over CONUS using the NLDAS test bed. J. Geophys. Res. Atmos. 119:13751–13770. doi:10.1002/2014JD022113

Campbell, G.S. 1974. Simple method for determining unsaturated conductivity from moisture retention data. Soil Sci. 117:311–314. doi:10.1097/00010694-197406000-00001

Carsel, R.F., and R.S. Parrish. 1988. Developing joint probability distributions of soil water retention characteristics. Water Resour. Res. 24:755–769. doi:10.1029/WR024i005p00755

Celia, M.A., E.T. Bouloutas, and R.L. Zarba. 1990. A general mass-conservative numerical solution for the unsaturated flow equation. Water Resour. Res. 26:1483–1496. doi:10.1029/WR026i007p01483

Chadburn, S., E. Burke, R. Essery, J. Boike, M. Langer, M. Heikenfeld, et al. 2015a. An improved representation of physical permafrost dynamics in the JULES land-surface model. Geosci. Model Dev. 8:1493–1508. doi:10.5194/gmd-8-1493-2015

Chadburn, S.E., E.J. Burke, R.L.H. Essery, J. Boike, M. Langer, M. Heikenfeld, et al. 2015b. Impact of model developments on present and future simulations of permafrost in a global land-surface model. Cryosphere 9:1505–1521. doi:10.5194/tc-9-1505-2015

Chamberlain, E.J., and A.J. Gow. 1979. Effect of freezing and thawing on the permeability and structure of soils. Eng. Geol. 13:73–92. doi:10.1016/0013-7952(79)90022-X

Chen, J. and P. Kumar. 2001. Topographic influence on the seasonal and interannual variation of water and energy balance of basins in North America. J. Climate 14:1989–2014. doi:10.1175/1520-0442(2001)014<1989:Tiotsa>2.0.Co;2

Childs, E.C. 1969. An introduction to the physical basis of soil water phenomena. John Wiley & Sons, New York.

Childs, E.C., and M. Bybordi. 1969. The vertical movement of water in stratified porous material: 1. Infiltration. Water Resour. Res. 5:446–459. doi:10.1029/WR005i002p00446

Choi, H.I., P. Kumar, and X.Z. Liang. 2007. Three-dimensional volume-averaged soil moisture transport model with a scalable parameterization of subgrid topographic variability. Water Resour. Res. 43:W04414. doi:10.1029/2006WR005134

Chow, V.T., D.R. Maidment, and L.W. Mays. 1988. Applied hydrology. McGraw-Hill, Singapore.

Chu, S.T., C.A. Onstad, and W.J. Rawls. 1986. Field evaluation of layered Green–Ampt model for transient crust conditions. Trans. ASAE 29:1268–1272. doi:10.13031/2013.30307

Chu, X., and M.A. Marino. 2005. Determination of ponding condition and infiltration in layered soils under unsteady rainfall. J. Hydrol. 313:195–207. doi:10.1016/j.jhydrol.2005.03.002

Clapp, R.B., and G.M. Hornberger. 1978. Empirical equations for some soil hydraulic properties. Water Resour. Res. 14:601–604. doi:10.1029/WR014i004p00601

Clark, D.B., and N. Gedney. 2008. Representing the effects of subgrid variability of soil moisture on runoff generation in a land surface model. J. Geophys. Res. Atmos. 113:D10111. doi:10.1029/2007JD008940

Clark, D.B., L.M. Mercado, S. Sitch, C.D. Jones, N. Gedney, M.J. Best, et al. 2011. The Joint UK Land Environment Simulator (JULES), model description: 2. Carbon fluxes and vegetation dynamics. Geosci. Model Dev. 4:701–722. doi:10.5194/gmd-4-701-2011

Clark, M.P., Y. Fan, D.M. Lawrence, J.C. Adam, D. Bolster, D.J. Gochis, et al. 2015. Improving the representation of hydrologic processes in earth system models. Water Resour. Res. 51:5929–5956. doi:10.1002/2015WR017096

Clothier, B.E. 2001. Infiltration. In: K.A. Smith and C.E. Mullins, editors, Soil and environmental analysis: Physical methods. 2nd ed. Marcel Dekker, New York. p. 239–280.

Colman, E.A., and G.B. Bodman. 1945. Moisture and energy conditions during downward entry of water into moist and layered soils. Soil Sci. Soc. Am. Proc. 9:3–11. doi:10.2136/sssaj1945.036159950009000C0001x

Corradini, C., A. Flammini, R. Morbidelli, and R.S. Govindaraju. 2011. A conceptual model for infiltration in two-layered soils with a more permeable upper layer: From local to field scale. J. Hydrol. 410:62–72. doi:10.1016/j.jhydrol.2011.09.005

Corradini, C., R.S. Govindaraju, and R. Morbidelli. 2002. Simplified modelling of areal average infiltration at the hillslope scale. Hydrol. Processes 16:1757–1770. doi:10.1002/hyp.394

Corradini, C., F. Melone, and R.E. Smith. 1994. Modeling infiltration during complex rainfall sequences. Water Resour. Res. 30:2777–2784. doi:10.1029/94WR00951

Corradini, C., F. Melone, and R.E. Smith. 1997. A unified model for infiltration and redistribution during complex rainfall patterns. J. Hydrol. 192:104–124. doi:10.1016/S0022-1694(96)03110-1

Cosby, B.J., G.M. Hornberger, R.B. Clapp, and T.R. Ginn. 1984. A statistical exploration of the relationships of soil moisture characteristics to the physical properties of soils. Water Resour. Res. 20:682–690. doi:10.1029/WR020i006p00682

Cosh, M.H., J.R. Stedinger, and W. Brutsaert. 2004. Variability of surface soil moisture at the watershed scale. Water Resour. Res. 40:W12513. doi:10.1029/2004WR003487

Craig, J.R., G. Liu, and E.D. Soulis. 2010. Runoff–infiltration partitioning using an upscaled Green–Ampt solution. Hydrol. Processes 24:2328–2334. doi:10.1002/hyp.7601

Crockford, H., S. Topalidis, and D.P. Richardson. 1991. Water repellency in a dry sclerophyll eucalypt forest: Measurements and processes. Hydrol. Processes 5:405–420. doi:10.1002/hyp.3360050408

Cueto-Felgueroso, L., and R. Juanes. 2009. A phase field model of unsaturated flow. Water Resour. Res. 45:W10409. doi:10.1029/2009WR007945

Cuntz, M., and V. Haverd. 2018. Physically accurate soil freeze–thaw processes in a global land surface scheme. J. Adv. Model. Earth Syst. 10:54–77. doi:10.1002/2017MS001100

Cuntz, M., J. Mai, L. Samaniego, M. Clark, V. Wulfmeyer, O. Branch, et al. 2016. The impact of standard and hard-coded parameters on the hydrologic fluxes in the Noah-MP land surface model. J. Geophys. Res. Atmos. 121:10676–10700. doi:10.1002/2016JD025097

Dagan, G., and E. Bresler. 1983. Unsaturated flow in spatially variable fields: 1. Derivation of models of infiltration and redistribution. Water Resour. Res. 19:413–420. doi:10.1029/WR019i002p00413

Dahan, O., B. Tatarsky, Y. Enzel, C. Kulls, M. Seely, and G. Benito. 2008. Dynamics of flood water infiltration and ground water recharge in hyperarid desert. Groundwater 46:450–461. doi:10.1111/j.1745-6584.2007.00414.x

Darcy, H. 1856. Les fontaines publiques de la ville de Dijon: Exposition et application des principes a suivre et des formulesa employer dans les questions de distribution d'eau. V. Dalmont, Paris.

Das, N.N., B.P. Mohanty, and E.G. Njoku. 2008. A Markov chain Monte Carlo algorithm for upscaled soil–vegetation–atmosphere-transfer modeling to evaluate satellite-based soil moisture measurements. Water Resour. Res. 44:W05416. doi:10.1029/2007WR006472

Davidson, J., D. Nielsen, and J.W. Biggar. 1963. The measurement and description of water flow through Columbia silt loam and Hesperia sandy loam. Hilgardia 34:601–617. doi:10.3733/hilg.v34n15p601

Davidson, S.E., and J.B. Page. 1956. Factors influencing swelling and shrinking in soils. Soil Sci. Soc. Am. J. 20:320–324. doi:10.2136/sssaj1956.03615995002000030007x

de Boer, F. 2016. HiHydroSoil: A high resolution soil map of hydraulic properties, Version 1.2. FutureWater Rep. 134. FutureWater, Wageningen, the Netherlands.

Decharme, B., A. Boone, C. Delire, and J. Noilhan. 2011. Local evaluation of the Interaction between Soil Biosphere Atmosphere soil multilayer diffusion scheme using four pedotransfer functions. J. Geophys. Res. 116:D20126. doi:10.1029/2011jd016002

Decharme, B., E. Brun, A. Boone, C. Delire, P. Le Moigne, and S. Morin. 2016. Impacts of snow and organic soils parameterization on northern Eurasian soil temperature profiles simulated by the ISBA land surface model. Cryosphere 10:853–877. doi:10.5194/tc-10-853-2016

Decharme, B., and H. Douville. 2006. Introduction of a sub-grid hydrology in the ISBA land surface model. Clim. Dyn. 26:65–78. doi:10.1007/s00382-005-0059-7

Decharme, B., E. Martin, and S. Faroux. 2013. Reconciling soil thermal and hydrological lower boundary conditions in land surface models. J. Geophys. Res. Atmos. 118:7819–7834. doi:10.1002/jgrd.50631

Decker, M. 2015. Development and evaluation of a new soil moisture and runoff parameterization for the CABLE LSM including subgrid-scale processes. J. Adv. Model. Earth Syst. 7:1788–1809. doi:10.1002/2015MS000507

De Lannoy, G.J.M., R.D. Koster, R.H. Reichle, S.P.P. Mahanama, and Q. Liu. 2014. An updated treatment of soil texture and associated hydraulic properties in a global land modeling system. J. Adv. Model. Earth Syst. 6:957–979. doi:10.1002/2014MS000330

Delleur, J.W. 2006. The handbook of groundwater engineering. CRC Press, Boca Raton, FL.

Demaria, E.M., B. Nijssen, and T. Wagener. 2007. Monte Carlo sensitivity analysis of land surface parameters using the Variable Infiltration Capacity model. J. Geophys. Res. Atmos. 112:D11113. doi:10.1029/2006JD007534

de Rosnay, P., J. Polcher, M. Bruen and K. Laval. 2002. Impact of a physically based soil water flow and soil–plant interaction representation for modeling large-scale land surface processes. J. Geophys. Res. 107(D11). doi:10.1029/2001JD000634.

DiCarlo, D.A. 2004. Experimental measurements of saturation overshoot on infiltration. Water Resour. Res. 40: W04215. doi:10.1029/2003WR002670

DiCarlo, D.A. 2013. Stability of gravity-driven multiphase flow in porous media: 40 Years of advancements. Water Resour. Res. 49:4531–4544. doi:10.1002/wrcr.20359

Dinka, T.M., and R.J. Lascono. 2012. Review paper: Challenges and limitations in studying the shrink–swell and crack dynamics of Vertisol soils. Open J. Soil Sci. 2:82–90. doi:10.4236/ojss.2012.22012

Dirmeyer, P.A., and F.R.J. Zeng. 1999. Precipitation infiltration in the simplified SiB land surface scheme. J. Meteorol. Soc. Jpn. 77:291–303. doi:10.2151/jmsj1965.77.1B_291

Doerr, S.H., R.A. Shakesby, and R.P.D. Walsh. 2000. Soil water repellency: Its causes, characteristics and hydro-geomorphological significance. Earth Sci. Rev. 51:33–65. doi:10.1016/S0012-8252(00)00011-8

Doerr, S.H. and A.D. Thomas. 2000. The role of soil moisture in controlling water repellency: New evidence from forest soils in Portugal. J. Hydrol. 231–232:134–147. doi:10.1016/S0022-1694(00)00190-6

d'Orgeval, T., J. Polcher, and P. de Rosnay. 2008. Sensitivity of the West African hydrological cycle in ORCHIDEE to infiltration processes. Hydrol. Earth Syst. Sci. 12:1387–1401. doi:10.5194/hess-12-1387-2008

Ducharne, A., R.D. Koster, M.J. Suarez, M. Stieglitz, and P. Kumar. 2000. A catchment-based approach to modeling land surface processes in a general circulation model: 2. Parameter estimation and model demonstration. J. Geophys. Res. 105(D20):24823–24838. doi:10.1029/2000JD900328

Ducharne, A., K. Laval, and J. Polcher. 1998. Sensitivity of the hydrological cycle to the parameterization of soil hydrology in a GCM. Clim. Dyn. 14:307–327. doi:10.1007/s003820050226

Ducharne, A., C. Ottlé, F. Maignan, N. Vuichard, J. Ghattas, F. Wang, et al. 2017. The hydrol module of ORCHIDEE: Scientific documentation [rev 3977] and on, work in progress, towards CMIP6v1. Tech. Rep. Inst. Pierre Simon Laplace, Paris.

Dümenil, L., and E. Todini. 1992. A rainfall–runoff scheme for the use in the Hamburg climate model. In: J.P. O'Kane, editor, Advances in theoretical hydrology: A tribute to James Dooge. Elsevier, Amsterdam. p. 129–157. doi:10.1016/B978-0-444-89831-9.50016-8

Dunkerley, D. 2012. Effects of rainfall intensity fluctuations on infiltration and runoff: Rainfall simulation on dryland soils, Fowlers Gap, Australia. Hydrol. Processes 26:2211–2224. doi:10.1002/hyp.8317

Dunkerley, D. 2017. An approach to analysing plot scale infiltration and runoff responses to rainfall of fluctuating intensity. Hydrol. Processes 31:191–206. doi:10.1002/hyp.10990

Dunne, T. 1978. Field studies of hillslope flow processes and their significance. In: M.J. Kirkby, editor, Hillslope hydrology. Wiley-Interscience, New York. p. 227–293.

Dunne, T., and R.D. Black. 1970. An experimental investigation of runoff production in permeable soils. Water Resour. Res. 6:478–490. doi:10.1029/WR006i002p00478

Edwards, L.M. 1991. The effect of alternate freezing and thawing on aggregate stability and aggregate size distribution of some Prince Edward Island soils. J. Soil Sci. 42:193–204. doi:10.1111/j.1365-2389.1991.tb00401.x

Egorov, A.G., R.Z. Dautov, J.L. Nieber, and A.Y. Sheshukov. 2003. Stability analysis of gravity-driven infiltrating flow. Water Resour. Res. 39:1266. doi:10.1029/2002WR001886

Eigenbrod, K.D. 1996. Effects of cyclic freezing and thawing on volume changes and permeabilities of soft fine-gained soils. Can. Geotech. J. 33:529–537. doi:10.1139/t96-079-301

Eliassi, M., and R.J. Glass. 2002. On the porous-continuum modeling of gravity-driven fingers in unsaturated materials: Extension of standard theory with a hold-back-pile-up effect. Water Resour. Res. 38(11):1234. doi:10.1029/2001WR001131

Entekhabi, D. and P.S. Eagleson. 1989. Land Surface hydrology parameterization for atmospheric general circulation models including subgrid scale spatial variability. J. Climate 2:816–831. doi:10.1175/1520-0442(1989)002<0816:lshpfa>2.0.co;2.

Everett, D.H. 1955. A general approach to hysteresis: 4. An alternative formulation of the domain model. Trans. Faraday Soc. 51:1551–1557. doi:10.1039/tf9555101551

Eyring, V., S. Bony, G.A. Meehl, C.A. Senior, B. Stevens, R.J. Stouffer, and K.E. Taylor. 2016. Overview of the Coupled Model Intercomparison Project Phase 6 (CMIP6) experimental design and organization. Geosci. Model Dev. 9:1937–1958. doi:10.5194/gmd-9-1937-2016

FAO. 1988. UNESCO soil map of the world, revised legend. World Resour. Rep. 60. FAO, Rome.

FAO. 2003. The digitized soil map of the world and derived soil properties. FAO Land and Water Digital Media Series 1. FAO, Rome.

FAO. 2009. Harmonized world soil database (version 1.1). FAO, Rome. http://webarchive.iiasa.ac.at/Research/LUC/External-World-soil-database/HTML/

Farrell, D.A., and W.E. Larson. 1972. Dynamics of the soil-water system during a rainstorm. Soil Sci. 113:88–95. doi:10.1097/00010694-197202000-00003

Feddes, R.A., E. Bresler, and S.P. Neuman. 1974. Field test of a modified numerical model for water uptake by root systems. Water Resour. Res. 10:1199–1206. doi:10.1029/WR010i006p01199

Flowers, M.D., and R. Lal. 1998. Axle load and tillage effects on soil physical properties and soybean grain yield on a Mollic Ochraqualf in northwest Ohio. Soil Tillage Res. 48:21–35. doi:10.1016/S0167-1987(98)00095-6

Fouli, Y., B.J. Cade-Menun, and H.W. Cutforth. 2013. Freeze–thaw cycles and soil water content effects on infiltration rate of three Saskatchewan soils. Can. J. Soil Sci. 93:485–496. doi:10.4141/cjss2012-060

Franzluebbers, A. 2002. Water infiltration and soil structure related to organic matter and its stratification with depth. Soil Tillage Res. 66:197–205. doi:10.1016/S0167-1987(02)00027-2

Frauenfeld, B., and C. Truman. 2004. Variable rainfall intensity effects on runoff and interrill erosion from two Coastal Plain Ultisols in Georgia. Soil Sci. 169:143–154. doi:10.1097/01.ss.0000117784.98510.46

Freeze, R.A. 1980. A stochastic-conceptual analysis of rainfall–runoff processes on a hillslope. Water Resour. Res. 16:391–408. doi:10.1029/WR016i002p00391

Frenkel, H., J.O. Goertzen, and J.D. Rhoades. 1978. Effects of clay type and content, exchangeable sodium percentage, and electrolyte concentration on clay dispersion and soil hydraulic conductivity. Soil Sci. Soc. Am. J. 42:32–39. doi:10.2136/sssaj1978.03615995004200010008x

Furman, A., A. Warrick, D. Zerihun, and C. Sanchez. 2006. Modified Kostiakov infiltration function: Accounting for Initial And Boundary Conditions. J. Irrig. Drain. Eng. 132:587–596. doi:10.1061/(ASCE)0733-9437(2006)132:6(587)

Gao, H., and M. Shao. 2015. Effects of temperature changes on soil hydraulic properties. Soil Tillage Res. 153:145–154. doi:10.1016/j.still.2015.05.003

Gardner, R. 1955. Relations of temperature to moisture tension of soils. Soil Sci. 79:257–266. doi:10.1097/00010694-195504000-00003

Gardner, W.R. 1960. Soil water relations in arid and semi-arid conditions. In: Arid Zone Research XVI: Plant–water relationships in arid and semi-arid conditions: Proceedings of the Madrid Symposium, Madrid, Spain. 24–30 Sept. 1959. UNESCO, Paris.

Garrote, L., and R.L. Bras. 1995. A distributed model for real-time flood forecasting using digital elevation models. J. Hydrol. 167:279–306. doi:10.1016/0022-1694(94)02592-Y

Gedney, N. and P.M. Cox. 2003. The sensitivity of global climate model simulations to the representation of soil moisture heterogeneity. J. Hydrometeorol. 4:1265–1275. doi:10.1175/1525-7541(2003)004<1265:Tsogcm>2.0.Co;2

Getirana, A., A. Boone, C. Peugeot, S. Boussetta, S. Ait-Mesbah, M. Anderson, et al. 2017. Streamflows over a West African basin from the ALMIP-2 model ensemble. J. Hydrometeorol. 18:1831–1845. doi:10.1175/JHM-D-16-0233.1

Getirana, A.C.V., E. Dutra, M. Guimberteau, J. Kam, H.-Y. Li, B. Decharme, et al. 2014. Water balance in the Amazon basin from a land surface model ensemble. J. Hydrometeorol. 15:2586–2614. doi:10.1175/JHM-D-14-0068.1

Ghanbarian, B., V. Taslimitehrani, G.Z. Dong, and Y.A. Pachepsky. 2015. Sample dimensions effect on prediction of soil water retention curve and saturated hydraulic conductivity. J. Hydrol. 528:127–137. doi:10.1016/j.jhydrol.2015.06.024

Giraldez, J.V., and G. Sposito. 1985. Infiltration in swelling soils. Water Resour. Res. 21:33–44. doi:10.1029/WR021i001p00033

Glass, R.J., T.S. Steenhuis, and J.-Y. Parlange. 1989. Mechanism for finger persistence in homogeneous, unsaturated, porous media: Theory and verification. Soil Sci. 148:60–70. doi:10.1097/00010694-198907000-00007

Gleeson, T., L. Smith, N. Moosdorf, J. Hartmann, H.H. Durr, A.H. Manning, et al. 2011. Mapping permeability over the surface of the Earth. Geophys. Res. Lett. 38:L02401. doi:10.1029/2010gl045565

Global Soil Data Task. 2014. Global soil data products CD-ROM contents (IGBP-DIS). [Dataset.] Oak Ridge Nat. Lab. Distributed Active Archive Ctr., Oak Ridge, TN. http://dx.doi.org/10.3334/ORNLDAAC/565.

Govindaraju, R.S., C. Corradini, and R. Morbidelli. 2006. A semi-analytical model of expected areal-average infiltration under spatial heterogeneity of rainfall and soil saturated hydraulic conductivity. J. Hydrol. 316:184–194. doi:10.1016/j.jhydrol.2005.04.019

Govindaraju, R.S., C. Corradini, and R. Morbidelli. 2012. Local- and field-scale infiltration into vertically non-uniform soils with spatially-variable surface hydraulic conductivities. Hydrol. Processes 26:3293–3301. doi:10.1002/hyp.8454

Govindaraju, R.S., R. Morbidelli, and C. Corradini. 2001. Areal infiltration modeling over soils with spatially correlated hydraulic conductivities. J. Hydrol. Eng. 6:150–158. doi:10.1061/(ASCE)1084-0699(2001)6:2(150)

Grant, S.A., and J. Bachmann. 2002. Effect of temperature on capillary pressure. In: P.A.C. Raats et al., editors, Environmental mechanics, water, mass and energy transfer in the biosphere. Geophys. Monogr. Ser. 129. Am. Geophys. Union, Washington, DC. p. 199–212. doi:10.1029/129GM18

Grant, S.A., and A. Salehzadeh. 1996. Calculation of temperature effects on wetting coefficients of porous solids and their capillary pressure functions. Water Resour. Res. 32:261–270. doi:10.1029/95WR02915

Green, W.H., and G. Ampt. 1911. Studies on soil physics. J. Agric. Sci. 4:1–24. doi:10.1017/S0021859600001441

Greene, R.S.B., and P.B. Hairsine. 2004. Elementary processes of soil–water interaction and thresholds in soil surface dynamics: A review. Earth Surf. Processes Landforms 29:1077–1091. doi:10.1002/esp.1103

Gudmundsson, L., L.M. Tallaksen, K. Stahl, D.B. Clark, E. Dumont, S. Hagemann, et al. 2012. Comparing large-scale hydrological model simulations to observed runoff percentiles in Europe. J. Hydrometeorol. 13:604–620. doi:10.1175/JHM-D-11-083.1

Habets, F., J. Noilhan, C. Golaz, J.P. Goutorbe, P. Lacarrère, E. Leblois, et al. 1999. The ISBA surface scheme in a macroscale hydrological model applied to the Hapex-Mobilhy area: II. Simulation of streamflows and annual water budget. J. Hydrol. 217:97–118. doi:10.1016/S0022-1694(99)00020-7

Habets, F., and G.M. Saulnier. 2001. Subgrid runoff parameterization. Phys. Chem. Earth, Part B 26:455–459. doi:10.1016/S1464-1909(01)00034-X

Hagemann, S., and L.D. Gates. 2003. Improving a subgrid runoff parameterization scheme for climate models by the use of high resolution data derived from satellite observations. Clim. Dyn. 21:349–359. doi:10.1007/s00382-003-0349-x

Hagemann, S., and T. Stacke. 2015. Impact of the soil hydrology scheme on simulated soil moisture memory. Clim. Dyn. 44:1731–1750. doi:10.1007/s00382-014-2221-6

Hailegeorgis, T.T., Y.S. Abdella, K. Alfredsen, and S. Kolberg. 2015. Evaluation of regionalization methods for hourly continuous streamflow simulation using distributed models in boreal catchments. J. Hydrol. Eng. 20(11). doi:10.1061/(ASCE)HE.1943-5584.0001218

Haines, W.B. 1930. Studies in the physical properties of soil: V. The hysteresis effect in capillary properties, and the modes of moisture distribution associated therewith. J. Agric. Sci. 20:97–116. doi:10.1017/S002185960008864X

Hamza, M.A., and W.K. Anderson. 2005. Soil compaction in cropping systems: A review of the nature, causes and possible solutions. Soil Tillage Res. 82:121–145. doi:10.1016/j.still.2004.08.009

Hanks, R.J., and S.A. Bowers. 1962. Numerical solution of the moisture flow equation for infiltration into layered soils. Soil Sci. Soc. Am. Proc. 26:530–534. doi:10.2136/sssaj1962.03615995002600060007x

Hanks, R.J., A. Klute, and E. Bresler. 1969. A numeric method for estimating infiltration, redistribution, drainage, and evaporation of water from soil. Water Resour. Res. 5:1064–1069. doi:10.1029/WR005i005p01064

Hannes, M., U. Wollschläger, T. Wöhling, and H.-J. Vogel. 2016. Revisiting hydraulic hysteresis based on long-term monitoring of hydraulic states in lysimeters. Water Resour. Res. 52:3847–3865. doi:10.1002/2015WR018319

Hansen, S., P. Abrahamsen, C.T. Petersen, and M. Styczen. 2012. Daisy: Model use, calibration, and validation. Trans. ASABE 55:1315–1333. doi:10.13031/2013.42244

Haverd, V., and M. Cuntz. 2010. Soil-Litter-Iso: A one-dimensional model for coupled transport of heat, water and stable isotopes in soil with a litter layer and root extraction. J. Hydrol. 388:438–455. doi:10.1016/j.jhydrol.2010.05.029

Haverd, V., M. Cuntz, L.P. Nieradzik, and I.N. Harman. 2016. Improved representations of coupled soil–canopy processes in the CABLE land surface model (Subversion revision 3432). Geosci. Model Dev. 9:3111–3122. doi:10.5194/gmd-9-3111-2016

Haverkamp, R., J.-Y. Parlange, R. Cuenca, P.J. Ross, and T.S. Steenhuis. 1998. Scaling of the Richards equation and its application to watershed modelling. In: G. Sposito, editor, Scale dependence and scale invariance in hydrology. Cambridge Univ. Press, Cambridge, UK. p. 190–223. doi:10.1017/CBO9780511551864.008

Haverkamp, R., J.-Y. Parlange, J. Starr, G. Schmitz, and C. Fuentes. 1990. Infiltration under ponded conditions: 3. A predictive equation based on physical parameters. Soil Sci. 149:292–300. doi:10.1097/00010694-199005000-00006

Healy, R.W. 2008. Simulating water, solute, and heat transport in the subsurface with the VS2DI software package. Vadose Zone J. 7:632–639. doi:10.2136/vzj2007.0075

Hengl, T., J.M. de Jesus, G.B.M. Heuvelink, M.R. Gonzalez, M. Kilibarda, A. Blagotic, et al. 2017. SoilGrids250m: Global gridded soil information based on machine learning. PLoS One 12. doi:10.1371/journal.pone.0169748

Hengl, T., J.M. de Jesus, R.A. MacMillan, N.H. Batjes, G.B.M. Heuvelink, E. Ribeiro, et al. 2014. SoilGrids1km: Global soil information based on automated mapping. PLoS One 9. doi:10.1371/journal.pone.0105992

Herbst, M., B. Diekkrüger, and J. Vanderborght. 2006. Numerical experiments on the sensitivity of runoff generation to the spatial variation of soil hydraulic properties. J. Hydrol. 326:43–58. doi:10.1016/j.jhydrol.2005.10.036

Hillel, D. 1980. Fundamentals of soil physics. Academic Press, San Diego.

Hillel, D. 1998. Environmental soil physics. Academic Press, San Diego.

Hillel, D., and W.R. Gardner. 1969. Steady infiltration into crust topped profiles. Soil Sci. 108:137–142. doi:10.1097/00010694-196908000-00010

Hillel, D., and W.R. Gardner. 1970. Transient infiltration into crust topped profiles. Soil Sci. 109:69–76. doi:10.1097/00010694-197002000-00001

Hirmas, D.R., D. Giménez, A. Nemes, R. Kerry, N.A. Brunsell, and C.J. Wilson. 2018. Climate-induced changes in continental-scale soil macroporosity may intensify water cycle. Nature 516:100–103. doi:10.1038/s41586-018-0463-x

Hogarth, W.L., J. Hopmans, J.-Y. Parlange, and R. Haverkamp. 1988. Application of a simple soil-water hysteresis model. J. Hydrol. 98:21–29. doi:10.1016/0022-1694(88)90203-X

Hogue, T.S., L.A. Bastidas, H.V. Gupta, and S. Sorooshian. 2006. Evaluating model performance and parameter behavior for varying levels of land surface model complexity. Water Resour. Res. 42:W08430. doi:10.1029/2005WR004440

Hopmans, J. 1989. Stochastic description of field-measured infiltration data. Trans. ASAE 32:1987–1993. doi:10.13031/2013.31252

Hopmans, J.W., and J.H. Dane. 1986. Temperature dependence of soil hydraulic properties. Soil Sci. Soc. Am. J. 50:4–9. doi:10.2136/sssaj1986.03615995005000010001x

Hopmans, J.W., J.-Y. Parlange, and S. Assouline. 2007. Infiltration. In: J.W. Delleur, editor The handbook of groundwater engineering. 2nd ed. CRC Press, Boca Raton, FL.

Horton, R.E. 1933. The role of infiltration in the hydrologic cycle. Eos Trans. AGU 14:446–460.

Horton, R.E. 1940. The infiltration-theory of surface-runoff. Eos Trans. AGU 21:541. doi:10.1029/TR021i002p00541-1

Horton, R.E. 1941. An approach toward a physical interpretation of infiltration-capacity. Soil Sci. Soc. Am. J. 5(C):399–417. doi:10.2136/sssaj1941.036159950005000C0075x

Huang, H.-C., Y.-C. Tan, C.-W. Liu, and C.-H. Chen. 2005. A novel hysteresis model in unsaturated soil. Hydrol. Processes 19:1653–1665. doi:10.1002/hyp.5594

Huang, M., X. Liang, and Y. Liang. 2003. A transferability study of model parameters for the variable infiltration capacity land surface scheme. J. Geophys. Res. Atmos. 108(D22):8864. doi:10.1029/2003JD003676

Huang, S.C., R. Kumar, M. Florke, T. Yang, Y. Hundecha, P. Kraft, et al. 2017. Evaluation of an ensemble of regional hydrological models in 12 large-scale river basins worldwide. Clim. Change 141:381–397. doi:10.1007/s10584-016-1841-8

Hugelius, G., C. Tarnocai, G. Broll, J.G. Canadell, P. Kuhry, and D.K. Swanson. 2013. The Northern Circumpolar Soil Carbon Database: Spatially distributed datasets of soil coverage and soil carbon storage in the northern permafrost regions. Earth Syst. Sci. Data 5:3–13. doi:10.5194/essd-5-3-2013

Huyakorn, P.S., E.P. Springer, V. Guvanasen, and T.D. Wadsworth. 1986. A three-dimensional finite-element model for simulating water flow in variably saturated porous media. Water Resour. Res. 22:1790–1808. doi:10.1029/WR022i013p01790

Ibrahim, H.A., and W. Brutsaert. 1968. Intermittent infiltration into soils with hysteresis. J. Hydraul. Div., Proc. Am. Soc. Civ. Eng. 94(HY1):113–137.

IGBP. 2000. Global Soil Data Task (IGBP-DIS, ISO-image of CD). International Geosphere–Biosphere Program, PANGAEA, Alfred Wegener Inst., Univ. of Bremen, Bremen, Germany. doi:10.1594/PANGAEA.869912

Imeson, A.C., J.M. Verstraten, E.J. van Mulligen, and J. Sevink. 1992. The effects of fire and water repellency on infiltration and runoff under Mediterranean type forest. Catena 19:345–361. doi:10.1016/0341-8162(92)90008-Y

Jame, Y.-W. 1977. Heat and mass transfer in freezing unsaturated soil. Univ. of Saskatchewan, Saskatoon, SK.

Jana, R., and B. Mohanty. 2011. Enhancing PTFs with remotely sensed data for multi-scale soil water retention estimation. J. Hydrol. 399:201–211. doi:10.1016/j.jhydrol.2010.12.043

Jana, R., and B. Mohanty. 2012a. On topographic controls of soil hydraulic parameter scaling at hillslope scales. Water Resour. Res. 48:2518. doi:10.1029/2011WR011204

Jana, R.B., and B.P. Mohanty. 2012b. A comparative study of multiple approaches to soil hydraulic parameter scaling applied at the hillslope scale. Water Resour. Res. 48:W02520. doi:10.1029/2010WR010185

Jana, R.B., and B.P. Mohanty. 2012c. A topography-based scaling algorithm for soil hydraulic parameters at hillslope scales: Field testing. Water Resour. Res. 48:W02519. doi:10.1029/2011WR011205

Jana, R.B., B.P. Mohanty, and E.P. Springer. 2008. Multiscale Bayesian neural networks for soil water content estimation. Water Resour. Res. 44:W08408. doi:10.1029/2008WR006879

Jansson, P.E. 2012. CoupModel: Model use, calibration, and validation. Trans. ASABE 55:1337–1344. doi:10.13031/2013.42245

Jarvis, N.J. 2007. A review of non-equilibrium water flow and solute transport in soil macropores: Principles, controlling factors and consequences for water quality. Eur. J. Soil Sci. 58:523–546. doi:10.1111/j.1365-2389.2007.00915.x

Jorda, H., M. Bechtold, N. Jarvis, and J. Koestel. 2015. Using boosted regression trees to explore key factors controlling saturated and near-saturated hydraulic conductivity. Eur. J. Soil Sci. 66:744–756. doi:10.1111/ejss.12249

Jury, W.A., W.R. Gardner, and W.H. Gardner. 1991. Soil physics. 5th ed. John Wiley & Sons, New York.

Jury, W.A., Z. Wang, and A. Tuli. 2003. A conceptual model of unstable flow in unsaturated soil during redistribution. Vadose Zone J. 2:61–67. doi:10.2136/vzj2003.6100

Kale, R., and B. Sahoo. 2011. Green–Ampt infiltration models for varied field conditions: A revisit. Water Resour. Manage. 25:3505–3536. doi:10.1007/s11269-011-9868-0

Keune, J., F. Gasper, K. Goergen, A. Hense, P. Shrestha, M. Sulis, and S. Kollet. 2016. Studying the influence of groundwater representations on land surface-atmosphere feedbacks during the European heat wave in 2003. J. Geophys. Res. Atmos. 121:13301–13325. doi:10.1002/2016JD025426

Kim, D., R.L. Ray, and M. Choi. 2017. Simulations of energy balance components at snow-dominated montane watershed by land surface models. Environ. Earth Sci. 76:337. doi:10.1007/s12665-017-6655-0

Kim, J., and B. Mohanty. 2017. A physically-based hydrological connectivity algorithm for describing spatial patterns of soil moisture in the unsaturated zone: Hydrologic connectivity in soil moisture. J. Geophys. Res. Atmos. 122:2096–2114. doi:10.1002/2016JD025591

Kim, K.H., and W.P. Miller. 1996. Effect of rainfall electrolyte concentration and slope on infiltration and erosion. Soil Technol. 9:173–185. doi:10.1016/S0933-3630(96)00011-6

King, P.M. 1981. Comparison of methods for measuring severity of water repellence of sandy soils and assessment of some factors that affect its measurement. Aust. J. Soil Res. 19:275–285. doi:10.1071/SR9810275

Kishné, A.S., C.L.S. Morgan, Y. Ge, and W.L. Miller. 2010. Antecedent soil moisture affecting surface cracking of a Vertisol in field conditions. Geoderma 157:109–117. doi:10.1016/j.geoderma.2010.03.020

Kollet, S.J., and R.M. Maxwell. 2006. Integrated surface-groundwater flow modeling: A free-surface overland flow boundary condition in a parallel groundwater flow model. Adv. Water Resour. 29:945–958. doi:10.1016/j.advwatres.2005.08.006

Kollet, S.J., and R.M. Maxwell. 2008a. Capturing the influence of groundwater dynamics on land surface processes using an integrated, distributed watershed model. Water Resour. Res. 44:W02402. doi:10.1029/2007wr006004

Kollet, S.J., and R.M. Maxwell. 2008b. Demonstrating fractal scaling of baseflow residence time distributions using a fully-coupled groundwater and land surface model. Geophys. Res. Lett. 35:L07402. doi:10.1029/2008GL033215

Koren, V., J. Schaake, K. Mitchell, Q.Y. Duan, F. Chen, and J.M. Baker. 1999. A parameterization of snowpack and frozen ground intended for NCEP weather and climate models. J. Geophys. Res. Atmos. 104:19569–19585. doi:10.1029/1999JD900232

Koster, R.D., M.J. Suarez, A. Ducharne, M. Stieglitz, and P. Kumar. 2000. A catchment-based approach to modeling land surface processes in a general circulation model: 1. Model structure. J. Geophys. Res. Atmos. 105:24809–24822. doi:10.1029/2000JD900327

Kostiakov, A.N. 1932. On the dynamics of the coefficients of water percolation in soils and on the necessity of studying it from a dynamic point of view for purpose of amelioration. In: O. Fauser, editor, Transactions of the 6th Commission of the International Society of Soil Science, Russia. Vol. A. Martinus Nijhoff, Groningen, the Netherlands. p. 17–21.

Kowalczyk, E.A., L. Stevens, R.M. Law, M.R. Dix, Y.P. Wang, I.N. Harman, et al. 2013. The land surface model component of ACCESS: Description and impact on the simulated surface climatology. Aust. Meteorol. Oceanogr. J. 63:65–82. doi:10.22499/2.6301.005

Kowalczyk, E.A., Y.P. Wang, R.M. Law, H.L. Davies, J.L. McGregor, and G. Abramowitz. 2006. The CSIRO Atmosphere Biosphere Land Exchange (CABLE) model for use in climate models and as an offline model. Pap. 013. CSIRO Mar. Atmos. Res., Aspendale, VIC, Australia.

Kutilek, M., V. Kuraz, and M. Krejca. 1993. Measurement time and spatial variability of field infiltration. Int. Agrophys. 7:133–140.

Kværnø, S.H., and L. Øygarden. 2006. The influence of freeze–thaw cycles and soil moisture on aggregate stability of three soils in Norway. Catena 67:175–182. doi:10.1016/j.catena.2006.03.011

Laliberte, G.E., A.T. Corey, and R.H. Brooks. 1966. Properties of unsaturated porous media. Hydrol. Pap. 17. Colorado State Univ., Fort Collins.

Lange, B., P. Lüescher, and P.F. Germann. 2009. Significance of tree roots for preferential infiltration in stagnic soils. Hydrol. Earth Syst. Sci. 13:1809–1821. doi:10.5194/hess-13-1809-2009

Lawrence, D.M., K.W. Oleson, M.G. Flanner, P.E. Thornton, S.C. Swenson, P.J. Lawrence, et al. 2011. Parameterization improvements and functional and structural advances in Version 4 of the Community Land Model. J. Adv. Model. Earth Syst. 3:M03001. doi:10.1029/2011MS00045

Lawrence, D.M., and A.G. Slater. 2008. Incorporating organic soil into a global climate model. Clim. Dyn. 30:145–160. doi:10.1007/s00382-007-0278-1

Lehmann, P., and D. Or. 2012. Hydromechanical triggering of landslides: From progressive local failures to mass release. Water Resour. Res. 48:W03535. doi:10.1029/2011WR010947

Lehrsch, G.A. 1998. Freeze–thaw cycles increase near-surface aggregate stability. Soil Sci. 163:63–70. doi:10.1097/00010694-199801000-00009

Lehrsch, G.A., R.E. Sojka, D.L. Carter, and P.M. Jolley. 1991. Freezing effects on aggregate stability affected by texture, mineralogy, and organic matter. Soil Sci. Soc. Am. J. 55:1401–1406. doi:10.2136/sssaj1991.03615995005500050033x

Letts, M.G., N.T. Roulet, N.T. Comer, M.R. Skarupa, and D.L. Verseghy. 2000. Parametrization of peatland hydraulic properties for the Canadian Land Surface Scheme. Atmos.-Ocean 38:141–160. doi:10.1080/07055900.2000.9649643

Le Vine, N., A. Butler, N. McIntyre, and C. Jackson. 2016. Diagnosing hydrological limitations of a land surface model: Application of JULES to a deep-groundwater chalk basin. Hydrol. Earth Syst. Sci. 20:143–159. doi:10.5194/hess-20-143-2016

Levy, G.J., H.J.C. Smith, and M. Agassi. 1989. Water temperature effect on hydraulic conductivity and infiltration rate of soils. S. Afr. J. Plant Soil 6:240–244. doi:10.1080/02571862.1989.10634520

Lewis, M. 1937. The rate of infiltration of water in irrigation-practice. Eos Trans. AGU 18:361–368.

Li, Q., S.F. Sun, and Y.K. Xue. 2010. Analyses and development of a hierarchy of frozen soil models for cold region study. J. Geophys. Res. Atmos. 115:D03107. doi:10.1029/2009jd012530

Liang, X., D.P. Lettenmaier, E.F. Wood, and S.J. Burges. 1994. A simple hydrologically based model of land surface water and energy fluxes for GSMs. J. Geophys. Res. 99(D7):14415–14428. doi:10.1029/94JD00483

Liang, X., and Z. Xie. 2001. A new surface runoff parameterization with subgrid-scale soil heterogeneity for land surface models. Adv. Water Resour. 24:1173–1193. doi:10.1016/S0309-1708(01)00032-X

Lin, H.S., K.J. McInnes, L.P. Wilding, and C.T. Hallmark. 1998. Macroporosity and initial moisture effects on infiltration rates in Vertisols and vertic intergrades. Soil Sci. 163:2–8. doi:10.1097/00010694-199801000-00002

Loague, K., and G.A. Gander. 1990. R-5 revisited: 1. Spatial variability of infiltration on a small rangeland catchment. Water Resour. Res. 26:957–971. doi:10.1029/WR026i005p00957

Logsdon, S.D., and D.B. Jaynes. 1996. Spatial variability of hydraulic conductivity in a cultivated field at different times. Soil Sci. Soc. Am. J. 60. doi:10.2136/sssaj1996.03615995006000030003x

MacDonald, M.K., J.W. Pomeroy, and R.L.H. Essery. 2017. Water and energy fluxes over northern prairies as affected by chinook winds and winter precipitation. Agric. For. Meteorol. 2017:372–385. doi:10.1016/j.agrformet.2017.10.025

Mantoglou, A., and L.W. Gelhar. 1987a. Capillary tension head variance, mean soil moisture content, and effective specific soil moisture capacity of transient unsaturated flow in stratified soils. Water Resour. Res. 23:47–56. doi:10.1029/WR023i001p00047

Mantoglou, A., and L.W. Gelhar. 1987b. Effective hydraulic conductivity of transient unsaturated flow in stratified soils. Water Resour. Res. 23:57–67. doi:10.1029/WR023i001p00057

Materia, S., P.A. Dirmeyer, Z.C. Guo, A. Alessandri, and A. Navarra. 2010. The sensitivity of simulated river discharge to land surface representation and meteorological forcings. J. Hydrometeorol. 11:334–351. doi:10.1175/2009JHM1162.1

McGhie, D.A., and A.M. Posner. 1981. The effect of plant top material on the water repellence of fired sands and water repellent soils. Aust. J. Agric. Res. 32:609–620. doi:10.1071/AR9810609

McNeal, B.L., and N.T. Coleman. 1966. Effect of solution composition on soil hydraulic conductivity. Soil Sci. Soc. Am. J. 30:308–312. doi:10.2136/sssaj1966.03615995003000030007x

Mein, R.G., and C.L. Larson. 1973. Modeling infiltration during a steady rain. Water Resour. Res. 9:384–394. doi:10.1029/WR009i002p00384

Meng, H., J.D. Salas, T. Green, and L. Ahuja. 2006. Scaling analysis of space–time infiltration based on the universal multifractal model. J. Hydrol. 322:220–235. doi:10.1016/j.jhydrol.2005.03.016

Mertens, J., D. Raes, and J. Feyen. 2002. Incorporating rainfall intensity into daily rainfall records for simulating runoff and infiltration into soil profiles. Hydrol. Processes 16:731–739. doi:10.1002/hyp.1005

Mezencev, V. 1948. Theory of formation of the surface runoff. Meteorol. Hidrol. 3:33–40.

Miller, D.E., and W.H. Gardner. 1962. Water infiltration into stratified soil. Soil Sci. Soc. Am. J. 26:115–119. doi:10.2136/sssaj1962.03615995002600020007x

Miller, E.E., and R.D. Miller. 1956. Physical theory for capillary flow phenomena. J. Appl. Phys. 27:324–332. doi:10.1063/1.1722370

Milly, P.C.D., and P.S. Eagleson. 1988. Effect of storm scale on surface runoff volume. Water Resour. Res. 24:620–624. doi:10.1029/WR024i004p00620

Milovac, J., J. Ingwersen, and K. Warrach-Sagi. 2014. Soil texture forcing data for the whole world for the Weather Research and Forecasting (WRF) model of the University of Hohenheim (UHOH) based on the Harmonized World Soil Database (HWSD) at 30 arc-second horizontal resolution. World Data Ctr. for Climate, German Climate Computing Ctr., Hamburg.

Mis, J. 1982. Formulation and solution of fundamental problems of vertical infiltration. Vodohosp. Cas. 30:304–311.

Mohammed, A., B. Kurylyk, E. Cey, and M. Hayashi. 2018. Snowmelt infiltration and macropore flow in frozen soils: Overview, knowledge and a conceptual framework. Vadose Zone J. 17:180084. doi:10.2136/vzj2018.04.0084

Mohanty, B.P. 1999. Scaling hydraulic properties of a macroporous soil. Water Resour. Res. 35:1927–1931. doi:10.1029/1999WR900050

Mohanty, B.P., and J. Zhu. 2007. Effective hydraulic parameters in horizontally and vertically heterogeneous soils for steady-state land–atmosphere interaction. J. Hydrometeorol. 8:715–729. doi:10.1175/JHM606.1

Montzka, C., M. Herbst, L. Weihermüller, A. Verhoef, and H. Vereecken. 2017. A global data set of soil hydraulic properties and sub-grid variability of soil water retention and hydraulic conductivity curves. Earth Syst. Sci. Data 9:529–543. doi:10.5194/essd-9-529-2017

Moore, I.D. 1981a. Effect of surface sealing on infiltration. Trans. ASAE 24:1546–1552. doi:10.13031/2013.34488

Moore, I.D. 1981b. Infiltration equations modified for surface effect. J. Irrig. Drain. Div., Am. Soc. Civ. Eng. 107:71–86.

Moore, R.J. 1985. The probability-distributed principle and runoff production at point and basin scales. Hydrol. Sci. J. 30:273–297. doi:10.1080/02626668509490989

Morbidelli, R., C. Corradini, and R.S. Govindaraju. 2006. A field-scale infiltration model accounting for spatial heterogeneity of rainfall and soil saturated hydraulic conductivity. Hydrol. Processes 20:1465–1481. doi:10.1002/hyp.5943

Morbidelli, R., C. Saltalippi, A. Flammini, and R.S. Govindaraju. 2018. Role of slope on infiltration: A review. J. Hydrol. 557:878–886. doi:10.1016/j.jhydrol.2018.01.019

Mualem, Y. 1974. A conceptual model of hysteresis. Water Resour. Res. 10:514–520. doi:10.1029/WR010i003p00514

Mualem, Y. 1976. A new model for predicting the hydraulic conductivity of unsaturated porous media. Water Resour. Res. 12:513–522. doi:10.1029/WR012i003p00513

Mualem, Y., and S. Assouline. 1989. Modeling soil seal as a nonuniform layer. Water Resour. Res. 25:2101–2108. doi:10.1029/WR025i010p02101

Mualem, Y., and S. Assouline. 1996. Soil sealing, infiltration and runoff. In: A.S. Issar and S.D. Resnick, editors, Runoff, infiltration and subsurface flow of water in arid and semi-arid regions. Water Science and Technology Library. Kluwer Acad., Dordrecht, the Netherlands. p. 131–181. doi:10.1007/978-94-017-2929-1_4

Mualem, Y., and S. Assouline. 1992. Flow processes in sealing soils: Conceptions and solutions. In: M.E. Sumner and B.A. Stewart, editors, Soil crusting: Chemical and physical processes. Lewis Publ., Boca Raton, FL.

Mualem, Y., and A. Beriozkin. 2009. General scaling rules of the hysteretic water retention function based on Mualem's domain theory. Eur. J. Soil Sci. 60:652–661. doi:10.1111/j.1365-2389.2009.01130.x

Mualem, Y., and G. Dagan. 1975. A dependent domain model of capillary hysteresis. Water Resour. Res. 11:452–460. doi:10.1029/WR011i003p00452

Mueller, A., E. Dutra, H. Cloke, A. Verhoef, G. Balsamo, and F. Pappenberger. 2016. Water infiltration and redistribution in land surface models. Eur. Ctr. for Medium-Range Weather Forecasts Tech. Mem. Research Dep., Univ. of Reading, Reading, UK.

Neuman, S.P. 1973. Saturated–unsaturated seepage by finite elements. J. Hydraul. Div., Am. Soc. Civ. Eng. 99:2233–2250.

Neuman, S.P. 1976. Wetting front pressure head in the infiltration model of Green and Ampt. Water Resour. Res. 12:564–566. doi:10.1029/WR012i003p00564

Neuman, S.P., R.A. Feddes, and E. Bresler. 1974. Finite element simulation of flow in saturated–unsaturated soils considering water uptake by plants. 3rd Annu. Rep. Hydraulic Engineering Lab., Technion, Haifa, Israel.

Nielsen, D., J. Biggar, and K. Erh. 1973. Spatial variability of field-measured soil-water properties. Hilgardia 42:215–259. doi:10.3733/hilg.v42n07p215

Nielsen, D.R., J.W. Hopmans, and K. Reichardt. 1998. An emerging technology for scaling field soil-water behavior. In: G. Sposito, editor, Scale dependence and scale invariance in hydrology. Cambridge Univ. Press, Cambridge, UK. p. 136–166. doi:10.1017/CBO9780511551864.006

Nimmo, J.R. 1992. Semiempirical model of soil water hysteresis. Soil Sci. Soc. Am. J. 56:1723–1730. doi:10.2136/sssaj1992.03615995005600060011x

Nimmo, J.R., and E.E. Miller. 1986. The temperature dependence of isothermal moisture vs. potential characteristics of soils. Soil Sci. Soc. Am. J. 50:1105–1113. doi:10.2136/sssaj1986.03615995005000050004x

Nimmo, J.R., K.S. Perkins, K.M. Schmidt, D. Miller, J.D. Stock, and K. Singha. 2009. Hydrologic characterization of desert soils with varying degrees of pedogenesis: 1. Field experiments evaluating plant-relevant soil water behavior. Vadose Zone J. 8:480–495. doi:10.2136/vzj2008.0052

Nissen, T.M., and M.M. Wander. 2003. Management and soil-quality effects on fertilizer-use efficiency and leaching. Soil Sci. Soc. Am. J. 67:1524–1532. doi:10.2136/sssaj2003.1524

Niu, G.-Y., and Z.-L. Yang. 2007. An observation-based formulation of snow cover fraction and its evaluation over large North American river basins. J. Geophys. Res. D Atmos. 112: D21101. doi:10.1029/2007JD008674

Niu, G.Y., Z.L. Yang, R.E. Dickinson, and L.E. Gulden. 2005. A simple TOPMODEL-based runoff parameterization (SIMTOP) for use in global climate models. J. Geophys. Res. 110:D21106. doi:10.1029/2005JD006111

Niu, G.-Y., Z.-L. Yang, K.E. Mitchell, F. Chen, M.B. Ek, M. Barlage, et al. 2011. The community Noah land surface model with multiparameterization options (Noah-MP): 1. Model description and evaluation with local-scale measurements. J. Geophys. Res. 116:D12109. doi:10.1029/2010JD015139

Noilhan, J., and P. Lacarrère. 1995. GCM gridscale evaporation from mesoscale modelling. J. Clim. 8:206–223. doi:10.1175/1520-0442(1995)008<0206:GGSEFM>2.0.CO;2

Nuth, M., and L. Laloui. 2008. Advances in modelling hysteretic water retention curve in deformable soils. Comput. Geotech. 35:835–844. doi:10.1016/j.compgeo.2008.08.001

Ogden, F.L., W. Lai, R.C. Steinke, J. Zhu, C.A. Talbot, and J.L. Wilson. 2015. A new general 1-D vadose zone flow solution method. Water Resour. Res. 51:4282–4300. doi:10.1002/2015WR017126

Oleson, K.W., D.M. Lawrence, G.B. Bonan, B. Drewniak, M. Huang, C.D. Koven, et al. 2013. Technical description of version 4.5 of the Community Land Model (CLM). NCAR Tech. Note NCAR/TN-503+STR. Natl. Ctr. for Atmos. Res., Boulder, CO.

Oleson, K.W., G.-Y. Niu, Z.-L. Yang, D.M. Lawrence, P.E. Thornton, P.J. Lawrence, et al. 2008. Improvements to the Community Land Model and their impact on the hydrological cycle. J. Geophys. Res. 113:G01021. doi:10.1029/2007JG000563

Or, D. 2008. Scaling of capillary, gravity and viscous forces affecting flow morphology in unsaturated porous media. Adv. Water Resour. 31:1129–1136. doi:10.1016/j.advwatres.2007.10.004

Or, D., F.J. Leij, V. Snyder, and T.A. Ghezzehei. 2000. Stochastic model for posttillage soil pore space evolution. Water Resour. Res. 36:1641–1652. doi:10.1029/2000WR900092

Pachepsky, Y., and R.L. Hill. 2017. Scale and scaling in soils. Geoderma 287:4–30. doi:10.1016/j.geoderma.2016.08.017

Paniconi, C., and M. Putti. 1994. A comparison of Picard and Newton iteration in the numerical solution of multidimensional variably saturated flow problems. Water Resour. Res. 30:3357–3374. doi:10.1029/94WR02046

Paniconi, C., and M. Putti. 2015. Physically based modeling in catchment hydrology at 50: Survey and outlook. Water Resour. Res. 51:7090–7129. doi:10.1002/2015WR017780

Parhi, P.K., S.K. Mishra, and R. Singh. 2007. A modification to Kostiakov and Modified Kostiakov infiltration models. Water Resour. Manage. 21:1973–1989. doi:10.1007/s11269-006-9140-1

Park, S.-E., A. Bartsch, D. Sabel, W. Wagner, V. Naeimi, and Y. Yamaguchi. 2011. Monitoring freeze/thaw cycles using ENVISAT ASAR Global Mode. Remote Sens. Environ. 115:3457–3467. doi:10.1016/j.rse.2011.08.009

Parlange, J.-Y. 1976. Capillary hysteresis and relationship between drying and wetting curves. Water Resour. Res. 12:224–228. doi:10.1029/WR012i002p00224

Parlange, J.-Y. 1980. Water transport in soils. Annu. Rev. Fluid Mech. 12:77–102. doi:10.1146/annurev.fl.12.010180.000453

Parlange, J.-Y., R. Haverkamp, and J. Touma. 1985. Infiltration under ponded conditions: 1. Optimal analytical solution and comparison with experimental observations. Soil Sci. 139:305–311. doi:10.1097/00010694-198504000-00003

Parlange, J.-Y., and D.E. Hill. 1976. Theoretical analysis of wetting front instability in soils. Soil Sci. 122:236–239. doi:10.1097/00010694-197610000-00008

Parlange, J.-Y., W.L. Hogarth, and M.B. Parlange. 1984. Optimal analysis of the effect of a surface crust. Soil Sci. Soc. Am. J. 48:494–497. doi:10.2136/sssaj1984.03615995004800030004x

Parlange, J.-Y., I.G. Lisle, R.D. Braddock, and R.E. Smith. 1982. The three-parameter infiltration equation. Soil Sci. 133:337–341. doi:10.1097/00010694-198206000-00001

Parlange, J.-Y., T.S. Steenhuis, R. Haverkamp, D.A. Barry, P.J. Culligan, W.L. Hogarth, et al. 1999. Soil properties and water movement. In: M.B. Parlange and J.W. Hopmans, editors, Vadose zone hydrology: Cutting across disciplines. Oxford Univ. Press, New York. p. 99–129.

Parlange, M.B., A.T. Cahill, D.R. Nielsen, J.W. Hopmans, and O. Wendroth. 1998. Review of heat and water movement in field soils. Soil Tillage Res. 47:5–10. doi:10.1016/S0167-1987(98)00066-X

Peck, A.J. 1983. Field variability of soil physical properties. In: D. Hillel, editor, Advances in irrigation. Vol. 2. Academic Press, San Diego. p. 189–221.

Philip, J.R. 1957. The theory of infiltration: 1. The infiltration equation and its solution. Soil Sci. 83:345–358. doi:10.1097/00010694-195705000-00002

Philip, J.R. 1967. Sorption and infiltration in heterogeneous media. Aust. J. Soil Res. 5:1–10. doi:10.1071/SR9670001

Philip, J.R. 1969. Theory of infiltration. Adv. Hydrosci. 5:215–296.

Philip, J.R. 1970. Flow in porous media. Annu. Rev. Fluid Mech. 2:177–204. doi:10.1146/annurev.fl.02.010170.001141

Philip, J.R. 1975. Stability analysis of infiltration. Soil Sci. Soc. Am. Proc. 39:1042–1049. doi:10.2136/sssaj1975.03615995003900060013x

Philip, J.R., and D.A. de Vries. 1957. Moisture movement in porous materials under temperature gradients. Eos Trans. AGU 38:222–232. doi:10.1029/TR038i002p00222

Philip, J.R., and J.H. Knight. 1974. On solving the unsaturated flow equation: 3. New quasi-analytical technique. Soil Sci. 117:1–13. doi:10.1097/00010694-197401000-00001

Poesen, J., J. Nachtergaele, G. Verstraeten, and C. Valentin. 2003. Gully erosion and environmental change: Importance and research needs. Catena 50:91–133. doi:10.1016/S0341-8162(02)00143-1

Poulovassilis, A. 1962. Hysteresis of pore water: An application of the concept of independent domains. Soil Sci. 93:405–412. doi:10.1097/00010694-196206000-00007

Prasad, S.N., and M.J.M. Römkens. 1982. An approximate integral solution of vertical infiltration under changing boundary conditions. Water Resour. Res. 18:1022–1028. doi:10.1029/WR018i004p01022

Pruess, K. 1991. TOUGH2: A general-purpose numerical simulator for multiphase fluid and heat flow. Lawrence Berkeley Lab., Berkeley, CA. doi:10.2172/5212064

Puigdefábregas, J. 2005. The role of vegetation patterns in structuring runoff and sediment fluxes in drylands. Earth Surf. Processes Landforms 30:133–147. doi:10.1002/esp.1181

Qi, J., P.A. Vermeer, and G. Cheng. 2006. A review of the influence of freeze–thaw cycles on soil geotechnical properties. Permafrost Periglacial Processes 17:245–252. doi:10.1002/ppp.559

Qu, W., H.R. Bogena, J.A. Huisman, J. Vanderborght, M. Schuh, E. Priesack, and H. Vereecken. 2015. Predicting subgrid variability of soil water content from basic soil information. Geophys. Res. Lett. 42:789–796. doi:10.1002/2014GL062496

Quirk, J.P. 1994. Interparticle forces: A basis for the interpretation of soil physical behaviour. Adv. Agron. 53:121–183. doi:10.1016/S0065-2113(08)60614-8

Quirk, J.P., and R.K. Schofield. 1955. The effect of electrolyte concentration of soil permeability. J. Soil Sci. 6:163–178. doi:10.1111/j.1365-2389.1955.tb00841.x

Raats, P.A.C. 1973. Unstable wetting fronts in uniform and nonuniform soils. Soil Sci. Soc. Am. J. 37:681–685. doi:10.2136/sssaj1973.03615995003700050017x

Raats, P.A.C. 2001. Developments in soil-water physics since the mid 1960s. Geoderma 100:355–387. doi:10.1016/S0016-7061(01)00028-3

Raats, P.A.C., and A. Klute. 1969. One-dimensional simultaneous motion of the aqueous phase and the solid phase of saturated and partially saturated porous media. Soil Sci. 107:329–333. doi:10.1097/00010694-196905000-00003

Raats, P.A.C., D. Smiles, and A.W. Warrick, editors. 2002. Environmental mechanics: Water, mass and energy transfer in the biosphere. Geophys, Monogr. Ser. 129. Am. Geophys. Union, Washington, DC.

Rahman, M., and R. Rosolem. 2017. Towards a simple representation of chalk hydrology in land surface modelling. Hydrol. Earth Syst. Sci. 21:459–471. doi:10.5194/hess-21-459-2017

Rahmati, M., L. Weihermüller, J. Vanderborght, Y.A. Pachepsky, L. Mao, S.H. Sadeghi, et al. 2018. Development and analysis of the Soil Water

Infiltration Global database. Earth Syst. Sci. Data 10:1237–1263. doi:10.5194/essd-10-1237-2018

Regalado, C.M., and A. Ritter. 2008. Cokriging spatial interpolation of soil water dependent repellency parameters determined with two different tests. Soil Sci. Soc. Am. J. 72:1683–1693. doi:10.2136/sssaj2008.0008

Rengasamy, P., and K. Olsson. 1991. Sodicity and soil structure. Aust. J. Soil Res. 29:935–952. doi:10.1071/SR9910935

Reynolds, C.A., T.J. Jackson, and W.J. Rawls. 2000. Estimating soil water-holding capacities by linking the Food and Agriculture Organization soil map of the world with global pedon databases and continuous pedotransfer functions. Water Resour. Res. 36:3653–3662. doi:10.1029/2000WR900130

Reynolds, W.D., and D.E. Eldrick. 1985. In situ measurements of field-saturated hydraulic conductivity, sorptivity and a-parameter using the Guelph permeameter. Soil Sci. 140:292–302. doi:10.1097/00010694-198510000-00008

Richards, L.A. 1931. Capillary conduction of liquids through porous mediums. Physics 1:318–333. doi:10.1063/1.1745010

Ritsema, C.J., and L.W. Dekker. 1998. Three-dimensional patterns of moisture, water repellency, bromide and pH in a sandy soil. J. Contam. Hydrol. 31:295–313. doi:10.1016/S0169-7722(97)00067-3

Roeckner, E., G. Bäuml, L. Bonaventura, R. Brokopf, M. Esch, M. Giorgetta, et al. 2003. The atmospheric general circulation model ECHAM 5: I. Model description. MPI Rep. 349. Max Planck Inst., Hamburg.

Römkens, M.J.M., R.L. Baumhardt, J.-Y. Parlange, F.D. Whisler, M.B. Parlange, and S.N. Prasad. 1986a. Effect of rainfall characteristics on seal hydraulic conductance. In: F. Callebaut et al., editors, Assessment of soil surface sealing and crusting. Ghent Univ. Press, Ghent, Belgium. p. 228–235.

Römkens, M.J.M., R.L. Baumhardt, M. Parlange, F.D. Whisler, J.-Y. Parlange, and S.N. Prasad. 1986b. Rain-induced surface seals: Their effect on ponding and infiltration. Ann. Geophys. 4:417–424.

Römkens, M.J.M., and S.N. Prasad. 1992. A spectral series approach to infiltration for crusted and non-crusted soils. In: M.E. Sumner and B.A. Stewart, editors, Soil crusting: Chemical and physical processes. Lewis Publ., Boca Raton, FL. p. 151–178.

Ross, P.J., R. Haverkamp, and J.-Y. Parlange. 1996. Calculating parameters for infiltration equations from soil hydraulic functions. Transp. Porous Media 24:315–339. doi:10.1007/BF00154096

Rubin, J., and R. Steinhardt. 1964. Soil water relations during rain infiltration: III. Water uptake at incipient ponding. Soil Sci. Soc. Am. J. 28:614–619. doi:10.2136/sssaj1964.03615995002800050013x

Russo, D. 2005. Salinity/Physical effects. In: D. Hillel, editor, Encyclopedia of soils in the environment 3. Elsevier Ltd, Oxford, UK. p. 442–453. doi:10.1016/B0-12-348530-4/00529-4

Russo, D., I. Russo, and A. Laufer. 1997. On the spatial variability of parameters of the unsaturated hydraulic conductivity. Water Resour. Res. 33:947–956. doi:10.1029/96WR03947

Sadeghi, M., B. Ghahraman, A.N. Ziaei, K. Davary, and K. Reichardt. 2012. Additional scaled solutions to Richards' equation for infiltration and drainage. Soil Tillage Res. 119:60–69. doi:10.1016/j.still.2011.12.004

Sahoo, A.K., P.A. Dirmeyer, P.R. Houser, and M. Kafatos. 2008. A study of land surface processes using land surface models over the Little River Experimental Watershed, Georgia. J. Geophys. Res. 113:D20121. doi:10.1029/2007JD009671

Samaniego, L., R. Kumar, and S. Attinger. 2010. Multiscale parameter regionalization of a grid-based hydrologic model at the mesoscale. Water Resour. Res. 46:W05523. doi:10.1029/2008WR007327

Samaniego, L., R. Kumar, S. Thober, O. Rakovec, M. Zink, N. Wanders, et al. 2017. Toward seamless hydrologic predictions across spatial scales. Hydrol. Earth Syst. Sci. 21:4323–4346. doi:10.5194/hess-21-4323-2017

Sato, N., P.J. Sellers, D.A. Randall, E.K. Schneider, J. Shukla, J.L. Kinter III, et al. 1989. Effects of implementing the simple biosphere model in a general circulation model. J. Atmos. Sci. 46: 2757–2782. doi:10.1175/1520-0469(1989)046<2757:Eoitsb>2.0.Co;2

Saulnier, G.M., and R. Datin. 2004. Analytical solution to a bias in the TOPMODEL framework balance. Hydrol. Processes 18:1195–1218. doi:10.1002/hyp.1346

Scanlon, B. 2004. Review of HYDRUS-1D. Southw. Hydrol. 3(4):37.

Schaake, J.C., V.I. Koren, Q.Y. Duan, K. Mitchell, and F. Chen. 1996. Simple water balance model for estimating runoff at different spatial and temporal scales. J. Geophys. Res. 101(D3):7461–7475. doi:10.1029/95JD02892

Schaap, M.G., and F.J. Leij. 1998. Database-related accuracy and uncertainty of pedotransfer functions. Soil Sci. 163:765–779. doi:10.1097/00010694-199810000-00001

Schaap, M.G., F.J. Leij, and M.Th. van Genuchten. 2001. ROSETTA: A computer program for estimating soil hydraulic parameters with hierarchical pedotransfer functions. J. Hydrol. 251:163–176. doi:10.1016/S0022-1694(01)00466-8

Schlüter, S., J. Vanderborght, and H.J. Vogel. 2012. Hydraulic non-equilibrium during infiltration induced by structural connectivity. Adv. Water Resour. 44:101–112. doi:10.1016/j.advwatres.2012.05.002

Scott, P.S., G.J. Farquhar, and N. Kouwen. 1983. Hysteretic effects on net infiltration. In: Advances in infiltration: Proceedings of the National Conference on Advances in Infiltration, Chicago. 12–13 Dec. 1983. ASAE Publ. 83-11. Am. Soc. Agric. Eng., St. Joseph, MI. p. 163–170.

Selker, J.S., and S. Assouline. 2017. An explicit, parsimonious, and accurate estimate for ponded infiltration into soils using the Green and Ampt approach. Water Resour. Res. 53:7481–7487. doi:10.1002/2017WR021020

Selker, J.S., J. Duan, and J.-Y. Parlange. 1999. Green and Ampt infiltration into soils of variable pore size with depth. Water Resour. Res. 35:1685–1688. doi:10.1029/1999WR900008

Sellers, P.J., Y. Mintz, Y.C. Sud, and A. Dalcher. 1986. A simple biosphere model (Sib) for use within general-circulation models. J. Atmos. Sci. 43:505–531. doi:10.1175/1520-0469(1986)043<0505:Asbmfu>2.0.Co;2.

Sellers, P.J., D.A. Randall, G.J. Collatz, J.A. Berry, C.B. Field, D.A. Dazlich, et al. 1996. A revised land surface parameterization (SiB2) for atmospheric GCMS: I. Model formulation. J. Climate 9: 676–705. doi:10.1175/1520-0442(1996)009<0676:Arlspf>2.0.Co;2.

Seneviratne, S.I., T. Corti, E.L. Davin, M. Hirschi, E.B. Jaeger, I. Lehner, et al. 2010. Investigating soil moisture–climate interactions in a changing climate: A review. Earth Sci. Rev. 99:125–161. doi:10.1016/j.earscirev.2010.02.004

Sharma, M.L., G.A. Gander, and C.G. Hunt. 1980. Spatial variability of infiltration in a watershed. J. Hydrol. 45:101–122. doi:10.1016/0022-1694(80)90008-6

Sharma, M.L., and E. Seely. 1979. Spatial variability and its effects on areal infiltration. In: Proceedings Hydrology and Water Resources Symposium, Perth, WA. 10–12 Sept. 1979. Inst. Eng., Perth, WA, Australia. p. 69–73.

Sharma, S.K., B.P. Mohanty, and J. Zhu. 2006. Including topography and vegetation attributes for developing pedotransfer functions. Soil Sci. Soc. Am. J. 70:1430–1440. doi:10.2136/sssaj2005.0087

She, H.Y., and B.E. Sleep. 1998. The effect of temperature on capillary pressure–saturation relationships for air–water and perchloroethylene–water systems. Water Resour. Res. 34:2587–2597. doi:10.1029/98WR01199

Shellito, P.J., E.E. Small, and M.H. Cosh. 2016. Calibration of Noah soil hydraulic property parameters using surface soil moisture from SMOS and basinwide in situ observations. J. Hydrometeorol. 17:2275–2292. doi:10.1175/JHM-D-15-0153.1

Shi, Y.N., K.J. Davis, F.Q. Zhang, and C.J. Duffy. 2014. Evaluation of the parameter sensitivities of a coupled land surface hydrologic model at a critical zone observatory. J. Hydrometeorol. 15:279–299. doi:10.1175/JHM-D-12-0177.1

Shouse, P.J., and B.P. Mohanty. 1998. Scaling of near-saturated hydraulic conductivity measured using disc infiltrometers. Water Resour. Res. 34:1195–1205. doi:10.1029/98WR00318

Silva, V.R., D.J. Reinert, and J.M. Reichert. 2000. Soil density, chemical attributes and maize root distribution as affected by grazing and soil management. (In Portuguese, with English abstract.) Rev. Bras. Cienc. Solo 24:191–199. doi:10.1590/S0100-06832000000100021

Šimůnek, J., N.J. Jarvis, M.Th. van Genuchten, and A. Gärdenäs. 2003. Review and comparison of models for describing non-equilibrium and preferential flow and transport in the vadose zone. J. Hydrol. 272:14–35. doi:10.1016/S0022-1694(02)00252-4

Šimůnek, J., and M.Th. van Genuchten. 2008. Modeling nonequilibrium flow and transport processes using HYDRUS. Vadose Zone J. 7:782–797. doi:10.2136/vzj2007.0074

Šimůnek, J., M.Th. van Genuchten, and M. Šejna. 2008. Development and applications of the HYDRUS and STANMOD software packages and related codes. Vadose Zone J. 7:587–600. doi:10.2136/vzj2007.0077

Šimůnek, J., M.Th. van Genuchten, and M. Šejna. 2016. Recent developments and applications of the HYDRUS computer software packages. Vadose Zone J. 15(7). doi:10.2136/vzj2016.04.0033

Sisson, J.B., and P.J. Wierenga. 1981. Spatial variability of steady-state infiltration rates as a stochastic process. Soil Sci. Soc. Am. J. 45:699–704. doi:10.2136/sssaj1981.03615995004500040005x

Sivapalan, M., and E.F. Wood. 1986. Spatial heterogeneity and scale in the infiltration response of catchments. In: V.K. Gupta, et al., editors, Scale problems in hydrology. D. Reidel, Hingham, MA. p. 81–106. doi:10.1007/978-94-009-4678-1_5

Sivapalan, M., and R.A. Woods. 1995. Evaluation of the effects of general-circulation models subgrid variability and patchiness of rainfall and soil-moisture on land-surface water-balance fluxes. Hydrol. Processes 9:697–717. doi:10.1002/hyp.3360090515

Skaggs, R.W. 1982. Infiltration. In: C.T. Haan et al., editors, Hydrologic modeling of small watersheds. ASAE Monogr. 5. Am. Soc. Agric. Eng., St. Joseph, MI. p. 121–166.

Smiles, D.E. 1974. Infiltration into a swelling material. Soil Sci. 117:140–147. doi:10.1097/00010694-197403000-00002

Smith, R.E. 1972. The infiltration envelope: Results from a theoretical infiltrometer. J. Hydrol. 17:1–22. doi:10.1016/0022-1694(72)90063-7

Smith, R.E. 1990. Analysis of infiltration through a two-layer soil profile. Soil Sci. Soc. Am. J. 54:1219–1227. doi:10.2136/sssaj1990.03615995005400050004x

Smith, R.E., C. Corradini, and F. Melone. 1999. A conceptual model for infiltration and redistribution in crusted soils. Water Resour. Res. 35:1385–1393. doi:10.1029/1998WR900046

Smith, R.E., and D.C. Goodrich. 2000. Model For rainfall excess patterns on randomly heterogeneous areas. J. Hydrol. Eng. 5:355–362. doi:10.1061/(ASCE)1084-0699(2000)5:4(355)

Smith, R.E., and R.H.B. Hebbert. 1979. A Monte Carlo analysis of the hydrologic effects of spatial variability of infiltration. Water Resour. Res. 15:419–429. doi:10.1029/WR015i002p00419

Smith, R.E., K.R.J. Smettem, P. Broadbridge, and D.A. Woolhiser. 2002. Infiltration theory for hydrologic applications. Water Resour. Monogr. 15. Am. Geophys. Union, Washington, DC. doi:10.1029/WM015

Soet, M., R.J. Ronda, J.N.M. Stricker, and A.J. Dolman. 2000. Land surface scheme conceptualisation and parameter values for three sites with contrasting soils and climate. Hydrol. Earth Syst. Sci. 4:283–294. doi:10.5194/hess-4-283-2000

Sposito, G. 1975. Steady vertical flows in swelling soils. Water Resour. Res. 11:461–464. doi:10.1029/WR011i003p00461

Stange, C., and R. Horn. 2005. Modeling the soil water retention curve for conditions of variable porosity. Vadose Zone J. 4:602–613. doi:10.2136/vzj2004.0150

Strudley, M.W., T.R. Green, and J.C. Ascough. 2008. Tillage effects on soil hydraulic properties in space and time: State of the science. Soil Tillage Res. 99:4–48. doi:10.1016/j.still.2008.01.007

Sun, S.F., and Y.K. Xue. 2001. Implementing a new snow scheme in simplified simple biosphere model. Adv. Atmos. Sci. 18:335–354. doi:10.1007/BF02919314

Swartzendruber, D. 1987. Rigorous derivation and interpretation of the Green and Ampt equation. In: Y.S. Fok, editor, Infiltration development and application. Water Resour. Res. Ctr., Univ. of Hawaii, Honolulu.

Talsma, T., and J.-Y. Parlange. 1972. One dimensional vertical infiltration. Aust. J. Soil Res. 10:143–150. doi:10.1071/SR9720143

Täumer, K., H. Stoffregen, and G. Wessolek. 2005. Determination of repellency distribution using soil organic matter and water content. Geoderma 125:107–115. doi:10.1016/j.geoderma.2004.07.004

Thomas, P.J., J.C. Baker, L.W. Zelazny, and D.R. Hatch. 2000. Relationship of map unit variability to shrink–swell indicators. Soil Sci. Soc. Am. J. 64:262–268. doi:10.2136/sssaj2000.641262x

Tillotson, P.M., and D.R. Nielsen. 1984. Scale factors in soil science. Soil Sci. Soc. Am. J. 48:953–959. doi:10.2136/sssaj1984.03615995004800050001x

Topp, G.C. 1971. Soil-water hysteresis: The domain theory extended to pore interaction conditions. Soil Sci. Soc. Am. J. 35:219–225. doi:10.2136/sssaj1971.03615995003500020017x

Tyler, S.W., and S.W. Wheatcraft. 1990. Fractal processes in soil water retention. Water Resour. Res. 26:1047–1054. doi:10.1029/WR026i005p01047

Unger, P.W. 1991. Overwinter changes in physical properties of no-tillage soil. Soil Sci. Soc. Am. J. 55:778–782. doi:10.2136/sssaj1991.03615995005500030024x

van Dam, J.C., P. Groenendijk, R.F.A. Hendriks, and J.G. Kroes. 2008. Advances of modeling water flow in variably saturated soils with SWAP. Vadose Zone J. 7:640–653. doi:10.2136/vzj2007.0060

van Dam, J.C., J.M.H. Hendrickx, H.C. Van Ommen, M.H. Bannink, M.Th. van Genuchten, and L.W. Dekker. 1990. Water and solute movement in a coarse-textured water-repellent field soil. J. Hydrol. 120:359–379. doi:10.1016/0022-1694(90)90159-U

van den Hurk, B., and P. Viterbo. 2003. The Torne-Kalix PILPS 2(e) experiment as a test bed for modifications to the ECMWF land surface scheme. Global Planet. Change 38:165–173. doi:10.1016/S0921-8181(03)00027-4

Vandervaere, J.-P., M. Vauclin, R. Haverkamp, C. Peugeot, J.-L. Thony, and M. Gilfedder. 1998. Prediction of crust-induced surface runoff with disc infiltrometer data. Soil Sci. 163:9–21. doi:10.1097/00010694-199801000-00003

van Genuchten, M.Th. 1980. A closed-form equation for predicting the hydraulic conductivity of unsaturated soils. Soil Sci. Soc. Am. J. 44:892–898. doi:10.2136/sssaj1980.03615995004400050002x

Van Looy, K., J. Bouma, M. Herbst, J. Koestel, B. Minasny, U. Mishra, et al. 2017. Pedotransfer functions in Earth system science: Challenges and perspectives. Rev. Geophys. 55:1199–1256. doi:10.1002/2017RG000581

Vaught, R., K.R. Brye, and D.M. Miller. 2006. Relationships among coefficient of linear extensibility and clay fractions in expansive, stoney soils. Soil Sci. Soc. Am. J. 70:1983–1990. doi:10.2136/sssaj2006.0054

Vereecken, H., R. Kasteel, J. Vanderborght, and T. Harter. 2007. Upscaling hydraulic properties and soil water flow processes in heterogeneous soils: A review. Vadose Zone J. 6:1–28. doi:10.2136/vzj2006.0055

Vereecken, H., J. Maes, and J. Feyen. 1990. Estimating unsaturated hydraulic conductivity from easily measured soil properties. Soil Sci. 149:1–12. doi:10.1097/00010694-199001000-00001

Vereecken, H., J. Maes, J. Feyen, and P. Darius. 1989. Estimating the soil-moisture retention characteristics from texture, bulk-density, and carbon content. Soil Sci. 148:389–403. doi:10.1097/00010694-198912000-00001

Vereecken, H., M. Weynants, M. Javaux, Y. Pachepsky, M.G. Schaap, and M.Th. van Genuchten. 2010. Using pedotransfer functions to estimate the van Genuchten–Mualem soil hydraulic properties: A review. Vadose Zone J. 9:795–820. doi:10.2136/vzj2010.0045

Verhoef, A., and G. Egea-Cegarra. 2013. Soil water and its management. In: P.J. Gregory and S. Nortcliff, editors, Soil conditions and plant growth. Blackwell Publ., Chichester, UK. p. 269–322. doi:10.1002/9781118337295.ch9

Vieira, S.R., D.R. Nielsen, and J.W. Biggar. 1981. Spatial variability of field-measured infiltration rate. Soil Sci. Soc. Am. J. 45:1040–1048. doi:10.2136/sssaj1981.03615995004500060007x

Viterbo, P. and A.C.M. Beljaars. 1995. An improved land-surface parameterization scheme in the ECMWF model and its validation. J. Climate 8:2716–2748. doi:10.1175/1520-0442(1995)008<2716:ailsps>2.0.co;2

Vogel, H.-J., I. Cousin, O. Ippisch, and P. Bastian. 2006. The dominant role of structure for solute transport in soil: Experimental evidence and modelling of structure and transport in a field experiment. Hydrol. Earth Syst. Sci. 10:495–506. doi:10.5194/hess-10-495-2006

Vogel, H.-J., and O. Ippisch. 2008. Estimation of a critical spatial discretization limit for solving Richards' equation at large scales. Vadose Zone J. 7:112–114. doi:10.2136/vzj2006.0182

Vogel, H.J., and K. Roth. 1998. A new approach for determining effective soil hydraulic functions. Eur. J. Soil Sci. 49:547–556. doi:10.1046/j.1365-2389.1998.4940547.x

Vrugt, J.A., C.J.F. ter Braak, C.G.H. Diks, B.A. Robinson, J.M. Hyman and D. Higdon. 2009. Accelerating Markov chain Monte Carlo simulation by differential evolution with self-adaptive randomized

subspace sampling. Int. J. Nonlinear Sci. Numer. Simul. 10:273–290. doi:10.1515/IJNSNS.2009.10.3.273

Walko, R.L., and R. Avissar. 2008. The Ocean–Land–Atmosphere Model (OLAM): I. Shallow-water tests. Mon. Weather Rev. 136:4033–4044. doi:10.1175/2008MWR2522.1

Walko, R.L., L.E. Band, J. Baron, T.G.F. Kittel, R. Lammers, T.J. Lee, et al. 2000. Coupled atmosphere–biophysics–hydrology models for environmental modeling. J. Appl. Meteorol. 39:931–944. doi:10.1175/1520-0450(2000)039<0931:CABHMF>2.0.CO;2

Wang, L.L., D.H. Chen, and H.J. Bao. 2016. The improved Noah land surface model based on storage capacity curve and Muskingum method and application in GRAPES model. Atmos. Sci. Lett. 17:190–198. doi:10.1002/asl.642

Wang, Y.P., E. Kowalczyk, R. Leuning, G. Abramowitz, M.R. Raupach, B. Pak, et al. 2011. Diagnosing errors in a land surface model (CABLE) in the time and frequency domains. J. Geophys. Res. 116:G01034. doi:10.1029/2010jg001385

Wang, Z., J. Feyen, M.Th. van Genuchten, and D.R. Nielsen. 1998. Air entrapment effects on infiltration rate and flow instability. Water Resour. Res. 34:213–222. doi:10.1029/97WR02804

Wang, Z., A. Tuli, and W.A. Jury. 2003a. Unstable flow during redistribution in homogeneous soil. Vadose Zone J. 2:52–60. doi:10.2136/vzj2003.5200

Wang, Z., L.S. Wu, T. Harter, J.H. Lu, and W.A. Jury. 2003b. A field study of unstable preferential flow during soil water redistribution. Water Resour. Res. 39:1075. doi:10.1029/2001WR000903

Warrick, A.W. 2003. Soil water dynamics. Oxford Univ. Press, New York.

Warrick, A.W., and A.A. Hussen. 1993. Scaling of Richards' equation for infiltration and drainage. Soil Sci. Soc. Am. J. 57:15–18. doi:10.2136/sssaj1993.03615995005700010004x

Warrick, A.W., and D.R. Nielsen. 1980. Spatial variability of soil physical properties in the field. In: D. Hillel, editor, Applications of soil physics. Academic Press, San Diego. p. 319–344.

Warrick, A.W., and T.C.J. Yeh. 1990. One-dimensional, steady vertical flow in a layered soil profile. Adv. Water Resour. 13:207–210. doi:10.1016/0309-1708(90)90042-3

Warrilow, D.A., A.B. Sangster, and A. Slingo. 1986. Modelling of land surface processes and their influence on European climate. Dyn. Climatol. DCTN38. Meteorol. Office, Bracknell, UK.

Weynants, M., H. Vereecken, and M. Javaux. 2009. Revisiting Vereecken pedotransfer functions: Introducing a closed-form hydraulic model. Vadose Zone J. 8:86–95. doi:10.2136/vzj2008.0062

Whisler, F.D., A.A. Curtis, A. Niknam, and M.J.M. Römkens. 1979. Modeling infiltration as affected by soil crusting. In: H.J. Morel Seytoux, editor, Surface and subsurface hydrology: Proceedings of the Fort Collins Third International Hydrology Symposium on Theoretical and Applied Hydrology, Fort Collins, CO. 27–29 July 1977. Water Resour. Publ., Fort Collins, CO. p. 400–413.

White, I., and M.J. Sully. 1992. On the variability and use of the hydraulic conductivity alpha parameter in stochastic treatments of unsaturated flow. Water Resour. Res. 28:209–213. doi:10.1029/91WR02198

Williams, P.J., and T.P. Burt. 1974. Measurement of hydraulic conductivity of frozen soils. Can. Geotech. J. 11:647–650. doi:10.1139/t74-066

Witter, J.V., P.D. Jungerius, and M.J. ten Harkel. 1991. Modelling water erosion and the impact of water repellency. Catena 18:115–124. doi:10.1016/0341-8162(91)90011-L

Wood, E.F., D.P. Lettenmaier, X. Liang, D. Lohmann, A. Boone, S. Chang, et al. 1998. The Project for Intercomparison of Land-surface Parameterization Schemes (PILPS) Phase 2(c) Red–Arkansas River basin experiment: 1. Experiment description and summary intercomparisons. Global Planet. Change 19:115–135. doi:10.1016/S0921-8181(98)00044-7

Woolhiser, D.A., R.E. Smith, and J.-V. Giraldez. 1996. Effects of spatial variability of saturated hydraulic conductivity on Hortonian overland flow. Water Resour. Res. 32:671–678. doi:10.1029/95WR03108

Wösten, J.H.M., A. Lilly, A. Nemes, and C. Le Bas. 1999. Development and use of a database of hydraulic properties of European soils. Geoderma 90:169–185. doi:10.1016/S0016-7061(98)00132-3

Wösten, J.H.M., Y.A. Pachepsky, and W.J. Rawls. 2001. Pedotransfer functions: Bridging the gap between available basic soil data and missing soil hydraulic characteristics. J. Hydrol. 251:123–150. doi:10.1016/S0022-1694(01)00464-4

Xue, Y., P.J. Sellers, J.L. Kinter and J. Shukla. 1991. A simplified biosphere model for global climate studies. J. Climate 4:345–364. doi:10.1175/1520-0442(1991)004<0345:Asbmfg>2.0.Co;2

Xue, Y.K., F.J. Zeng, and C.A. Schlosser. 1996. SSiB and its sensitivity to soil properties: A case study using HAPEX-Mobilhy data. Global Planet. Change 13:183–194. doi:10.1016/0921-8181(95)00045-3

Yager, R.R. 2001. The power average operator. IEEE Trans. Syst. Man Cybern. A 31:724–731. doi:10.1109/3468.983429

Yang, K., T. Koike, B.S. Ye, and L. Bastidas. 2005. Inverse analysis of the role of soil vertical heterogeneity in controlling surface soil state and energy partition. J. Geophys. Res. 110:D08101. doi:10.1029/2004jd005500

Yang, Z.-L., and R.E. Dickinson. 1996. Description of the Biosphere–Atmosphere Transfer Scheme (BATS) for the Soil Moisture Workshop and evaluation of its performance. Global Planet. Change 13:117–134. doi:10.1016/0921-8181(95)00041-0

Yang, Z.-L., and G.-Y. Niu. 2003. The versatile integrator of surface and atmosphere processes: 1. Model description. Global Planet. Change 38:175–189. doi:10.1016/S0921-8181(03)00028-6

Young, I.M., and J.W. Crawford. 2004. Interactions and self-organization in the soil–microbe complex. Science 304:1634–1637. doi:10.1126/science.1097394

Zaslavsky, D. 1964. Theory of unsaturated flow into a non-uniform soil profile. Soil Sci. 97:400–410. doi:10.1097/00010694-196406000-00006

Zhan, X.W., Y.K. Xue, and G.J. Collatz. 2003. An analytical approach for estimating CO_2 and heat fluxes over the Amazonian region. Ecol. Modell. 162:97–117. doi:10.1016/S0304-3800(02)00405-2

Zhang, Y.Q., H.X. Zheng, F.H.S. Chiew, J. Pena-Arancibia, and X.Y. Zhou. 2016. Evaluating regional and global hydrological models against streamflow and evapotranspiration measurements. J. Hydrometeorol. 17:995–1010. doi:10.1175/JHM-D-15-0107.1

Zhao, W., and A. Li. 2015. A review on land surface processes modelling over complex terrain. Adv. Meteorol. 17:607181. doi:10.1155/2015/607181

Zhou, X.Y., Y.Q. Zhang, Y.P. Wang, H.Q. Zhang, J. Vaze, L. Zhang, et al. 2012. Benchmarking global land surface models against the observed mean annual runoff from 150 large basins. J. Hydrol. 470–471:269–279. doi:10.1016/j.jhydrol.2012.09.002

Zhu, J., and B.P. Mohanty. 2002a. Spatial averaging of van Genuchten hydraulic parameters for steady-state flow in heterogeneous soils: A numerical study. Vadose Zone J. 1:261–272. doi:10.2136/vzj2002.2610

Zhu, J., and B.P. Mohanty. 2002b. Upscaling of soil hydraulic properties for steady state evaporation and infiltration. Water Resour Res 38(9):1178. doi:10.1029/2001WR000704.

Zhu, J., and B.P. Mohanty. 2003. Effective hydraulic parameters for steady state vertical flow in heterogeneous soils. Water Resour. Res. 39:1227. doi:10.1029/2002WR001831

Zhu, J., and B.P. Mohanty. 2004. Soil hydraulic parameter upscaling for steady-state flow with root water uptake. Vadose Zone J. 3:1464–1470. doi:10.2136/vzj2004.1464

Zhu, J., and B.P. Mohanty. 2006. Effective scaling factor for transient infiltration in heterogeneous soils. J. Hydrol. 319:96–108. doi:10.1016/j.jhydrol.2005.07.004

Zhu, J., B.P. Mohanty, and N.N. Das. 2006. On the effective averaging schemes of hydraulic properties at the landscape scale. Vadose Zone J. 5:308–318. doi:10.2136/vzj2005.0035

Zhu, J., B.P. Mohanty, A.W. Warrick, and M.Th. van Genuchten. 2004. Correspondence and upscaling of hydraulic functions for steady-state flow in heterogeneous soils. Vadose Zone J. 3:527–533. doi:10.2136/vzj2004.0527

Zobler, L. 1986. A world soil file for global climate modeling. Tech. Mem. 87802. NASA Goddard Space Flight Ctr., Greenbelt, MD.

Zobler, L. 1999. Global soil types, 1-degree grid (Zobler). [Dataset.] Oak Ridge Natl. Lab. Distributed Active Archive Ctr., Oak Ridge, TN. doi:10.3334/ORNLDAAC/418